Takahashi, K., Ravelo, A.C., Alvarez Zarikian, C.A., and the Expedition 323 Scientists
Proceedings of the Integrated Ocean Drilling Program, Volume 323

Site U1342[1]

Expedition 323 Scientists[2]

Chapter contents

Background and objectives

The primary objective of drilling at Integrated Ocean Drilling Program (IODP) Site U1342 (proposed Site BOW-15A; Takahashi et al., 2009) was to study high-resolution Pliocene–Pleistocene paleoceanography at a relatively shallow water depth on Bowers Ridge (Fig. **F1**), where relatively low sedimentation rates were observed in an earlier site survey piston core study (Takahashi, 2005). Bowers Ridge is well situated to study the past extent of water mass exchange with the Pacific Ocean through adjacent Aleutian passes such as Amukta, Amchitka, and Buldir (Figs. **F2, F3, F4, F5**). As at other Bowers Ridge sites, the record of changes in the flow of the warm Alaskan Stream water mass into the Bering Sea and its impact on the distribution of past sea ice coverage (Katsuki and Takahashi, 2005) is of particular interest.

A previous site survey piston core study found more open water conditions during the Last Glacial Maximum (LGM) at proposed Site BOW-8A (Takahashi et al., 2009), which is located in almost the same spot as Site U1342, than at Site BOW-12A, near the ridge crest where IODP Site U1340 is located (Fig. **F1**). Although productivity in the Bering Sea in general is very high with respect to other parts of the global oceans, expected productivity at this site, as well as the other Bowers Ridge sites, is lower than at IODP Site U1339 on Umnak Plateau, which is substantially more influenced by the adjacent Bering Sea shelf. With its relatively shallow water depth of 818 m, Site U1342 is the shallowest of the Bowers Ridge sites (Site U1340, water depth = 1295 m, and IODP Site U1341, water depth = 2140 m); therefore, Site U1342 provides an important constraint on the intensity and depth of the water column oxygen minimum zone (OMZ). A previous site survey piston core study reported sedimentation rates of ~32 m/m.y. (Takahashi, 2005), and Pliocene-age sediments at the bottom of the sedimentary section are expected.

This drill site at Bowers Ridge can also be used to study the impact of subseafloor microbes on biogeochemical fluxes. Organic-fueled subseafloor respiration and its impact on biogeochemistry in such a highly productive region have not previously been quantified. To do so, sediments drilled at Site U1342 will be used to determine subseafloor cell abundances and to investigate the link between the mass and characteristics of subseafloor microbes and the extent of export productivity from the surface ocean (Takahashi et al., 2000). Compared to other IODP Expedition 323 drill

[1] Expedition 323 Scientists, 2011. Site U1342. *In* Takahashi, K., Ravelo, A.C., Alvarez Zarikian, C.A., and the Expedition 323 Scientists, *Proc. IODP,* 323: Tokyo (Integrated Ocean Drilling Program Management International, Inc.). doi:10.2204/iodp.proc.323.106.2011
[2] **Expedition 323 Scientists' addresses.**

sites where detailed microbiological studies took place, Site U1342 is expected to have lower (but still high) surface-ocean productivity. As such, because of its more open ocean location farthest away from the high-productivity zone of the shelf, Site U1342 serves as the low-productivity end-member of the expedition's microbiological study.

Operations

Four holes were drilled at Site U1342 (Table T1). The first was cored using the advanced piston corer (APC) system to refusal. When refusal was met early, the extended core barrel (XCB) system was deployed to confirm formation material. The XCB recovered 0.5 m of basalt, effectively ending Hole U1342A. The second hole (U1342B) was dedicated to microbiology. Hole U1342C was cored with the APC system to 45.4 m drilling depth below seafloor (DSF), and Hole U1342D was APC cored to 44.0 m DSF. At that point, a center bit was dropped and the hole was drilled ahead 18.6 m to determine if the basalt was continuous. At a drilling break, the XCB system was deployed and used to take 13 cores of hard rock to the total hole depth of 127.7 m DSF. A complete set of site-specific tide tables was provided by the science party for Site U1342. These tables were used to make adjustments relative to initial mudline core and for each successive core in each hole. APC coring totaled 182 m penetrated, with 194.11 m recovered (a core recovery of 106.7%). XCB coring for Site U1342 totaled 66.1 m penetrated, with 41.54 m recovered (62.8% core recovery). The total cored interval was 248.1 m, with 235.65 m of core recovered, for a 95% total core recovery. The time spent at Site U1342 was 33.25 h (1.4 days).

Hole U1342A

Hole U1342A was spudded at 1320 h on 3 August 2009 (all times are ship local time, Universal Time Coordinated [UTC] – 11 h). The first APC barrel recovered 1.8 m of sediment, and an official seafloor depth was established at 829.7 m drilling depth below rig floor (DRF). APC coring continued through Core 323-U1342A-8H to 49.3 m DSF. Coring with the APC system was suspended after two successive short, incomplete strokes of the core barrel and apparent refusal. Three meters of hole was then drilled without coring with the APC/XCB bit, and the XCB system was deployed for a short core (1 m) to identify the material at APC refusal. Basalt was recovered and Hole U1342A was terminated. Overall core recovery for Hole U1342A using the APC coring system was 115.5%, with 56.93 m recovered. Core recovery using the XCB coring system was 46%, with 0.46 m recovered.

Hole U1342B

The vessel was offset 20 m east of Hole U1342A, and Hole U1342B was spudded at 2315 h on 3 August. The barrel recovered 5.33 m of core, and an official seafloor depth was established at 830.4 m DRF. APC coring continued through Core 323-U1342B-5H to 43.3 m DSF.

Hole U1342C

The vessel was offset 20 m east of Hole U1342B, and Hole U1342C was spudded at 0235 h on 4 August. The first APC barrel recovered 7.2 m of core, and an official seafloor depth was established at 830.3 m DRF. APC coring continued through Core 323-U1342C-6H to refusal. Overall core recovery for Hole U1342C using the APC coring system was 103.7%, with 47.06 m recovered.

Hole U1342D

The vessel was offset 20 m east of Hole U1342C, and Hole U1342D was spudded at 0830 h on 4 August. The first APC barrel recovered 6.0 m of core, and an official seafloor depth was established at 829.7 m DRF. APC coring continued through Core 323-U1342D-5H to 44.0 m DSF. On reaching refusal, the center bit was dropped and the hole was drilled ahead 18.6 m to see if there were sediments under the layer of hard rock (basalt). After a drilling break was observed, the XCB coring system was deployed and used successfully to core an additional 65.10 m into the formation. Overall core recovery for Hole U1342D using the APC coring system was 102.9%, with 45.29 m recovered. The XCB coring system recovered 41.08 m, for 63.1% core recovery.

Lithostratigraphy

Four holes were drilled at Site U1342; the deepest, Hole U1342D, reached 127.7 meters below seafloor (mbsf) and recovered basement rocks composed of dominantly volcaniclastic sedimentary rock below 62.6 mbsf. The sediments recovered at Site U1342 are a mixture of biogenic (mainly diatom frustules and foraminifers, with minor amounts of nannofossils, silicoflagellates, sponge spicules, and radiolarians), volcaniclastic (fine to coarse ash), and siliciclastic (clay- to pebble-sized clasts) sediments. In general, the color of the sediment reflects its lithologic characteristics: sediment composed of siliciclastic sediment or mixed lithologies tends to be very dark greenish gray to dark gray, whereas biogenic sediment is olive-gray to olive. Volcaniclastic ash layers are dark gray to black or shades of light gray to white. The recovered sediments and volcanic and volcaniclastic sedimentary rock are classified into three units based on major lithologic changes. The bottom boundary of Unit I (sediment composed mainly of diatoms, silt, and clay) is defined by a sharp change in grain size and diatom abundance. Unit II is predominantly sandy silt and silty sand. The bottom of Unit II is the contact between unconsolidated sediments and basement rock (Unit III), where drilling commenced.

Description of units

Unit I

Intervals: Sections 323-U1342A-1H-1, 0 cm, through 5H-4, 48 cm; 323-U1342C-1H-1, 0 cm, through 5H-2, 17 cm; and 323-U1342D-1H-1, 0 cm, through 5H-3, 40 cm

Depths: Hole U1342A, 0–35.3 mbsf; Hole U1342C, 0–37.0 mbsf; and Hole U1342D, 0–37.9 mbsf

Age: Pleistocene

Unit I is composed of two alternating, mainly siliciclastic and biogenic lithologies: silty clay to clayey silt and diatom ooze (Figs. **F6, F7, F8**) and is similar to Unit I described at other sites. The main siliciclastic lithologies are diatom-bearing to diatom- and foraminifer-rich silty clay or clayey silt. These lithologies tend to be very dark gray to olive-gray (5Y 4/1, 10Y 4/1, 5Y 3/2, 5Y 3/1, and 10Y 3/1). The main biogenic lithology is olive foraminifer-rich diatom ooze with variable amounts of dispersed vitric ash. The biogenic ooze is frequently laminated and ranges from olive to olive-gray (5Y 4/3, 5Y 4/4, and 5Y 4/2). Foraminifers occur scattered throughout all lithologies. The preservation of siliceous microfossils is poor in the siliciclastic lithologies (see **"Biostratigraphy"**).

The most dominant sedimentary features are thin to thick laminations that occur frequently in foraminifer-rich diatom ooze and occasionally contain nannofossils or silicoflagellates. Laminations are generally parallel, but occasionally cross-laminations occur. Laminated diatom ooze generally has a gradational top boundary characterized by burrows or mottling, whereas the lower boundary is either gradational or sharp. In some cases, a distinct, nearly monospecific layer of pennate diatoms (*Lioloma pacifium*) occurs at the bottom of the layer. Pennate diatom laminae are subhorizontal and are visible at the lower boundaries of laminated diatom ooze. These laminae are similar to those observed in Hole U1340D (Fig. **F10** in the "Site U1340" chapter).

Fifty laminated intervals were described in Holes U1342A, U1342C, and U1342D. Nineteen of these were correlated between all holes based on their core composite depth below seafloor (CCSF-A), lamina thickness, and other visual characteristics (Fig. **F9**). The remaining 31 laminated layers were recognized in only one or two holes. In these intervals, slightly to moderately bioturbated diatom ooze is likely to occur in the other hole without apparent lamination (Figs. **F9, F10**).

Bioturbation varies from slight to moderate throughout the unit and is typically characterized by a mottling defined by color or texture changes. Typically, individual burrows are well preserved at the upper boundary of the laminated intervals and even within the laminations. Where recognizable, trace fossils were mostly assigned to the *Chondrites* and *Skolithos* ichnofacies.

Clasts occur throughout the unit and do not appear to be associated with any particular lithology. Distinct ash layers occur mainly between 20 and 40 mbsf in all holes. Volcanic ash layers are gray (5YR 6/1 and 5Y 6/1), grayish brown (2.5Y 5/2), dark grayish brown (2.5Y 4/2), and black (5Y 2.5/2).

Unit II

Intervals: Sections 323-U1342A-5H-4, 48 cm, through 7H-5, 131 cm; 323-U1342C-5H-2, 17 cm, through 6H-CC, 16 cm; and 323-U1342D-5H-3, 40 cm, through 5H-CC, 13 cm

Depths: Hole U1342A, 35.3–49.3 mbsf; Hole U1342C, 37.0–45.4 mbsf; and Hole U1342D, 37.9–44.0 mbsf

Age: Pliocene to lower Pleistocene

Unit II is defined by a shift in texture from silt- to sand-sized grains and a corresponding decrease in biogenic components composed of sandy silt to silty sand (Fig. **F6**). The main lithologies are very dark greenish gray to gray diatom-bearing clay to sand and very dark gray to black (5Y 3/1 to 2.5N) diatom-rich sponge spicule–bearing fine-ashy sand. One dark gray ash layer is present in all three holes, and dispersed vitric ash mottles are present throughout. Isolated clasts were also observed. In general, the sediment is highly disturbed. The sand is composed of moderately to well-rounded igneous and metamorphic rock fragments, quartz, feldspar, pyroxene, sponge spicules, diatom frustules, and well-rounded glauconite grains (Fig. **F11;** see also **"Site U1342 thin sections"** and **"Site U1342 smear slides"** in "Core descriptions”). Bioturbation varies from moderate to strong throughout the unit and is characterized by large *Skolithos* burrows.

Because of the highly chaotic nature of the sediments, it is unclear whether the visible structures are a result of coring disturbance, slumping, or primary deposition. Bedding and parallel laminations were described in Hole U1342C; these features are also found in Holes U1342A and U1342D but were not described as such.

In Holes U1342A and U1342C (Sections 323-U1342A-5H-4, 88 cm, to 7H-CC and Sections 323-U1342C-5H-CC, 0 cm, to 5H-CC, 36 cm), black sand sediments are soupy and include no significant biogenic components as a result of sediment sorting by flow-in. Because of poor recovery and flow-in of sand, it is not possible to define the exact thickness of these sandy lithologic units. In Core 323-U1342A-7H, the APC was advanced 1 m but recovered 7.4 m of sediment. In Figure **F6**, only 1 m of sediment from Core 323-U1342A-7H is illustrated to show the depth of the drilled interval (323-U1342A-8D) and the rocks recovered in Core 323-U1342A-9X. The base of Unit II is defined by the termination of APC coring at Core 323-U1342A-7H (49.3 mbsf), where the lithified basement was reached.

Unit III

Intervals: Sections 323-U1342A-8D, 0 cm, through 9X-1 and 323-U1342D-6D, 0 cm, through 19X-4
Depths: Hole U1342A, 49.3–53.3 mbsf, and Hole U1342D, 44.0–127.7 mbsf
Age: unknown (age will be determined by shore-based studies)

Unit III is composed of mafic volcaniclastic rocks that range from sandstone to breccia and possibly minor basalt (Fig. **F12**). Basalt is present only in Core 323-U1342A-7X, extending from 52.30 to 52.76 mbsf. The basalt is porphyritic and vesicular, with a very dark gray interstitial groundmass. Phenocrysts are mostly plagioclase laths as large as 6 mm (~20%) and pyroxene as large as 2 mm (~2%). Many phenocrysts are in glomeroporphyritic aggregates. Vesicles are ovoid to irregular in shape and have a diameter as wide as 15 mm, with an average of 2–3 mm. They have a pale blue-gray or white mineral coating. The groundmass consists of plagioclase laths with brown glass in the interstices.

Below the basalt are interbedded gray, green, and red volcanogenic sandstone and breccia. The contact between the basalt and sedimentary rocks was not recovered. Most of the bedding contacts recovered in the volcaniclastic interval are parallel and are more or less sharp. Thin to thick laminations are common. The sandstone and some of the breccia beds are polymictic, consisting of a range of scoriaceous (black and red), vesicular, and nonvesicular glassy and porphyritic basalt fragments and plagioclase and pyroxene crystals. Monomict breccias with irregularly shaped porphyritic and vesicular mafic clasts are also present. Breccia clasts range from very angular to subangular and, less frequently, subrounded. Some mafic clasts have alteration rims, and rare clasts in the polymict breccia have cored lapilli consisting of a central mafic rock fragment and a coating of basalt. Most mafic clasts have flow-aligned plagioclase laths. The matrix of both breccia types is made up of glassy fragments. Most beds are moderately to well sorted, and some sandstone beds have dewatering structures. Some breccia beds are more poorly sorted. Beds are both massive and normally graded. One of the most common sedimentary structures in the laminated volcaniclastic layers is soft-sediment deformation. Tightly folded and tilted volcaniclastic beds were observed in Sections 323-U1342D-10X-2, 9X-2, 10X-3, and 12X-2. Faulted volcaniclastic layers showing ~3 cm of apparent vertical displacement (throw) were also observed; the largest was found in Section 323-U1342D-12X-2 above a slightly slumped interval (Fig. **F13**). The relative offset of the hanging wall and footwall indicates that this is probably normal faulting produced in an extensional regime. Based on regional information from the Aleutian Ridge, the volcanic basement rock of Bowers Ridge probably first formed in the Eocene and ceased to accumulate in the Miocene.

Discussion

Unit I is characterized by repeated alternations between laminated foraminifer-rich diatom ooze layers and siliciclastic layers. The occurrence of well-preserved laminations indicates the absence of bioturbating fauna and thus suggests low-oxygen conditions in bottom waters and within the surface sediments. Burrows or mottles at the gradational tops of laminated sediment intervals indicate an increase in oxygenation of bottom waters after the deposition of laminated sediments. In contrast, the sharp bottom boundaries could be the result of a decrease in bottom water oxygen and cessation of bioturbation at the onset of laminated intervals or a hiatus between the laminated sediments and underlying siliciclastic sediments. Occasional cross laminations indicate either migration of sediment by bottom currents or soft-sediment deformation. The sedimentation rate at this site is on average very low (3 cm/k.y.) (see **“Paleomagnetism”**). The winnowing of sediment by bottom currents may have caused the apparent low average sedimentation rate, and the sedimentary record may have inherited strongly variable sedimentation rates or even phases of nondeposition or erosion.

High values in color reflectance parameter b* correlate well with the laminated sediments in all holes (Fig. **F14**) because of the difference in color between siliciclastic sediments (dark gray to greenish gray) and diatom ooze (olive). Sudden changes in b* were also recognized at depths where prominent laminated intervals were found in other holes. The nonlaminated intervals are generally slightly to moderately bioturbated diatom oozes. This bioturbation indicates that these nonlaminated diatom oozes are likely the result of postdepositional bioturbation of the laminated structure (see example in Fig. **F10**) and might represent similar depositional conditions as their laminated equivalents.

The total number of well-correlated laminated intervals (16) is similar to the total number of interglacial cycles (15) that occurred during the last 1.1 m.y. (Lisiecki and Raymo, 2005). This match suggests that the changes controlling laminations occur on the same timescale as glacial–interglacial cycles. The laminations may be related to high biological production in the surface waters and elevated organic matter export, which create anoxic bottom water conditions that prevent bioturbation of the sediments by macrofauna. Biological production tends to increase during interglacial periods in the Bering Sea (Okazaki et al., 2005). A preliminary interpretation is that the occurrence of laminated ooze reflects interglacial times. This interpretation is consistent with the preliminary paleomagnetic age model (see **"Paleomagnetism"**). However, this interpretation is tentative because these laminated intervals have not yet been well dated.

Unit II is characterized by its sandy texture with low abundances of biogenic components (Figs. **F6, F7, F8**). Moderately to well-rounded and mixed volcaniclastic and metamorphic mineral or rock fragments in the sand suggest that the source is terrestrial. The contact between Units I and II is sharp. It is unclear whether the sand was redeposited from a shallower water depth by sediment gravity flows or the paleowater depth at this site was shallower than it is today. Seismic profiles that cross the crest of Bowers Ridge appear to document that its basement rock framework was truncated by wave-base erosion prior to subsidence to depths of 1 km and deeper. Furthermore, the age of the unit is also ambiguous. Several Miocene diatom species were observed in this unit (see **"Biostratigraphy"**), but the base of Unit I is dated to only 1.1 Ma. Thus, the occurrence of Miocene species can be explained by reworking by sediment gravity flows, an extremely low sedimentation rate, or a hiatus between Units I and II.

The basement volcanic rock (basalt) was most likely deposited as lava, as indicated by the flow alignment of the plagioclase laths and the vesicular texture. The volcaniclastic rocks beneath have a mafic volcanic source and contain both fragments and tephra fragments (scoria). The complexly zoned plagioclase shows resorbed and sieve-textured cores typical of arc lavas. The massive to graded nature of beds and the unmodified (angular) grain shapes suggest that rapid deposition by mass flows was one of the primary depositional mechanisms. However, other sedimentary structures, including the sorting of particles, soft-sediment deformation, and microfaulting, may indicate alternate depositional modes that reflect resedimentation by mass wasting of sediments having different degrees of coherence and lithification, which, together with the presence of lava flows, are common in stratovolcanoes. It is unclear at this stage whether the mass flows were subaerial or subaqueous and whether the flows are gas or water supported. The red color of many of the fragments suggests a subaerial and oxidized source, at least in part.

Biostratigraphy

Core catcher samples above 36 m CCSF-A at Site U1342 are dominated by diatom microfossils exhibiting high diversity and variably good to poor preservation. These samples also contain well-preserved, low-diversity assemblages of calcareous nannofossils and planktonic foraminifers typical of high latitudes, very high to low abundances of calcareous benthic foraminifers, and variable abundances of other siliceous microfossils. Palynological residues contain high to low abundances of dinoflagellate cysts, pollen, and other palynomorphs. Below 36 m CCSF-A, the majority of microfossils disappear, and samples contain only rare diatoms and palynomorphs and are barren of calcareous microfossils. Abundant sponge spicules and fragments occur. Biostratigraphy below 36 m CCSF-A is hampered by poor microfossil preservation. Eight biostratigraphic datum events were interpreted based on radiolarians, diatoms, silicoflagellates, and calcareous nannofossils. These, together with paleomagnetic datum events, indicate that the base of the microfossil-rich section (uppermost 36 m CCSF-A) is 1.0 Ma (Fig. **F15;** Table **T2**), giving a low sedimentation rate of 3.6 cm/k.y. compared to other Expedition 323 sites. Siliceous microfossils are mainly composed of high-latitude pelagic species similar to those found at nearby Sites U1340 and U1341. Dinoflagellate assemblages vary between low and high primary productivity indicators and indicate generally low sea-surface temperatures (SST) and low seasonal sea ice coverage. Calcareous planktonic microfossils at this site reflect a high-latitude environment, indicating variation in SST. Benthic foraminifers are dominated by species typical of environments within the OMZ. The appearance of Pliocene diatom specimens in shallow samples and Pleistocene specimens close to the basement rock suggest reworking at this site. Middle Miocene diatoms were observed below ~45 mbsf, and further investigation will be needed to determine the age of the basement.

Calcareous nannofossils

All core catcher samples from Holes U1342A–U1342D were sampled and examined to assess the abundance and state of preservation of calcareous nannofossils. Evaluations of the abundance of taxa within the assemblages were also made. The results (Table T3) show that *Coccolithus pelagicus* is the dominant taxon and is present in all samples containing calcareous nannofossils; small and medium gephyrocapsids are also frequently present. Other taxa include *Emiliania huxleyi*, *Pseudoemiliania lacunosa*, *Reticulofenestra minuta*, and *Calcidiscus leptoporus*. Reworked specimens occur in most samples from Hole U1342D, and some of these were identified as typical middle Miocene to Pliocene taxa. The sequences recovered at Site U1342 are also characterized by frequent barren intervals, particularly in all samples below ~36 m CCSF-A (Samples 323-U1342A-6H-CC and 7H-CC, 323-U1342B-2H-CC through 5H-CC, 323-U1342C-4H-CC through 6H-CC, and 323-U1342D-5H-CC and 9H-CC) and apparently at random in Holes U1342B and U1342C, hampering the continuity of the calcareous nannofossil record.

Emiliania huxleyi, which characterizes calcareous nannoplankton Zone NN21 (Martini, 1971), is present in Samples 323-U1342A-1H-CC and 323-U1342D-1H-CC and 2H-CC. Therefore, these samples can be assigned to Zone NN21, which ranges from 0.29 Ma to the present. Sample 323-U1342A-3H-CC contains *P. lacunosa* and is therefore assigned to calcareous nannofossil Zone NN19 (Martini, 1971), which ends at 0.44 Ma.

It was not possible to assign an age based on calcareous nannofossils to the sandy silt bottom sediments of Site U1342. The existence of Pliocene and middle Miocene reworked taxa in samples above this level may provide an age estimate for those sediments; however, long-distance transportation of reworked taxa cannot be discounted because warm-water *Discoaster* spp. was found among the reworked population.

Planktonic foraminifers

The >125 µm fraction of 25 core catcher samples from Holes U1342A–U1342D and an extra sample from Hole U1342C were analyzed for planktonic foraminifers (Table T4). Additionally, mudline samples from the top of Core 1H in all holes were analyzed using the same size fraction. High proportions of sand, sponge spicules, and diatoms were observed in the majority of samples, and Sample 323-U1342D-9X-CC contains only rock fragments. The uppermost samples of Site U1342 cores (uppermost ~36 m CCSF-A) contain dominant to few planktonic foraminifers, and samples are mostly barren of planktonic foraminifers below. The fauna is largely dominated by *Neogloboquadrina pachyderma* (sinistral). The frequency of subpolar species *Globigerina bulloides*, *Globigerina umbilicata*, and *Neogloboquadrina pachyderma* (dextral) varies between holes and cores. In Hole U1342A, both *G. bulloides* and *N. pachyderma* (dextral) are variably abundant, and *G. bulloides* is abundant in Sample 323-U1342D-4H-CC.

The dominating species at Site U1342, *N. pachyderma* (sinistral), is also the dominating species in the water column of the Bering Sea today (Asahi and Takahashi, 2007). The temporal variability of this species at this site shows how subpolar–polar sea-surface conditions prevailed over the last 1 m.y. *Globigerina bulloides* and *G. umbilicata* are controlled both by temperature and food availability (Reynolds and Thunell, 1985); however, studies in the Bering Sea show that in this region these species are mostly influenced by temperature (Asahi and Takahashi, 2007).

Benthic foraminifers

More than 20 species of benthic foraminifers were recovered in 29 samples from Holes U1342A–U1342D (Table T5). The majority of core catcher samples down to around Sample 4H-CC in all holes contain varyingly diverse calcareous assemblages ranging from high to low abundance. Occasionally dominant species are *Cassidulina* sp. and *Uvigerina peregrina*. Persistently occurring species include *Brizalina pygmaea*, *Brizalina spathula*, *Bulimina* aff. *exilis*, *Globobulimina pacifica*, and *Valvulineria* spp. This assemblage shows similarities to the assemblages found in the uppermost ~100 m of Sites U1339, U1340, and U1341 and also to those within or near the OMZ in the Sea of Okhotsk (Bubenshchikova et al., 2008). This fauna is likely strongly affected by the local OMZ, and variation in species abundance is probably linked to changes in oxygen concentrations and, in turn, surface water productivity and/or intermediate water ventilation. This assemblage does not appear to reflect shallow-water (shelf) deposition.

The assemblage largely disappears from Sample 5H-CC and below in all holes and is replaced with glauconite-rich sands likely derived from a more shallow (shelf) setting.

Ostracodes

No ostracodes were found in core catcher samples at Site U1342.

Diatoms

Diatom biostratigraphy is based on the analysis of core catcher samples from all cores from Holes U1342A–U1342D. Depth positions and age estimates of biostratigraphic marker events are shown in Figure **F15** and Table**T6.** Diatom preservation is poor to moderate in all holes, and abundance is common to rare throughout this Pleistocene record.

Only 5–6 cores were retrieved at Site U1342 before basement was reached. Continued drilling into the rock strata provided some interludes of softer material that were analyzed for diatoms (Samples 323-U1342A-7H-CC and 323-U1342B-7H-CC). However, little information could be derived from these older intervals, and clear reworking was evident from the presence of the early Pleistocene–Pliocene species *Neodenticula koizumii* and the Miocene species *Actinocyclus ingens*. The presence of this middle Miocene species suggests a minimum age of 14 Ma (Baldauf and Barron, 1980) for the basement at this site. This datum is, however, tentative and requires further investigation.

In Holes U1342A and U1342C, the last occurrence (LO) of *Proboscia curvirostris* was observed in Samples 323-U1342A-3H-CC and 323-U1342C-3H-CC. This datum, however, was observed at a shallower depth in Samples 323-U1342B-2H-CC and 323-U1342D-2H-CC and concurs with radiolarian datum *Spongodiscus* sp. (Table **T2**). Therefore, the stratigraphic marker observed at the shallower depths was used to assign an age of 0.3 Ma (Barron and Gladenkov, 1995; Yanagisawa and Akiba, 1998).

In general, diversity is higher in the *P. curvirostris* Zone in every hole, including the species *Neodenticula seminae*, *Actinocyclus curvatulus*, *Thalassiosira* spp. (*Thalassiosira antarctica* spores, *Thalassiosira latimarginata* s.l., and *Thalassiosira oestrupii*), *Thalassiothrix longissima*, and *Porosira glacialis*. In Hole U1342B, stratigraphic biomarker *Thalassiosira jouseae* co-occurs with *P. curvirostris*, and its absence in the other holes further suggests poor preservation at this site.

The last common occurrence (LCO) datum of *Actinocyclus oculatus* marks the following stratigraphic zonation and was not observed in any of the holes, although it was observed sporadically throughout the record. Therefore, no clear datum was defined beyond *P. curvirostris* Zone 11. The LO of *N. koizumii* was observed in Samples 323-U1342A-5H-CC, 323-U1342B-5H-CC, and 323-U1342D-5H-CC. This datum of 2.1 Ma could not be assigned because this zone is established by the LCO of *N. koizumii* according to Yanagisawa and Akiba (1998). Because of poor diatom preservation below Core 5H in all holes, biostratigraphic zonation was constrained by one species, *P. curvirostris*, which places *N. seminae* North Pacific Diatom (NPD) Zone 12 in Samples 323-U1342A-1H-CC through 2H-CC and 323-U1342C-1H-CC through 2H-CC (1.65–11.41 and 7.09–17.04 mbsf, respectively). In Holes U1342B and U1342D, Zone NPD12 is shallower and covers only Samples 323-U1342B-1H-CC and 323-U1342D-1H-CC (0–5.33 and 0–6.11 mbsf, respectively). In general, this short interval is poorer in diatom preservation than Zone 11 and is composed of *T. latimarginata* s.l., *T. antarctica* spores, *T. oestrupii*, and, to a lesser extent, *Rhizosolenia* spp.

Silicoflagellates and ebridians

Silicoflagellate and ebridian counting was conducted in Holes U1342A and U1342D (Table **T7**). Silicoflagellate and ebridian preservation at Site U1342 is essentially poor to moderate and is worse than the preservation at previous sites. Zonation datum events could not be defined at this site because of low abundances, poor skeleton preservation, and limited sample numbers. Based on the observed species, the age of the uppermost four cores from Holes U1342A and U1342D is probably Pleistocene. The age of Core 323-U1342A-5H and below may be older than 2.5 Ma based on the occurrence of *Ebriopsis antiqua antiqua*, assuming it is not reworked. The biostratigraphic results at this site are still unclear, but they will be revised with the increased sample numbers available for shore-based study.

Radiolarians

Radiolarian biostratigraphy is based on the analysis of core catcher samples from Holes U1342A–U1342D. The radiolarian zone defined during this expedition (see **"Biostratigraphy"** in the "Methods" chapter) could not be determined because there was no occurrence of *Stylatractus universus*. However, the stratigraphy at Site U1342 (Table **T8**) extends from the *Botryostrobus aquilonaris* Zone (upper Quaternary) to the *Eucyrtidium matuyamai* Zone (middle Quaternary) in the subarctic Pacific (Kamikuri et al., 2007). Six radiolarian datums derived in the subarctic Pacific were identified at this site (Table **T8**). These datums indicate lower sedimentation rates (~5 cm/k.y.) in the uppermost 20 m intervals of each hole than those at other Bowers Ridge sites (U1340 and U1341). The *Amphimelissa setosa* LO datum (0.08–0.10 Ma) was found only in Hole U1342C, probably because its small skeleton size passed through the 63 µm mesh. Note that the occurrence of *S. universus* in Sample 323-U1342A-7H-CC is not used as a datum because Samples 323-U1342A-6H-CC and 7H-CC possibly constitute flow-in materials. Although radiolarian datums in the lower intervals are scarce, the LO of *E. matuyamai* (0.9–1.5 Ma) was found in Sample 323-U1342B-4H-CC. This datum provides a constraint for age estimation for the lower intervals and an average sedimentation rate in Hole U1342B of 2–4 cm/k.y. Below 36 m CCSF-A, radiolarian abundances are very low and only a few Pleistocene species were found. No Miocene radiolarian species were found in the interval.

Radiolarian abundances and preservation are shown in Table **T9.** Radiolarian preservation is generally moderate to poor in all samples. The preservation conditions at this site are worse than those at other Bowers Ridge sites (U1340 and U1341). In particular, radiolarian skeletons in Sample 323-U1342A-3H-CC suffered significant dissolution and appear thin and frail, similar to specimens from deep-sea sediments found below 4000 m water depth. The dissolution is possibly related to sediment winnowing by bottom currents (see **"Lithostratigraphy"**). Radiolarian abundances are common to few in all holes at Site U1342 and very few in the lower intervals. Radiolarian assemblages are similar to those found at other Bowers Ridge sites (U1340 and U1341). However, the abundance of *Stylochlamydium venustum*, with its fragile skeletal parts, is apparently low, suggesting poor preservation. Interestingly, *Phorticium pylonium* Heackel, which is abundant in tropical to subtropical Pacific waters, was found in Sample 323-U1342D-1H-CC. With its characteristic squarelike cortical shell, this specimen differs from those found at low latitudes.

Palynology: dinoflagellate cysts, pollen, and other palynomorphs

Palynological assemblages were examined in core catcher samples from Holes U1342A and U1342B (Table **T10**). In spite of relatively poor diatom preservation compared to Sites U1340 and U1341, samples were difficult to process because of abundant detrital and biogenic silica. Pollen grains (mostly dominated by *Picea*) and pteridophyte spores occur throughout the sequence, with concentrations ranging between 10 and 900 grains/cm^3. The highest abundance occurs in Samples 323-U1342A-2H-CC and 3H-CC at ~11.86 and 22.02 m CCSF-A, respectively. Variable pollen concentrations indicate vegetation changes in the source area and/or changes in the strength and pattern of atmospheric and/or oceanic circulation trajectories. Reworked palynomorphs are common only in Samples 323-U1342B-3H-CC and 5H-CC and likely reflect detrital input. Organic linings of benthic foraminifers are common throughout the sequence. Their abundance could be related to moderate calcium carbonate dissolution or high benthic foraminifer production.

Dinoflagellate cysts are common to abundant in most samples, with concentrations ranging between 100 and >1000 cysts/cm^3. However, dinoflagellate cysts are very few to rare in the sandy layer (Samples 323-U1342A-6H-CC and 7H-CC). Poor preservation of organic-walled dinoflagellate cysts in the lower part of the sequence, particularly in the sandy layer (Samples 323-U1342A-6H-CC and 7H-CC and 323-U1342B-5H-CC), suggests significantly high oxygen concentrations in the bottom water, probably caused by sediment remobilization. The species composition of the assemblages is modern (Table **T10**), suggesting a Pleistocene age for all analyzed samples.

Discussion

Diatomaceous sediments above ~36 m CCSF-A span the last ~1.2 m.y. (Fig. **F15**). These sediments and those below contain occasional reworked diatoms and silicoflagellates. The age of the underlying rock strata could not be clearly defined; however, middle Miocene diatoms observed in the deepest sample (323-U1342A-7H-CC) suggest a tentative age older than 14 Ma. Biostratigraphic investigations will continue postexpedition and be improved with shore-based studies.

Planktonic foraminifer abundances are high throughout most of the record. Calcareous nannofossil abundances are low but follow the same general trend as planktonic foraminifers. At the top of the sandy silt basal unit (~36 m CCSF-A), both calcareous nannofossils and planktonic foraminifers are absent (Fig. **F16**). Barren intervals usually coincide with coarser sediments, which probably indicates the existence of winnowing processes that washed away the finer fraction during these intervals. The barren levels also match levels with lower percentages of $CaCO_3$. In fact, the large similarities between carbonate abundance and calcareous nannofossil records might indicate that most of the carbonate at this site accumulated within the clay fraction, as at

Site U1341. The percentages of heavily silicified diatom valves are low throughout the section except at ~42 m CCSF-A (Fig. **F16**), where there is a single peak.

Both dinoflagellate cyst assemblages and sea ice diatoms suggest low seasonal sea ice coverage, and planktonic foraminifers indicate polar to subpolar conditions (Fig. **F17**). In general, dinoflagellate cysts suggest high primary productivity, low SST, and seasonal sea ice coverage (Fig. **F17**). However, the codominance of the autotrophic-related productivity species *Operculodinium centrocarpum* and the heterotrophic *Brigantedinium* spp. in Sample 323-U1342A-3H-CC could be associated with relatively low primary productivity and/or an incursion of oceanic/oligotrophic waters. Ecological interpretation of diatom assemblages at this site is complicated by the low abundance of diatoms and sample intervals and may only be resolved by higher resolution work.

Benthic foraminifers generally have high abundances, and variation in species dominance is probably related to changes in oxygen levels caused by productivity changes and/or intermediate water ventilation, although it may also have been affected by current winnowing. Figure **F18** shows the variability in the proportions of two common genera, *Bulimina* spp. and *Uvigerina* spp., against gamma ray attenuation (GRA) bulk density data. *Uvigerina* is regarded as a shallow infaunal (intermediate oxygen) genus, and *Bulimina* is regarded as deep infaunal (low oxygen) (e.g., Bubenshchikova et al., 2008; Kaiho, 1994). Low-oxygen species abundance generally correlates with variations in GRA bulk density in the uppermost ~9 m because low GRA is associated with high biogenic production rates. Low oxygen at these times suggests that productivity was a factor affecting the OMZ extent; however, the OMZ may also have been affected by intermediate water ventilation during times of low production and possibly extensive sea ice coverage. Further analysis is needed to fully understand this relationship.

Paleomagnetism

The archive halves of all sediment cores recovered at Site U1342 were measured on the three-axis cryogenic magnetometer at 2.5 cm intervals. Natural remanent magnetization (NRM) was measured before (NRM step) and/or after (demagnetization step) stepwise alternating-field (AF) demagnetization in peak fields of up to 20 mT. Cores from Hole U1342A were measured at NRM step and 20 mT demagnetization step; other Site U1342 cores were measured only at 20 mT demagnetization step to keep up with core flow.

Inclination and intensity after 20 mT AF demagnetization from Holes U1342A, U1342C, and U1342D are plotted in Figure **F19.** The average inclination values are nearly 70° over the normal polarity intervals, which are close to the site axial dipole inclination (~72°), indicating that we can effectively remove overprint magnetization caused by the drill pipe and/or core barrel from the NRM records. All inclination records for cores from Holes U1342A, U1342C, and U1342D as well as the 60 point averages are plotted in Figure **F20.** A polarity zonation was defined from the inclination record and correlated to the polarity timescale based on micropaleontology datums (see **"Biostratigraphy"**). The Brunhes/Matuyama boundary and the base of the Jaramillo Subchron are clearly identified in Holes U1342A, U1342C, and U1342D. The top of the Jaramillo Subchron and both the top and the base of the Cobb Mountain Subchron are identified in Holes U1342C and U1342D but not in Hole U1342A. Three excursions were tentatively noted in Holes U1342A, U1342C, and U1342D: the Kamikatsura, Santa Rosa, and Punaruu excursions, the depths and ages of which are shown in Table **T11.**

Relative paleointensity estimates from Site U1341 were compared to estimates from Site U1342. Both estimates are based on normalizing the NRM after 20 mT AF demagnetization by magnetic susceptibility. Magnetic susceptibility was used as a correlation tool to determine if a reproducible relative paleointensity record could be developed for these two sites. Magnetic susceptibility and relative paleointensity for Site U1341 are plotted in Figure **F21.** Magnetic susceptibility and relative paleointensity for Site U1342 are plotted in Figure **F22.** The comparison was limited to the Brunhes Chron (last 781,000 y). It is possible to see a correlative pattern of relative paleointensity at the two sites, as indicated by the relative numbering scheme in Figures **F21** and **F22.** However, the relative paleointensity estimates are still significantly influenced by lithologic variability and should not be considered high-resolution estimates of true geomagnetic field intensity variations.

The age-depth relationship at Site U1342 was estimated by combining the information recovered from our estimates of polarity boundaries, excursions, and relative paleointensity (Brunhes only). The ages of excursions and relative paleointensity features are assigned using estimates of how each one is related to a specific marine isotope stage (Fig. **F22**). The final time-depth curve is shown in Figure **F23.** The fine-grained hemipelagic marine sediments are estimated to have been deposited during the last ~1.5 m.y., with essentially a constant sediment accumulation rate during the last 1 m.y.

Figure **F24** summarizes rock magnetic variability in Hole U1342A. Magnetic susceptibility is shown at the top, and magnetic remanence (after 20 mT AF demagnetization) is shown at the bottom. Note the discrete intervals where both magnetic parameters undergo more than order-of-magnitude decreases that indicate intervals of significant magnetic mineral dissolution. These intervals appear to be closely related to laminated sediment intervals, and both are probably related to enhanced rates of reduction diagenesis during those selected time intervals. The major dissolved intervals are noted in Table **T12.** Our chronostratigraphic estimates suggest that these dissolved intervals (and their associated laminations) occur in interglacial sediments (Table **T12**). A few narrow intervals of significantly stronger remanence (Table **T13**) are tentatively associated with authigenic greigite or ice-rafted pebbles, which always occur in glacial-stage sediments with lower porosity.

Geochemistry and microbiology

Interstitial water chemistry

Samples for interstitial water analyses were retrieved from Hole U1342A at 1.48, 4.7, 14.2, 20.2, 29.7, 39.2, 44.2, and 54.2 mbsf by the whole-round squeezing technique. Furthermore, high-resolution samples were taken from microbiology-dedicated Hole U1342B with a total number of 56 whole-round samples. To prevent oxidation, whole rounds were stored in a nitrogen-filled glove box at 7°C until squeezed. Aliquot samples were processed for routine shipboard analyses (see **"Geochemistry"** in the "Methods" chapter) and collected for shore-based analyses of sulfur and oxygen isotopes of sulfate and hydrogen sulfide, trace metals, dissolved organic carbon (DOC), and fatty acids.

Chlorinity, salinity, alkalinity, dissolved inorganic carbon, and pH

Interstitial water chloride concentrations at Site U1342 average 543 ± 16 mM (Fig. **F25F**), and salinity ranges from 35 to 37. Alkalinity increases subtly with depth in the uppermost 12 m from 3.0 to 5.1 mM and decreases to 3.5 mM at 54.2 mbsf (Fig. **F25C**). This trend is similar to the dissolved inorganic carbon (DIC) profile (Fig. **F25A**). DIC concentrations range from 2.7 to 5.1 mM in the uppermost 12 m and decrease to a minimum of 2.9 mM at 54.2 mbsf. At ~19 mbsf, DIC decreases to a local minimum of 3.9 mM. Interstitial water pH varies between 7.4 and 8.1, with a trend toward higher values below 30 mbsf (Fig. **F25B**). Dissolved sulfate and hydrogen sulfide.

Dissolved sulfate concentrations at Site U1342 decrease from concentrations close to seawater values at 0.05 mbsf to ~24 mM below 20 mbsf (Fig. **F25D**). Hydrogen sulfide concentrations above the detection limit of 0.5 µM were only observed sporadically and remain <1.5 µM (data not shown).

Dissolved ammonium, phosphate, and silica

Ammonium concentrations increase with depth from 0.02 mM in the uppermost 10 m to maximum values averaging 0.33 mM between 11 and 24 mbsf (Fig. **F25H**). Concentrations decrease slightly below 24 mbsf. Phosphate concentrations gradually increase from 3.2 µM at 0.05 mbsf to a maximum of 22.4 µM at 6.1 mbsf (Fig. **F25G**). Phosphate concentrations below this depth decrease to <5 µM at 33 mbsf. Dissolved silica concentrations increase from 470 µM at 0.05 mbsf to 940 µM at 25 mbsf and then decrease to 330 µM at 54 mbsf (Fig. **F26J**).

Dissolved calcium, magnesium, sodium, and potassium

Dissolved calcium, magnesium, sodium, and potassium concentrations were determined by ion chromatography. Calcium concentrations increase linearly from seawater values in the uppermost centimeters to a maximum concentration of 18 mM at 42.85 mbsf (Fig. **F26A**). In contrast, magnesium concentrations decrease from 52.5 mM at 0.05 mbsf to <45 mM below 30 mbsf (Fig. **F26B**). Sodium and potassium behave conservatively, with average values of 467 ± 15 mM and 11.3 ± 0.7 mM, respectively (Fig. **F26C, F26D**).

Dissolved manganese, iron, barium, boron, lithium, and strontium

Concentrations of dissolved minor elements, analyzed by inductively coupled plasma–atomic emission spectrometry (ICP-AES), are displayed in Figure **F26E–F26I**. Manganese concentrations increase throughout the uppermost 12 m to ~4.6 µM, are fairly constant with depth to ~25 mbsf, and increase again to a maximum of 9.8 µM at 37 mbsf. Dissolved iron concentrations are scattered and low, with no values exceeding 15 µM.

Dissolved barium is below detection limit at all depths. Dissolved lithium concentrations are fairly constant (~21 µM), with some scatter. Dissolved boron concentrations are fairly constant in the uppermost ~30 mbsf and decrease below this depth. Dissolved strontium concentrations slightly increase below 25 mbsf.

Volatile hydrocarbons

Forty-nine headspace samples were taken adjacent to whole rounds. Methane was the only hydrocarbon gas detected, and values are ≤7 ppmv (Fig. F25E).

Sedimentary bulk geochemistry

Forty-nine samples from Holes U1342A and U1342B were analyzed for solid-phase total carbon (TC), total nitrogen (TN), total sulfur (TS), and total inorganic carbon (TIC). From these analyses, total organic carbon (TOC) and calcium carbonate ($CaCO_3$) concentrations were calculated (see **"Geochemistry"** in the "Methods" chapter). $CaCO_3$ concentrations at Site U1342 range from 0.2 to 47.6 wt% (average = 6.5 wt%) (Fig. F27A). TOC concentrations range from 0.03 to 2.19 wt% (average = 0.85 wt%) (Fig. F27B). TN concentrations are 0.01–0.25 wt% (average = 0.11 wt%) (data not shown). TS concentrations are 0.01–1.35 wt% (average = 0.29 wt%) (Fig. F27C). The highest $CaCO_3$ and TOC concentrations were determined for the shallowest sample collected from Hole U1342B at 0.05 mbsf. Low values of $CaCO_3$, TOC, and TS were detected in the deepest sediment of Hole U1342A. A higher sampling resolution in Hole U1342B reveals that the values of each solid-phase constituent fluctuate within narrow depth intervals below ~10 mbsf. The variations of geochemical records were compared with the position of laminated sediment intervals, which were estimated by GRA bulk density in Hole U1342B. The results suggest that TOC and TS are markedly higher in the laminated layers (Fig. F28), in contrast to $CaCO_3$, which is not always high. To consider the formation processes of the laminated sediment in the Bering Sea, these data will provide useful information during shore-based research. Splits of squeeze cakes were also collected and treated for shore-based analyses of bulk elemental composition, iron mineral phases, and iron-monosulfide and pyrite content and sulfur isotope composition.

Microbiology

Samples for community structure and total prokaryotic cell abundance were collected adjacent to interstitial water whole rounds at the resolution described above. Samples were fixed according to the protocol described in **"Microbiology"** in the "Methods" chapter.

Conclusion

Interstitial water sulfate, DIC, phosphate, and ammonium profiles indicate that the sediment at Site U1342 is characterized by low rates of anaerobic carbon mineralization predominantly driven by organoclastic sulfate reduction. Additionally, small increases in manganese concentrations may indicate microbial manganese oxide reduction as an additional mineralization pathway. It is more likely, however, that dissolved manganese is released during the reaction of hydrogen sulfide with Fe/Mn (oxyhydr)oxides.

In contrast to Site U1341, a deeper site on Bowers Ridge, Site U1342 sediments have one order of magnitude lower ammonium concentrations and 50% lower phosphate concentrations. This highlights the extremely low mineralization rates at Site U1342 despite its shallower depth and similar TOC concentrations. The low extent of anaerobic carbon mineralization at this site may be attributed to the extremely low sedimentation rates (see **"Biostratigraphy"**). Very low sedimentation rates prolong the time that organic matter is degraded by oxic respiration and nitrate reduction in the oxic/suboxic sediment zone. This leaves refractory organic material that is inefficiently degraded during anaerobic carbon mineralization (Hulthe et al., 1998). Dissimilar ammonium and phosphate profiles indicate the removal of phosphate from the interstitial water due to the formation of solid-phase phosphate mineral phases rather than different mechanisms of production.

Solid-phase data, however, suggest that present-day interstitial water geochemistry may give limited insight into past conditions. High TOC concentrations that correlate strongly with high TS concentrations in several laminated intervals throughout the sediment column indicate events of high organic carbon input that resulted in high sulfate reduction rates and hence elevated hydrogen sulfide production. This is reflected in high pyrite (TS) concentrations.

Another striking feature at Site U1342 is the inverse relationship of the (almost linear) calcium and magnesium profiles, which indicates the influence of signals linked to the alteration of the underlying basalt on the interstitial water calcium and magnesium concentrations. Both profiles are most likely the result of diffusion between seawater and the relatively shallow basaltic basement. Low-temperature interactions of seawater with the basaltic basement, such as the dissolution of basaltic glass, calcic plagioclase, and olivine, result in the liberation of calcium, whereas the precipitation of smectite leads to the consumption of magnesium (e.g., Gieskes, 1981; Staudigel and Hart, 1983; Thompson, 1983; Lyons et al., 2000).

Physical properties

Site U1342 was spudded at a water depth of ~830 m just south of the summit area of Ulm Plateau, a wave-beveled platform cresting the western end of Bowers Ridge. Seismic reflection data reveal a thin blanket of sediment overlying the ridge's basement framework, which is known from a few dredge hauls and from coring to be constructed of arc igneous rock older than middle or early late Miocene. Recovered cores from Holes U1342A–U1342D were sectioned and placed on the Special Task Multisensor Logger (STMSL) "fast track" to record whole-core magnetic susceptibility and GRA bulk density values. Core sections were allowed to warm to laboratory temperature and were then scanned on the Whole-Round Multisensor Logger (WRMSL) for GRA, magnetic susceptibility, and *P*-wave measurements. Only sediment samples from Hole U1342C were collected to measure moisture and density (MAD) properties with shipboard MAD procedures.

The sediment blanket at Ulm Plateau was sampled in Hole U1342C to ~45 mbsf. At this subsurface depth, basement of dominantly volcaniclastic rock was encountered. In Hole U1342D, basement was cored to a subsediment depth of ~83 m (44–127 mbsf). The top ~18.6 m of basement was drilled without coring, below which 13 XCB cores recovered ~41 m of dominantly volcaniclastic rock.

The sedimentary column was divided into two lithologic units (see **"Lithostratigraphy"**): Unit I (silt and laminated diatom ooze; surface to ~36 mbsf) and Unit II (sponge spicule– and diatom-bearing sand; ~36–45 mbsf).

Magnetic susceptibility

Figure **F29** shows a downhole trend of decreasing magnetic susceptibility, from a near-surface value of ~100 SI units to about half this value at ~35 mbsf, the base of lithologic Unit I. Below this depth, magnetic susceptibility readings in Unit II increase in steps to as high as 350 SI units at 42 mbsf. The depth profile of magnetic susceptibility readings varies somewhat rhythmically between high and low excursions ranging from ~10 to 200 SI units in Unit I and from 50 to 350 SI units in Unit II (Fig. **F29**).

The cyclic fluctuations in Unit I readings presumably record alternating beds of dominantly biogenic and siliciclastic components. The downhole decreasing strength of magnetic susceptibility possibly records accumulating diagenetic degradation of magnetic properties. The higher values of Unit II likely track the downhole-increasing abundance of sandy material derived from the underlying volcanic basement, which a few recovered microfossils suggest was wave-base leveled sometime in the early late Miocene (see **"Biostratigraphy"** and **"Lithostratigraphy"**). In Hole U1342D, at a within-basement depth of ~73–74 mbsf (29–30 m below the sediment/basement contact), magnetic susceptibility values are much higher and average ~1500 SI units. At ~116–117 mbsf (~72–73 m into basement), magnetic susceptibility readings average ~750 SI units.

GRA wet bulk density

The WRMSL GRA data and MAD discrete sample measurements in Figure **F30** show a steady increase in density with depth. The overall increase in density is from 1.35 g/cm^3 near the seafloor to 1.65 g/cm^3 at ~36 mbsf, which is the base of the silt and diatom ooze of Unit I. Below this depth, bulk density increases at a steeper gradient to ~1.90 g/cm^3 just above basement at ~45 mbsf. The steeper gradient is within the sandy sediment of Unit II, which is presumably granular material derived during the final wave-beveling stage of destruction of a stratavolcano that formerly rose above Ulm Plateau. Core inspection implies that the increased density at the base of Unit II is a consequence of higher contents of siliciclastic and rock volcanic debris compared to biogenic components, in particular diatom frustules.

P-wave velocity

P-wave velocity increases downhole from near-seafloor readings of just over 1.45 km/s to ~1.55 km/s in Unit II near the contact with basement rock at ~45 mbsf (Fig. **F31**). In the sandy sediment of Unit II in Hole U1342D, *P*-wave velocity increased to ~1.60 km/s and somewhat higher. Velocity recorded in this unit is at a minimum because of serious drilling disturbance and the in-mixing of water.

Natural gamma radiation

The natural gamma radiation (NGR) readings displayed in Figure **F32** increase irregularly downhole from a near-seafloor average of ~18 counts/s to ~24 counts/s at the base of Unit I. The gradient of increasing values steepens within the sandy beds of Unit II to reach ~40 counts/s just above basement contact at ~44 mbsf. The elevated NGR readings presumably record a downsection increase in clay minerals that may be derived within Unit II from the underlying bedrock of arc lava and volcaniclastic deposits. Rock clasts recovered in core sections exhibit evidence of oxidation. Clay minerals that account for the higher NGR readings in the basal sediment of Unit II presumably reflect subaerial weathering of the stratavolcano that towered above Ulm Plateau prior to its presumed early late Miocene destruction. At ~72–73 m into basement (~116–117 mbsf) in Hole U1342D, NGR readings are quite low, ranging from ~1 to 6 counts/s, but the cored volcaniclastic sandstone and breccia are commonly oxidized and red in color.

MAD (discrete sample) wet bulk density

MAD physical properties of wet and dry bulk density, moisture content, porosity, and grain density were measured on sediment samples (~10 cm^3) taken from the working halves of split core sections. The samples were routinely collected from Sections 2, 4, and 6 of Hole U1342C cores (Table **T14**). The measured values of wet bulk density are shown in Figure **F30** as open circles plotted with WRMSL GRA bulk density. In general, MAD values track those of GRA but with much greater measurement spacing. The contrast between Unit I and denser Unit II sediments is nevertheless clearly shown by the MAD data.

MAD porosity and water content

As shown in Figure **F33,** sediment porosity and water or moisture content track in parallel, decreasing downhole. The near-surface porosity is ~80%, but porosity decreases to ~55% in the sandy sediment of Unit II and just above basement at 44 mbsf. The downhole trend of overall decreasing porosity and water content presumably reflects compaction of the section, with notable excursions to higher values in the basal 10–12 m of Unit I that may identify higher relative content of siliceous microfossils.

Grain density

Grain density decreases downsection in Unit I from ~2.82 to 2.53 g/cm^3 and possibly lower (Fig. **F34**). Grain density in underlying Unit II (siliceous microfossil–bearing sand) rapidly increases downhole to ~2.70 g/cm^3 as bedrock is approached. The elevated grain density in Unit I, as compared to the upper beds of Site U1341 on the deeper flank of Bowers Ridge, can be attributed to the availability of nearby bedrock sources for Site U1342 deposits. Seafloor exposures of probably pre-Miocene volcaniclastic and lava units or their occurrence in the shallow subcrop most likely occur on the summit area of Ulm Plateau, located ~10 km northwest of Site U1342. The rapid excursion near the base of Unit I to a low density of just over 2.2 g/cm^3 is probably a spurious measurement.

Stratigraphic correlation

The composite depth scale and splice at Site U1342 is complete and continuous from 0.0 to 46.54 m CCSF-A (as defined in **"Stratigraphic correlation"** in the "Methods" chapter). The splice ranges from the mudline at the top of Core 323-U1342D-1H to the bottom of Section 323-U1342D-5H-7 (Tables **T15, T16**). Sediment cores below the splice (Cores 323-U1342A-6H and 7H) are included in the composite depth framework by appending them with a constant affine value of 2.78 m. Core 323-U1342A-8D is a drilled interval with no recovery; Core 323-U1342A-9X recovered hard rock and is not included in the composite depth framework, nor are drilled interval 323-U1342D-6D and Cores 323-U1342D-7X through 19X, which had partial recovery of lithified sediments and volcanic rocks.

Correlations were accomplished using IODP Correlator software (version 1.656), and some intervals were checked with digital line-scan images with Correlyzer (version 1.3.3).

The composite (CCSF-A) and splice (CCSF-D) depth scales are based primarily on the stratigraphic correlation of WRMSL magnetic susceptibility data (Fig. **F35**), augmented with WRMSL GRA bulk density (Fig. **F36**) and NGR data (Fig. **F37**). Color reflectance data were also examined; the b* parameter was useful for correlation (Fig. **F38**), but the L* and a* parameters did not appear to correlate between holes (data not shown). GRA data from both the STMSL and WRMSL were calibrated prior to analyzing cores for each hole.

Construction of the CCSF-A and CCSF-D scales assumed that the uppermost sediment (the mudline) in Core 323-U1342A-1H was the sediment/water interface. A mudline was also recovered in Cores 323-U1342A-1H, 323-U1342B-1H, and 323-U1342C-1H, which confirmed the fidelity of the top of the recovered section. Core 323-U1342A-1H serves as the anchor in the composite depth scale and is the only core with depths that are the same on the mbsf and CCSF-A scales. However, because Core 323-U1342A-1H is a short core, we chose to start the splice with the longer Core 323-U1342D-1H, whose top starts at 0.03 mbsf. From this core we worked downhole, correlating the variations in core logging data on a core-by-core basis using Correlator. Hole U1342B was assigned affine values based on comparison of its STMSL GRA and magnetic susceptibility data to the WRMSL GRA and magnetic susceptibility data from other holes; however, Hole U1342B was largely consumed by microbiology studies, so it was excluded from the splice. All affine values that define the composite depth scale and all splice tie points are robust and well defined at Site U1342. The resulting spliced records of magnetic susceptibility, GRA bulk density, and NGR are illustrated in Figure **F39.**

Within the splice, the composite CCSF-A depth scale is defined as the CCSF-D depth scale. Note that CCSF-D rigorously applies only to the spliced interval. Intervals outside the splice, although available with CCSF-A composite depth assignments, should not be expected to correlate precisely with fine-scale details within the splice or with other holes because of normal variation in the relative spacing of features in different holes. Such apparent depth differences may reflect coring artifacts or fine-scale variations in sediment accumulation and preservation at and below the seafloor.

The cumulative offset between mbsf and CCSF-A depth scales is approximately linear (Fig. F40). The affine growth factor (a measure of the fractional stretching of the composite section relative to the drilled interval; see "Stratigraphic correlation" in the "Methods" chapter) at Site U1342 is 1.06 between 0 and 44.0 mbsf. Calculation of mass accumulation rates (MARs) based on the CCSF-A or CCSF-D scales should account for this affine growth factor by dividing apparent depth intervals by the appropriate growth factor. After it is divided by the growth factor (accounting for the different depth intervals), this scaled depth scale should be referred to as CCSF-B.

Downhole measurements

The only downhole measurements made at Site U1342 were two deployments of the third-generation advanced piston corer temperature tool (APCT-3) in Hole U1342C. The measured temperature was 4.46°C at 26.2 m DSF and 5.32°C at 35.0 m DSF (Table T17). These two measurements suggest a local geothermal gradient of 97.7°C/km (Fig. F41). A simple estimate of the heat flow can be obtained from the product of the geothermal gradient by the average thermal conductivity (0.991 W/[m·K]; see "Physical properties"), which gives a value of 96.9 mW/m^2, significantly higher than existing measurement in the area (the global heat flow database of the International Heat Flow Commission can be found at www.heatflow.und.edu/index.html).

Considering the variations in thermal conductivity with depth, a more accurate measure of the heat flow in a conductive regime can be given by a "Bullard plot." The thermal resistance of an interval is calculated by integrating the inverse of thermal conductivity over depth. If the thermal regime is purely conductive, the heat flow will be the slope of the temperature versus thermal resistance profiles (Bullard, 1939). The thermal resistance calculated over the intervals overlying the APCT-3 measurements is shown in Table T17, and the resulting linear fit of the temperature to the thermal resistance gives a heat flow value of 80.9 mW/m^2, which is closer to the other measurements in the Bowers Ridge area (Fig. F42).

References

Asahi, H., and Takahashi, K., 2007. A 9-year time-series of planktonic foraminifer fluxes and environmental change in the Bering Sea and the central subarctic Pacific Ocean, 1990–1999. *Prog. Oceanogr.,* 72(4):343–363. doi:10.1016/j.pocean.2006.03.021

Baldauf, J.G., and Barron, J.A., 1980. *Actinocyclus ingens* var. *nodus:* a new stratigraphically useful diatom of the circum-North Pacific. *Micropaleontology,* 26:103–110. doi:10.2307/1485279

Barron, J.A., and Gladenkov, A.Y., 1995. Early Miocene to Pleistocene diatom stratigraphy of Leg 145. *In* Rea, D.K., Basov, I.A., Scholl, D.W., and Allan, J.F. (Eds.), *Proc. ODP, Sci. Results,* 145: College Station, TX (Ocean Drilling Program), 3–19. doi:10.2973/odp.proc.sr.145.101.1995

Bubenshchikova, N., Nürnberg, D., Lembke-Jene, L., and Pavlova, G., 2008. Living benthic foraminifera of the Okhotsk Sea: faunal composition, standing stocks and microhabitats. *Mar. Micropaleontol.,* 69(3–4):314–333. doi:10.1016/j.marmicro.2008.09.002

Bullard, E.C., 1939. Heat flow in South Africa. *Proc. R. Soc. London, Ser. A,* 173:474–502.

Gieskes, J.M., 1981. Deep-sea drilling interstitial water studies: implications for chemical alteration of the oceanic crust, Layers I and II. *In* Warme, J.E., Douglas, R.G., and Winterer, E.L. (Eds.), *The Deep Sea Drilling Project: A Decade of Progress*. Spec. Publ.—Soc. Econ. Paleontol. Mineral., 32:149–167.

Hulthe, G., Hulth, S., and Hall, P.O.J., 1998. Effect of oxygen on degradation rate of refractory and labile organic matter in continental margin sediments. *Geochim. Cosmochim. Acta,* 62(8):1319–1328. doi:10.1016/S0016-7037(98)00044-1

Kaiho, K., 1994. Benthic foraminiferal dissolved-oxygen index and dissolved-oxygen levels in the modern ocean. *Geology,* 22(8):719–722. doi:10.1130/0091-7613(1994)022<0719:BFDOIA>2.3.CO;2

Kamikuri, S., Nishi, H., and Motoyama, I., 2007. Effects of late Neogene climatic cooling on North Pacific radiolarian assemblages and oceanographic conditions. *Palaeogeogr., Palaeoclimatol., Palaeoecol.,* 249(3–4):370–392. doi:10.1016/j.palaeo.2007.02.008

Katsuki, K., and Takahashi, K., 2005. Diatoms as paleoenvironmental proxies for seasonal productivity, sea-ice and surface circulation in the Bering Sea during the late Quaternary. *Deep-Sea Res., Part II,* 52(16–18):2110–2130. doi:10.1016/j.dsr2.2005.07.001

Lisiecki, L.E., and Raymo, M.E., 2005. A Pliocene–Pleistocene stack of 57 globally distributed benthic $\delta^{18}O$ records. *Paleoceanography,* 20(1):PA1003. doi:10.1029/2004PA001071

Lyons, T.W., Murray, R.W., and Pearson, D.G., 2000. A comparative study of diagenetic pathways in sediments of the Caribbean Sea: highlights from pore-water results. *In* Leckie, R.M., Sigurdsson, H., Acton, G.D., and Draper, G. (Eds.), *Proc. ODP, Sci. Results,* 165: College

Station, TX (Ocean Drilling Program), 287–298. doi:10.2973/odp.proc.sr.165.020.2000

Martini, E., 1971. Standard Tertiary and Quaternary calcareous nannoplankton zonation. *In* Farinacci, A. (Ed.), *Proc. 2nd Int. Conf. Planktonic Microfossils Roma:* Rome (Ed. Tecnosci.), 2:739–785.

Okazaki, Y., Takahashi, K., Asahi, H., Katsuki, K., Hori, J., Yasuda, H., Sagawa, Y., and Tokuyama, H., 2005. Productivity changes in the Bering Sea during the late Quaternary. *Deep-Sea Res., Part II,* 52(16–18):2150–2162. doi:10.1016/j.dsr2.2005.07.003

Reynolds, L., and Thunell, R.C., 1985. Seasonal succession of planktonic foraminifera in the subpolar North Pacific. *J. Foraminiferal Res.,* 15(4):282–301. doi:10.2113/gsjfr.15.4.282

Staudigel, H., and Hart, S.R., 1983. Alteration of basaltic glass: mechanisms and significance for the oceanic crust-seawater budget. *Geochim. Cosmochim. Acta,* 47(3):337–350. doi:10.1016/0016-7037(83)90257-0

Takahashi, K., 2005. The Bering Sea and paleoceanography. *Deep-Sea Res., Part II,* 52(16–18):2080–2091. doi:10.1016/j.dsr2.2005.08.003

Takahashi, K., Fujitani, N., Yanada, M., and Maita, Y., 2000. Long-term biogenic particle fluxes in the Bering Sea and the central subarctic Pacific Ocean, 1990–1995. *Deep-Sea Res., Part I,* 47(9):1723–1759. doi:10.1016/S0967-0637(00)00002-9

Takahashi, K., Ravelo, A.C., and Alvarez Zarikian, C.A., 2009. Pliocene–Pleistocene paleoceanography and climate history of the Bering Sea. *IODP Sci. Prosp.,* 323. doi:10.2204/iodp.sp.323.2009

Thompson, G., 1983. Basalt-seawater interaction. *In* Rona, P.A., Boström, K., Laubier, L., and Smith, K.L., Jr. (Eds.), *Hydrothermal Processes at Seafloor Spreading Centers:* New York (Plenum), 225–278.

Yanagisawa, Y., and Akiba, F., 1998. Refined Neogene diatom biostratigraphy for the northwest Pacific around Japan, with an introduction of code numbers for selected diatom biohorizons. *Chishitsugaku Zasshi,* 104:395–414.

Publication: 15 March 2011
MS 323-106

Figure F1. Location map for Site U1342 on Bowers Ridge. DSDP = Deep Sea Drilling Project.

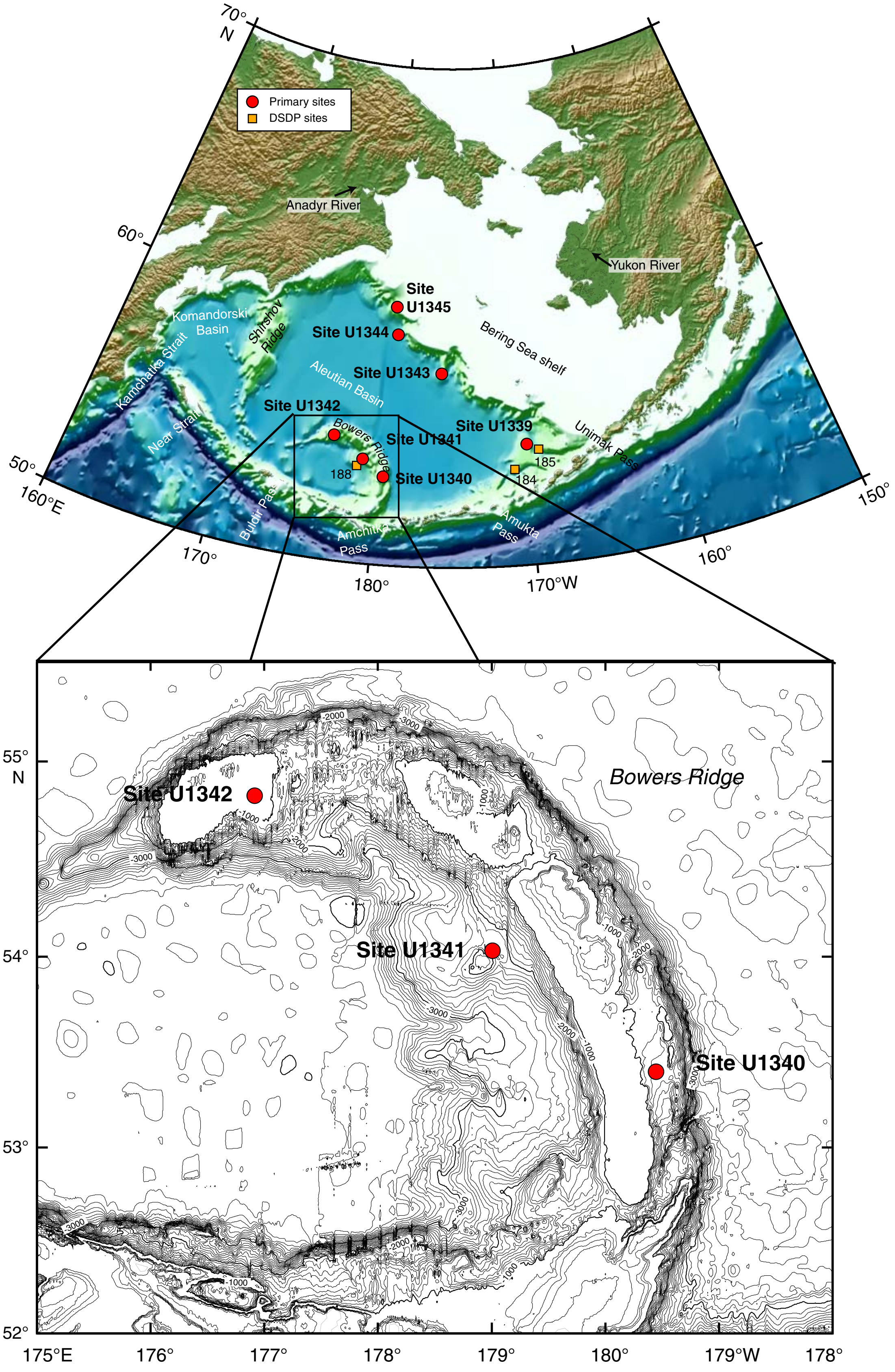

Figure F2. Seismic profile of *Hakuhou-Maru* Cruise KH99-3 Line Stk4-1 (north–south) near Site U1342.

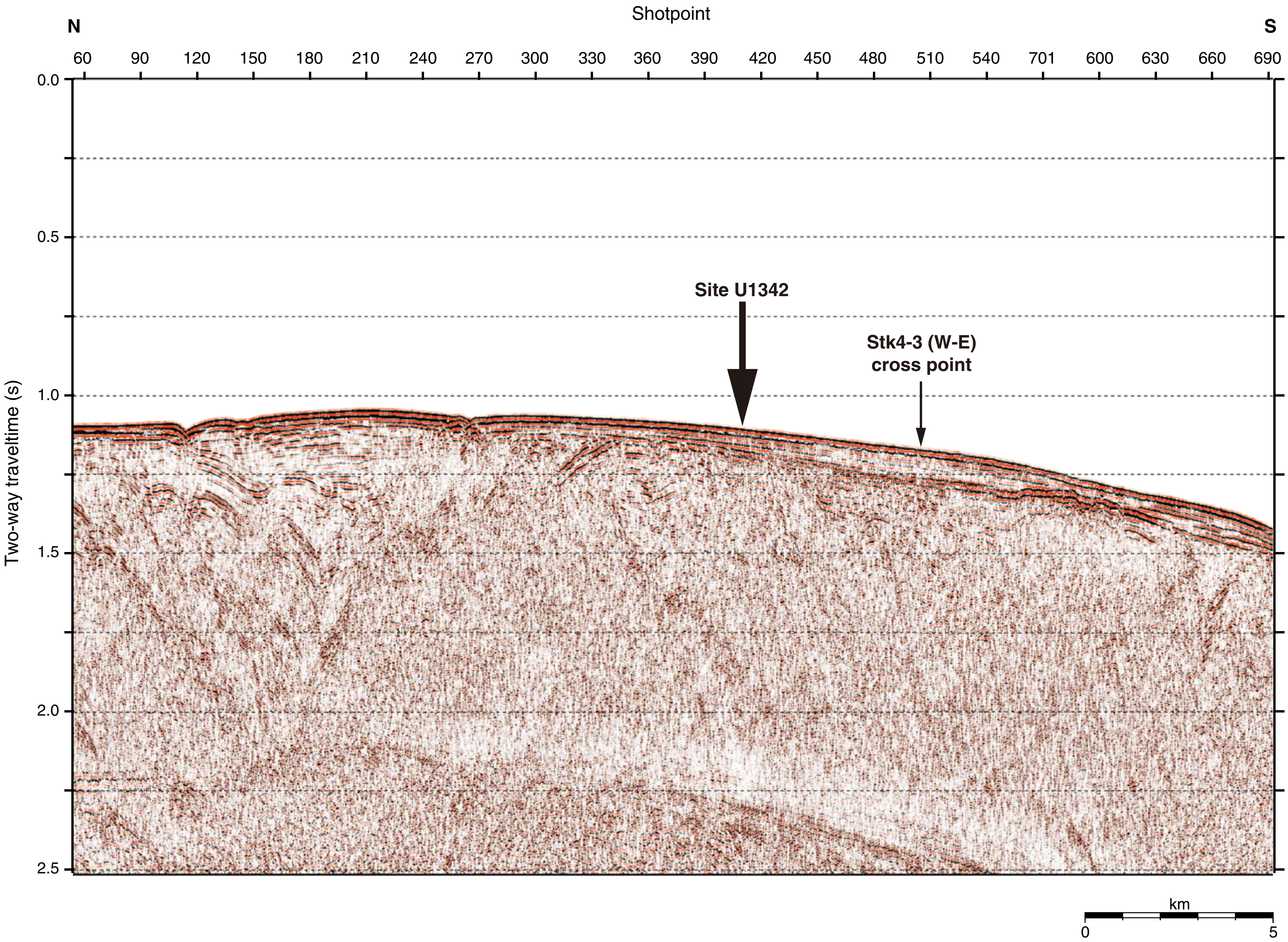

Figure F3. Navigation map of *Hakuhou-Maru* Cruise KH99-3 around Site U1342 for close-up seismic profiles found in Figures **F4** and **F5.**

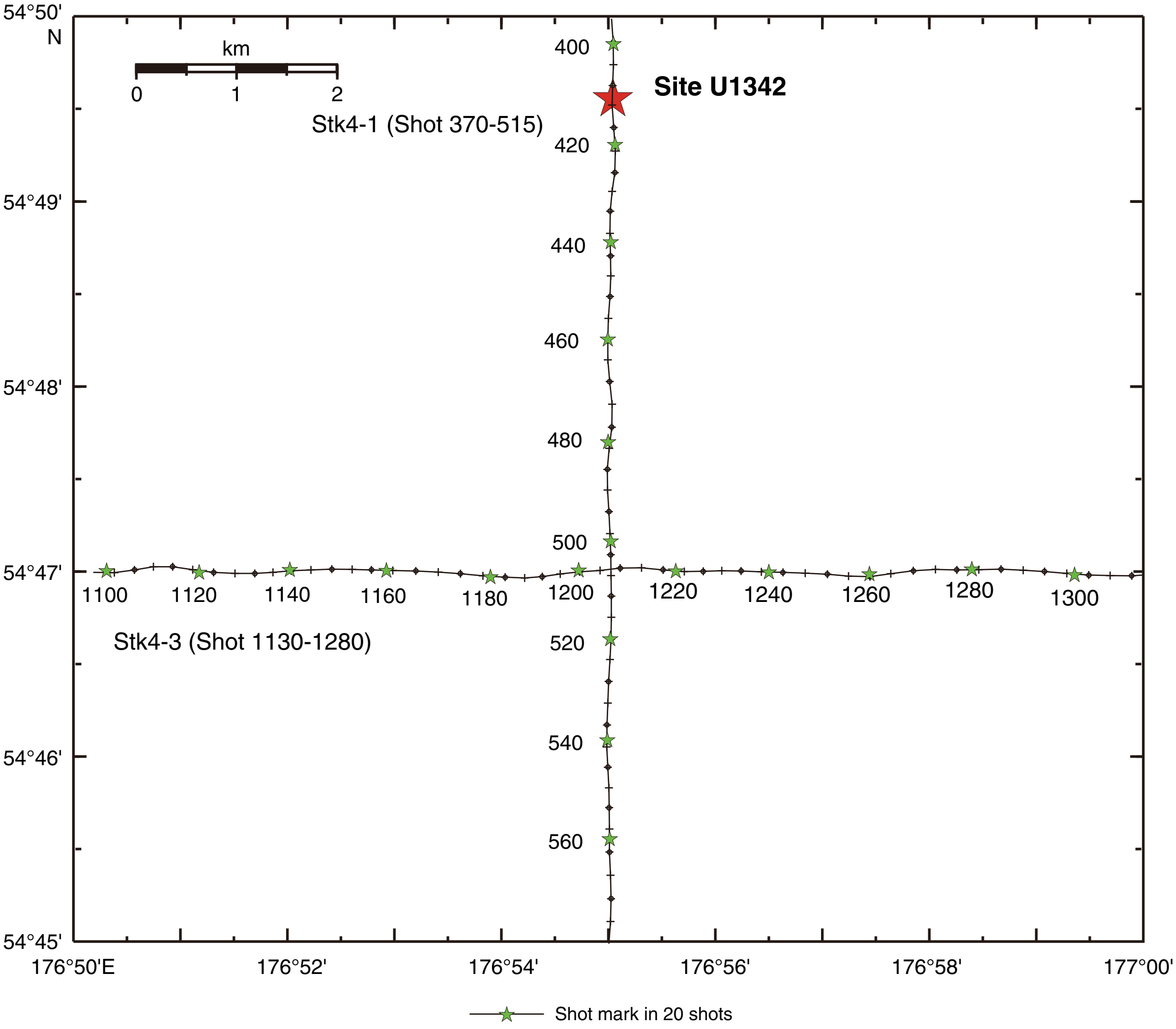

Figure F4. A. Close-up seismic profile of *Hakuhou-Maru* Cruise KH99-3 Line Stk4-3 (west–east) near Site U1342. Cross point with Line Stk4-1 (north–south) is at Shotpoint 1203. **B.** Time-depth curve estimated from results of velocity analyses on Lines Stk4-1 and Stk4-3.

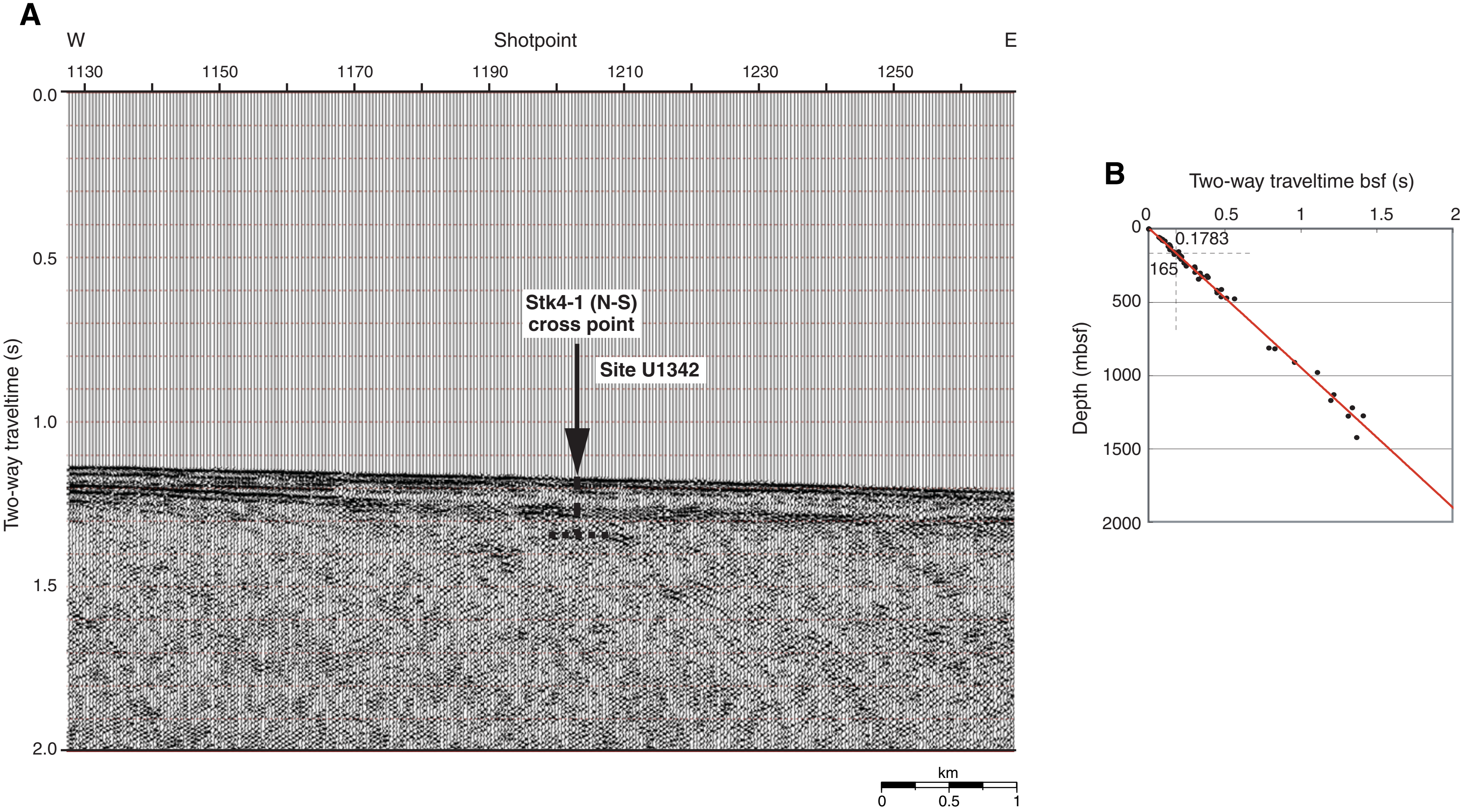

Figure F5. A. Close-up seismic profile of *Hakuhou-Maru* Cruise KH99-3 Line Stk4-1 (north–south) near Site U1342. Cross point with Line Stk4-3 (west–east) is at Shotpoint 505. **B.** Time-depth curve estimated from results of velocity analyses on Lines Stk4-1 and Stk4-3.

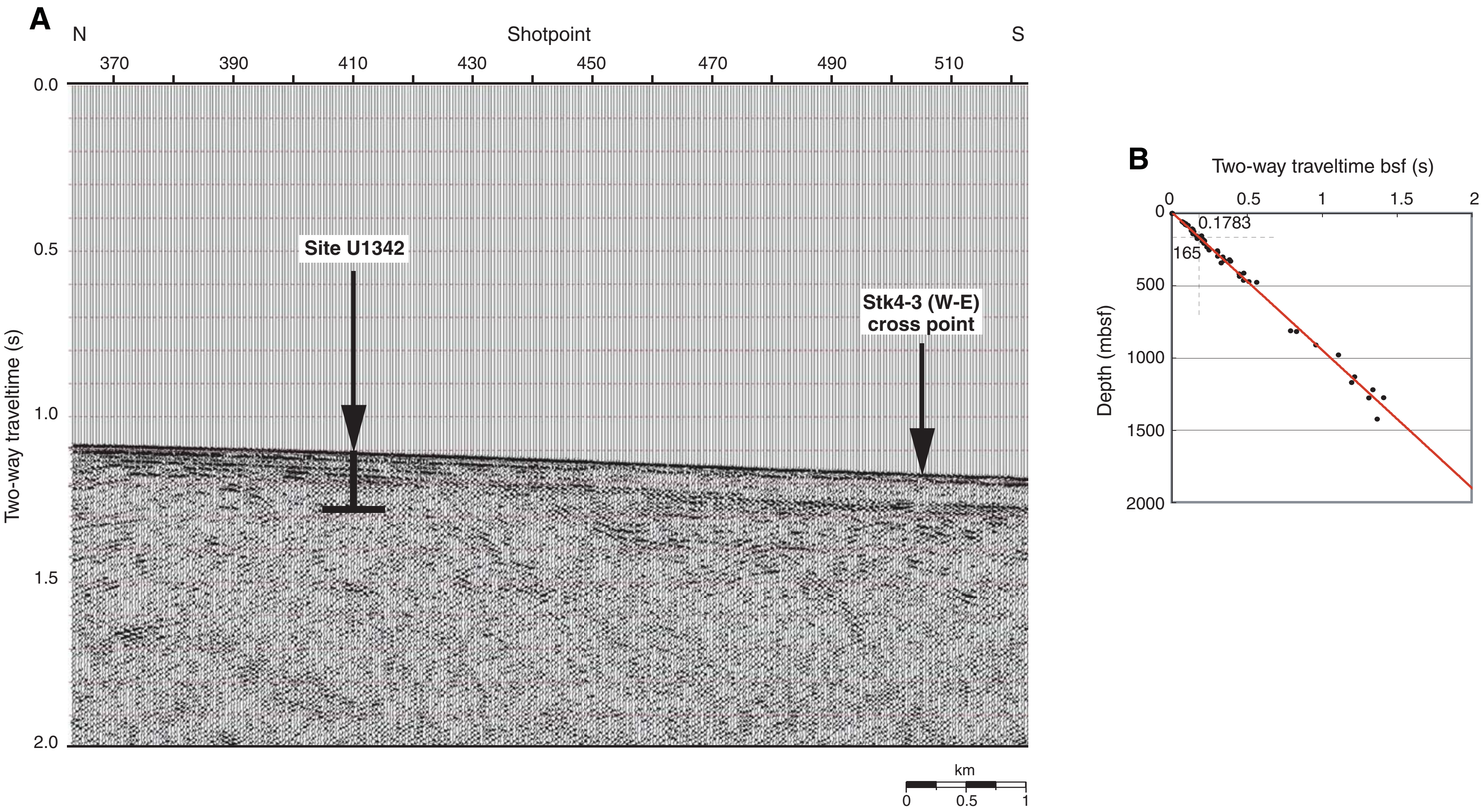

Figure F6. Summary of lithology, structures, accessories, microfossils, and physical properties, Hole U1342A. See legend in Figure F6 in the "Methods" chapter. Soft-sed = soft-sediment, auth = authigenic, calc = calcareous, NGR = natural gamma radiation, GRA = gamma ray attenuation, sed rate = sedimentation rate.

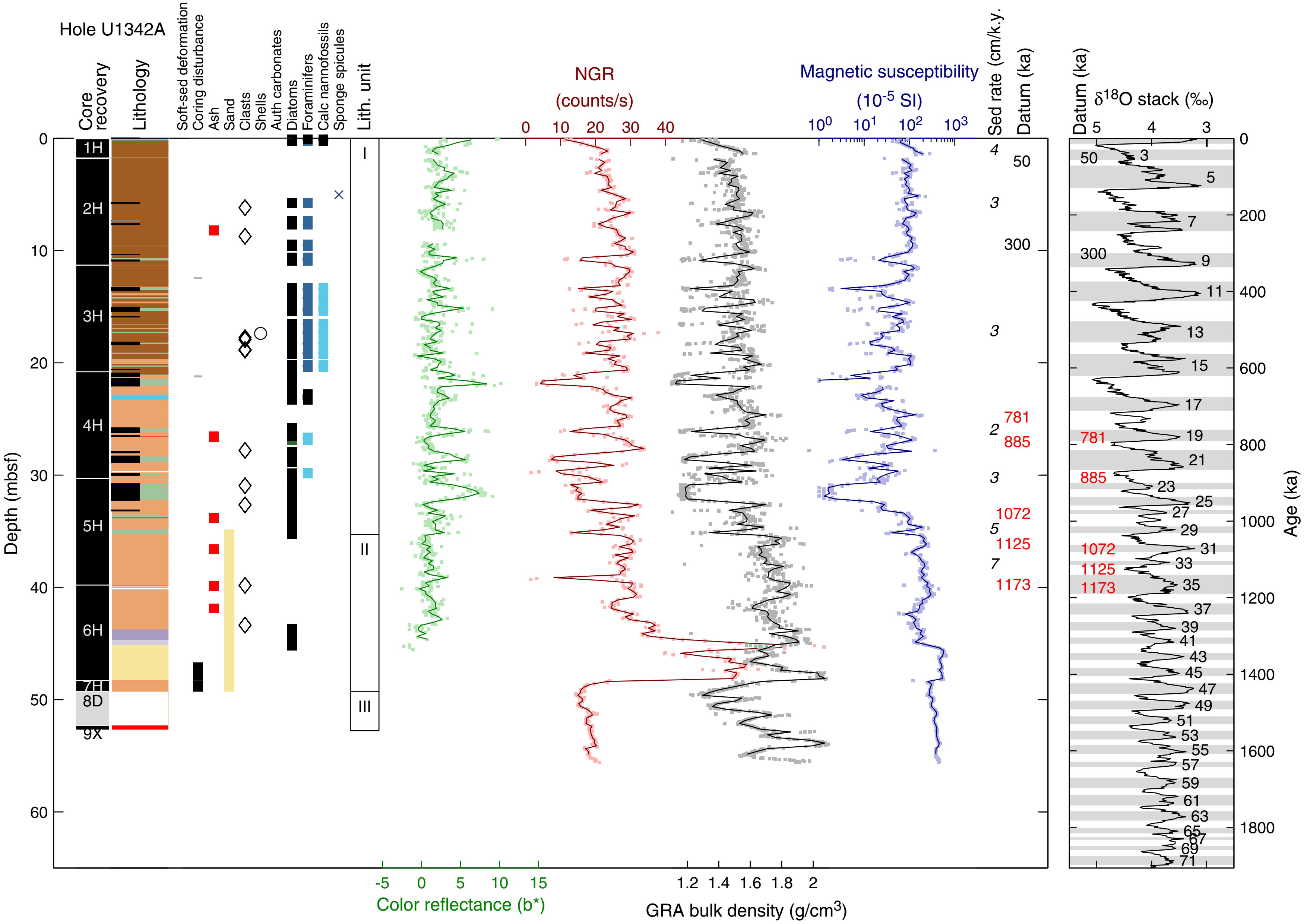

Figure F7. Summary of lithology, structures, accessories, microfossils, and physical properties, Hole U1342C. See legend in Figure F6 in the "Methods" chapter. Soft-sed = soft-sediment, auth = authigenic, calc = calcareous, NGR = natural gamma radiation, GRA = gamma ray attenuation, sed rate = sedimentation rate.

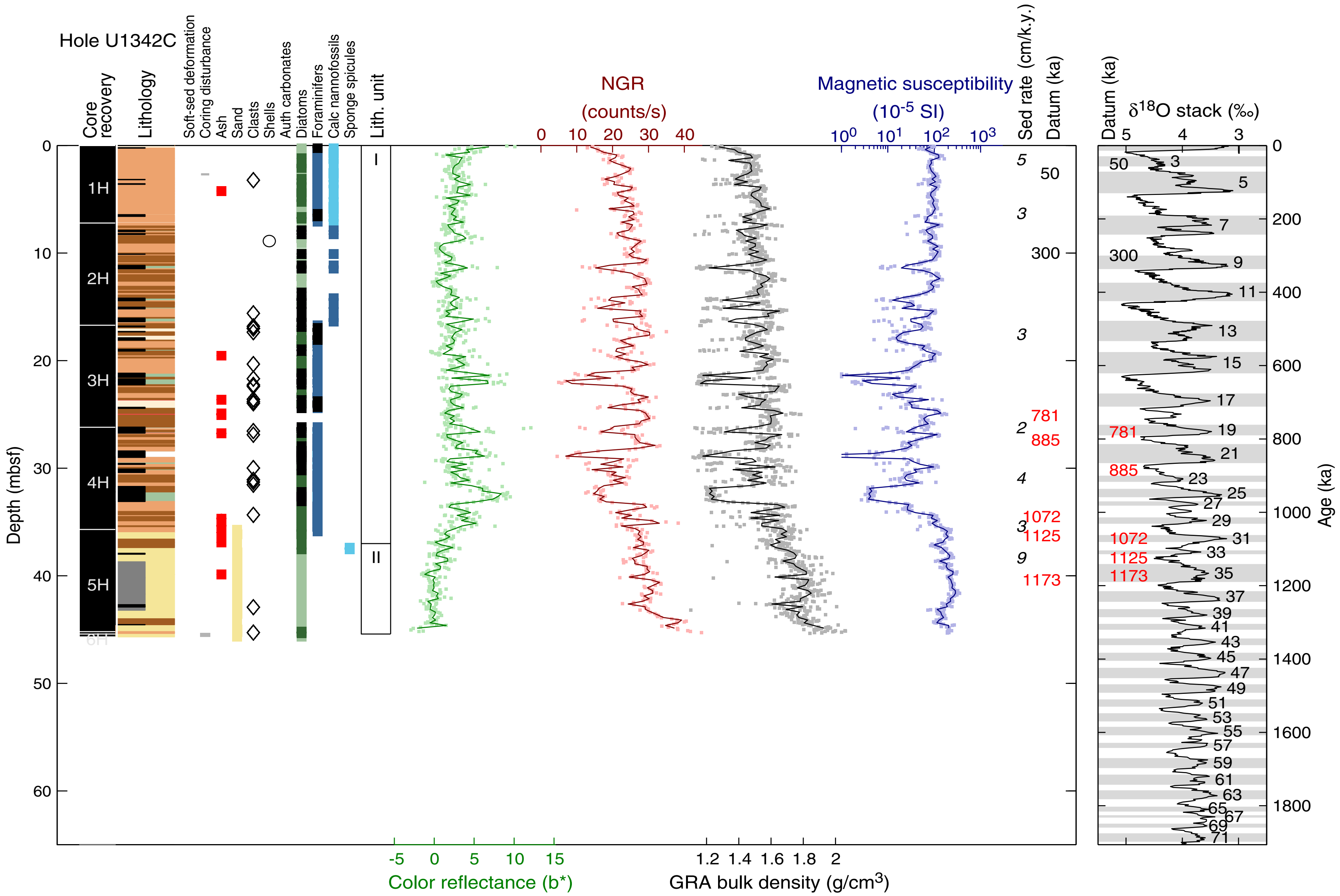

Figure F8. Summary of lithology, structures, accessories, microfossils, and physical properties, Hole U1342D. See legend in Figure F6 in the "Methods" chapter. Soft-sed = soft-sediment, auth = authigenic, calc = calcareous, NGR = natural gamma radiation, GRA = gamma ray attenuation, sed rate = sedimentation rate. **A.** 0–65 mbsf. (**Continued on next page.**)

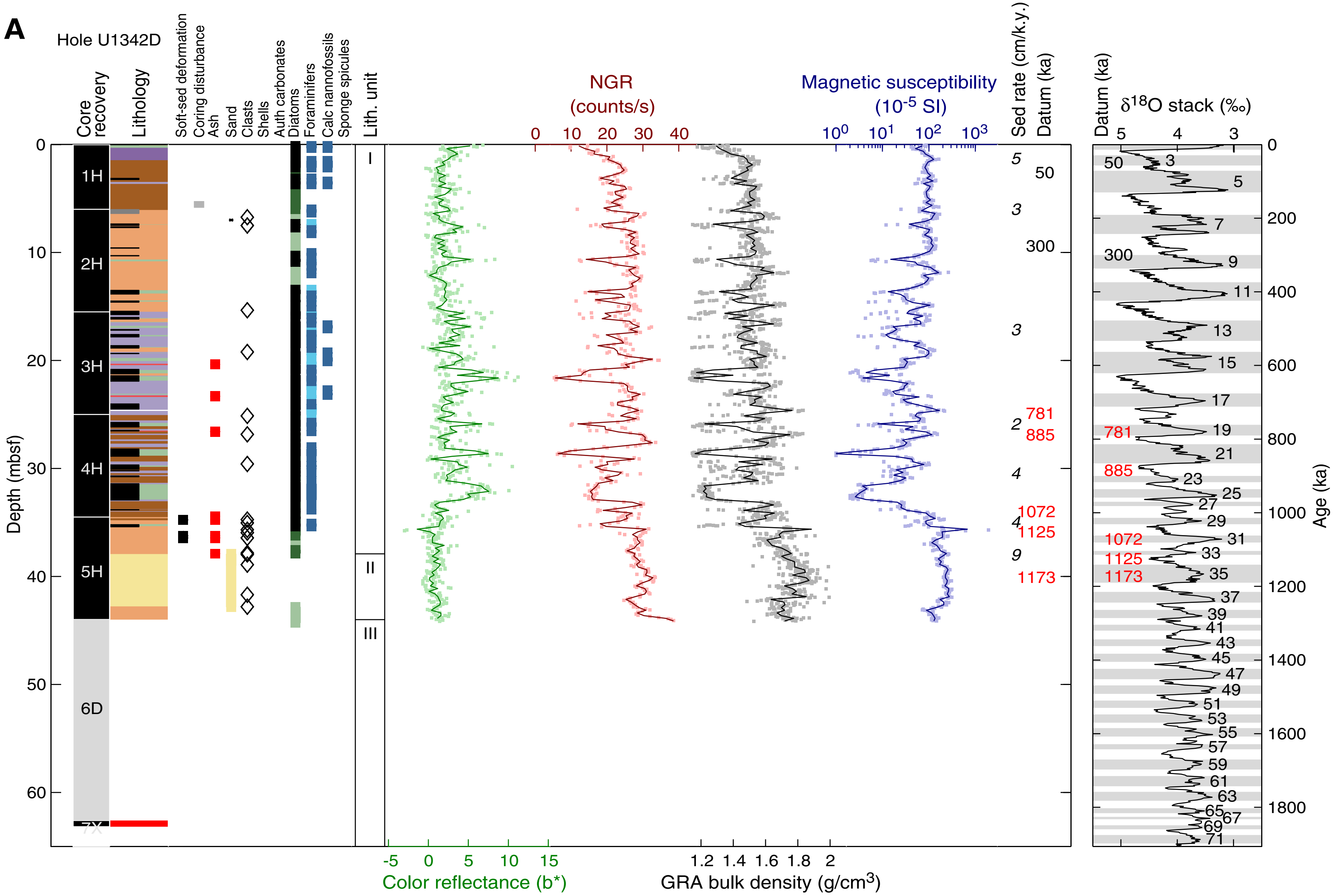

Figure F8 (continued). B. 65–130 mbsf.

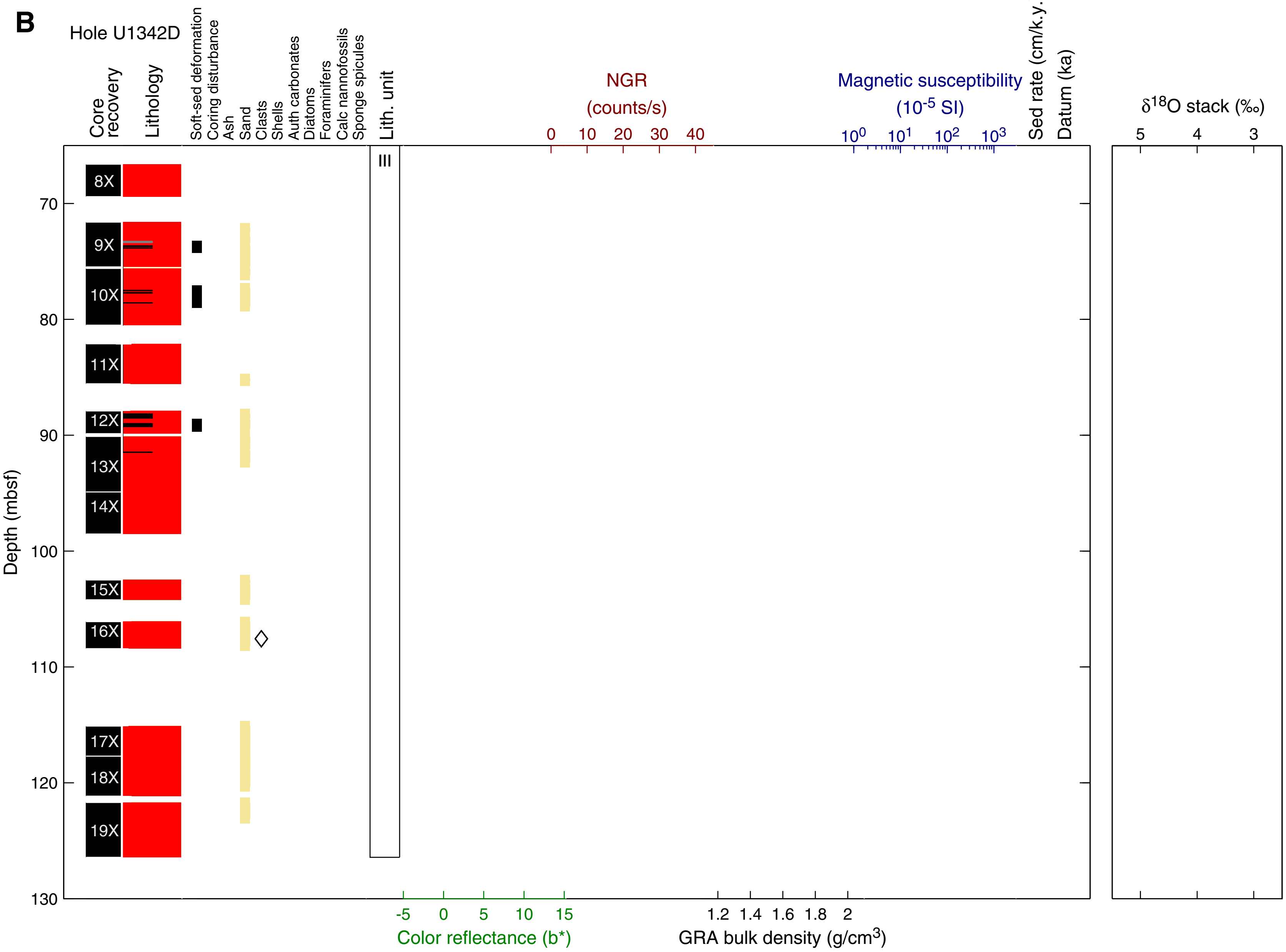

Figure F9. Correlation of laminated sediments, Holes U1342A, U1342C, and U1342D. The lithologic columns are from Figures F6, F7, and F8. Note that the depth of each laminated interval is converted into CCSF-A (m). Age estimates are determined by radiolarians (R), calcareous nannofossils (C), silicoflagellates (S), or paleomagnetism (P). Triangles = lamination depth in Hole U1342A, diamonds = lamination depth in Hole U1342C, circles = lamination depth in Hole U1342D. Green lines connect correlated laminations between holes. Benthic $\delta^{18}O$ stack is from Lisiecki and Raymo (2005).

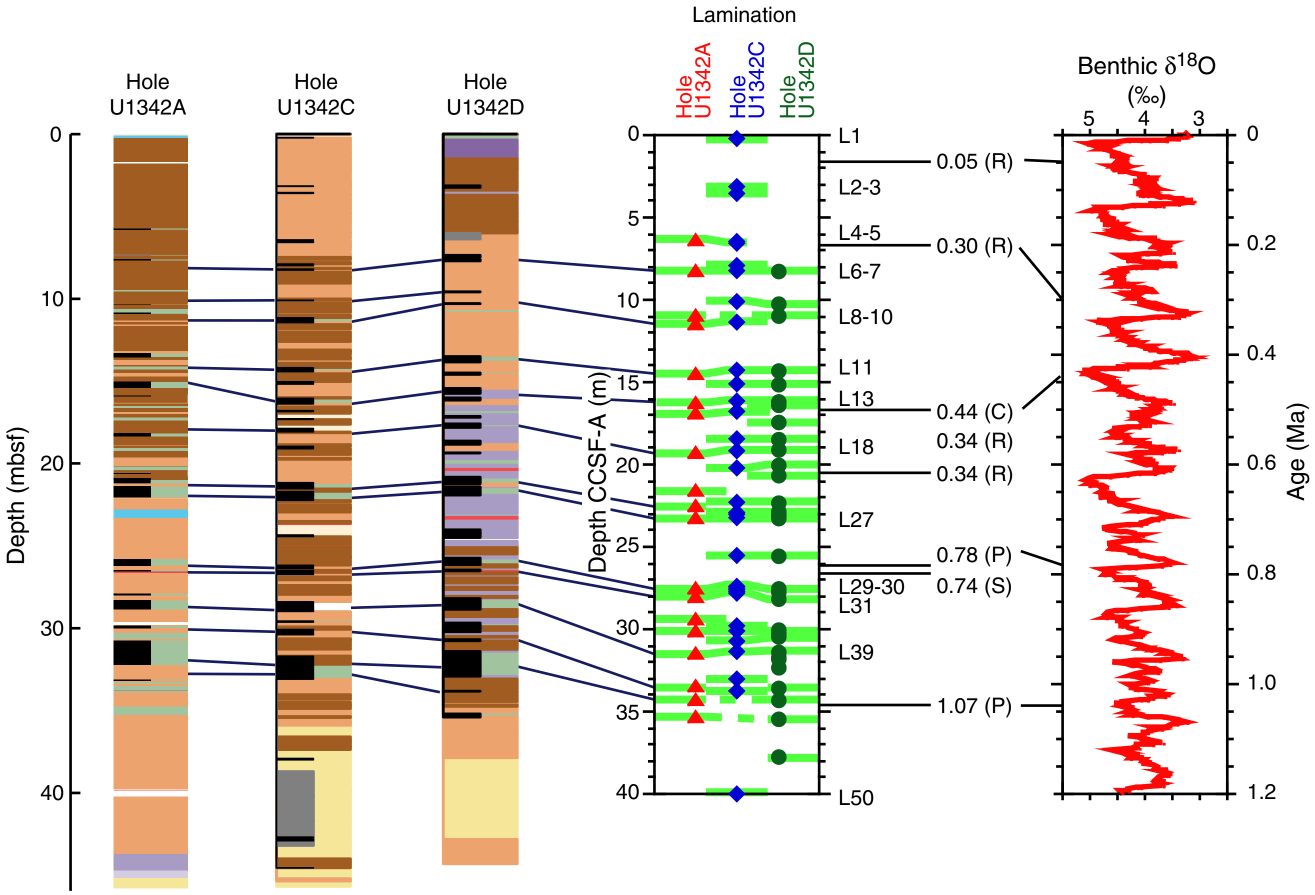

Figure F10. Core photographs of a laminated interval correlated between Holes U1342A, U1342C, and U1342D. **A.** Bioturbated diatom ooze (interval 323-U1342A-3H-2, 111–123 cm). **B.** Well-preserved laminated interval (323-U1342C-2H-7, 1–21 cm). **C.** Laminated interval (323-U1342D-3H-6, 31–43 cm).

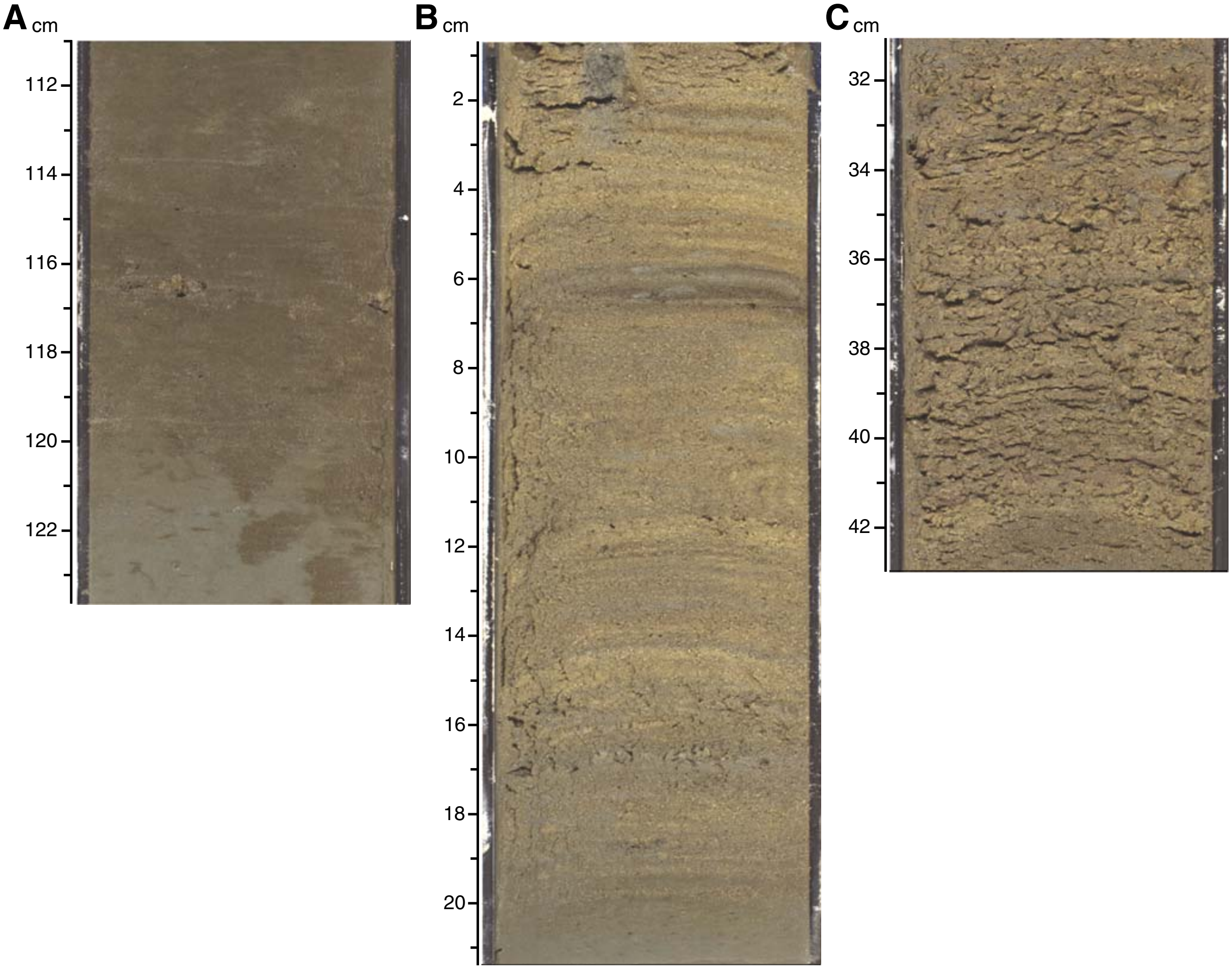

Figure F11. Sandy lithology in Unit II. **A.** Line-scan image (interval 323-U1342A-5H-4, 43–64 cm). **B.** Photomicrograph of grain mount from Section 323-U1342A-6H-6, 60 cm, under plane-polarized (above) and cross-polarized (below) light. The glauconite is the green grain in the center of the field of view.

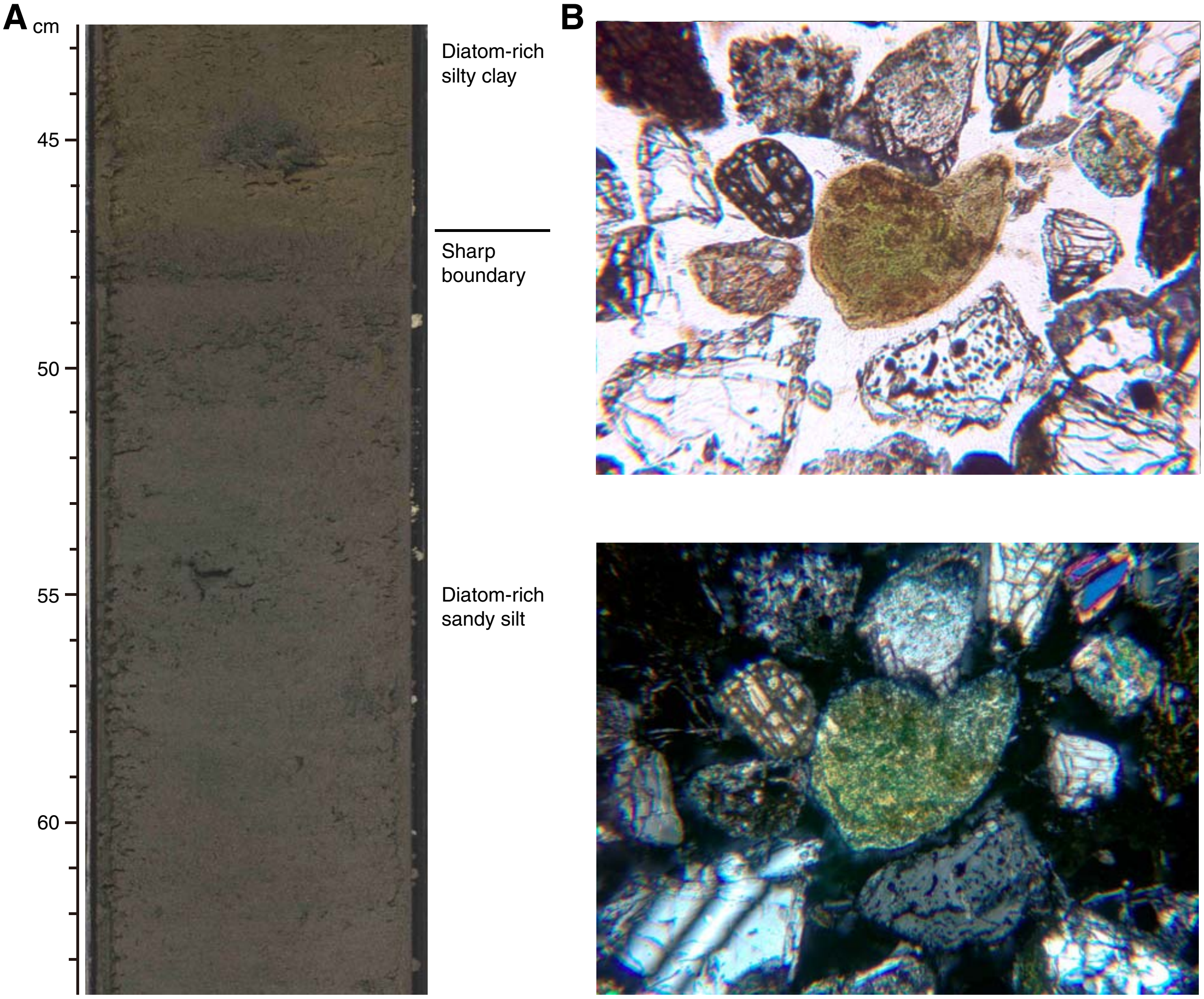

Figure F12. Igneous rock and volcanic sandstone in Unit III. **A.** Line-scan image of interval 323-U1342D-7X-1, 21–31. **B.** Thin section photomicrograph of igneous rock from Section 323-U1342D-7X-1. **C.** Line-scan image of interval 323-U1342D-8X-1, 63–74 cm. **D.** Thin section photomicrograph of volcanic sandstone from Section 323-U1342D-8X-1.

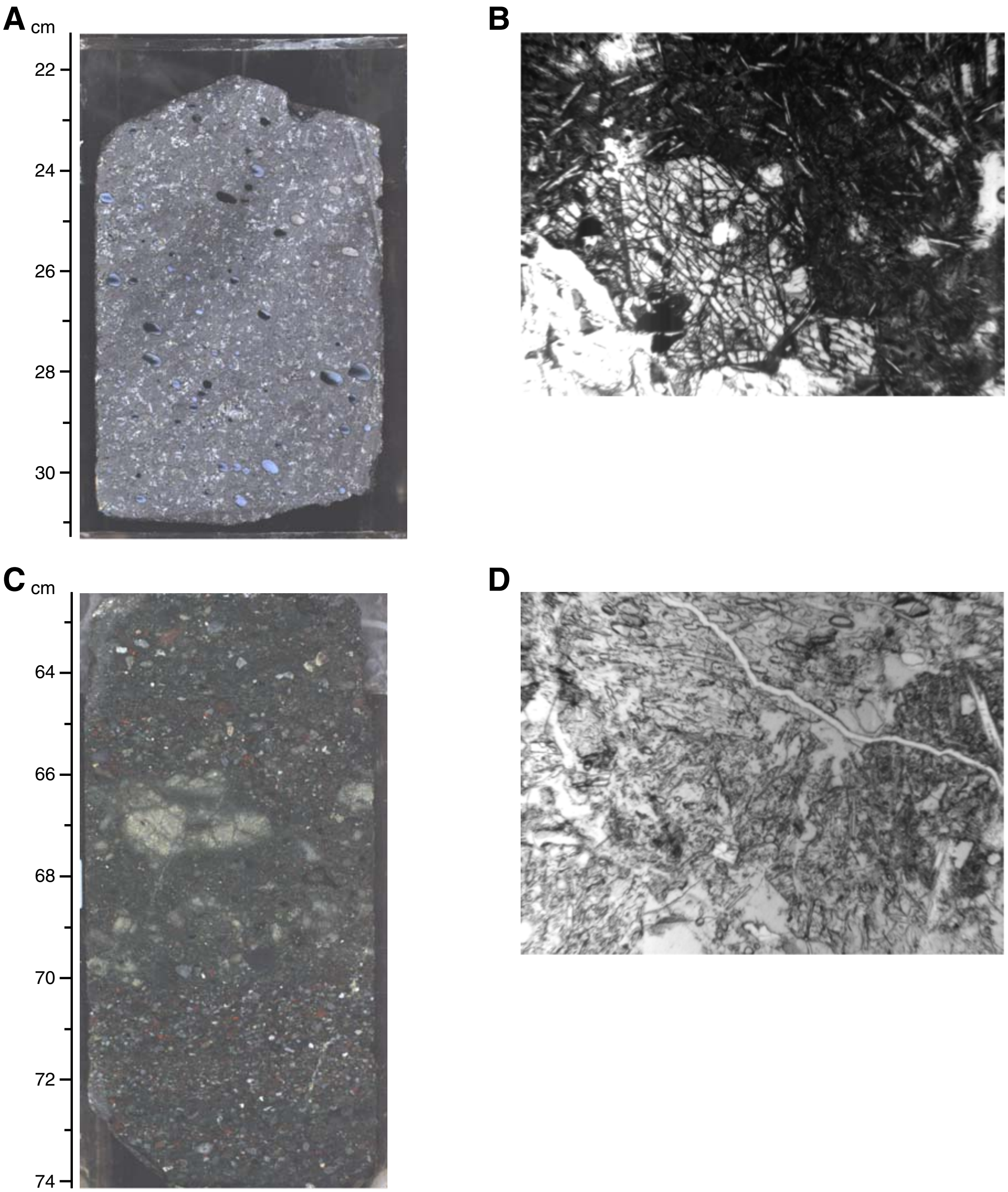

Figure F13. Core photographs of examples of (**A**) soft-sediment deformation in interval 323-U1342D-12X-2, 49–60 cm, and (**B**) a normal fault in interval 323-U1342D-12X-2, 5–26 cm.

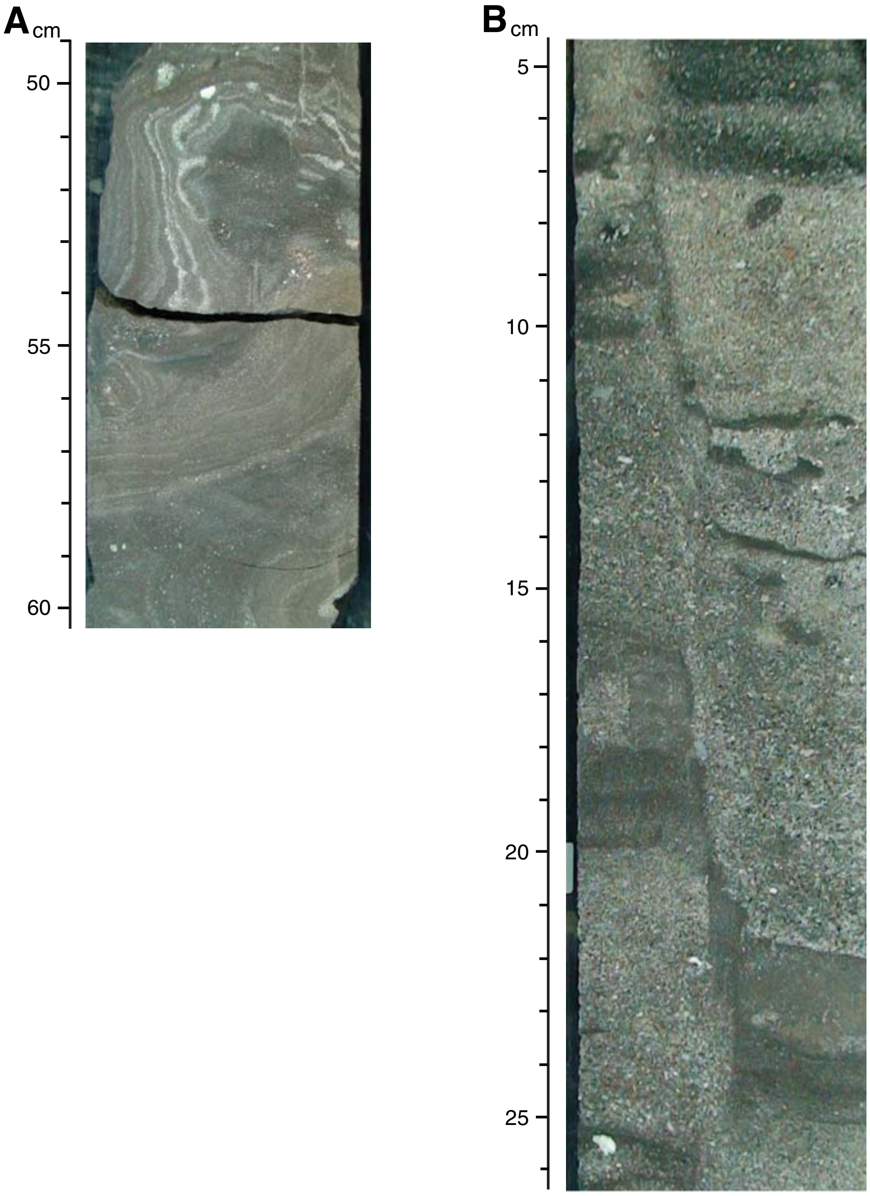

Figure F14. Comparison of laminated interval locations and color reflectance parameters L* and b*, Hole U1342A. Age estimates are determined by radiolarians (R), calcareous nannofossils (C), silicoflagellates (S), or paleomagnetism (P). Calc = calcareous. Gray triangles indicate range of biostratigraphic error.

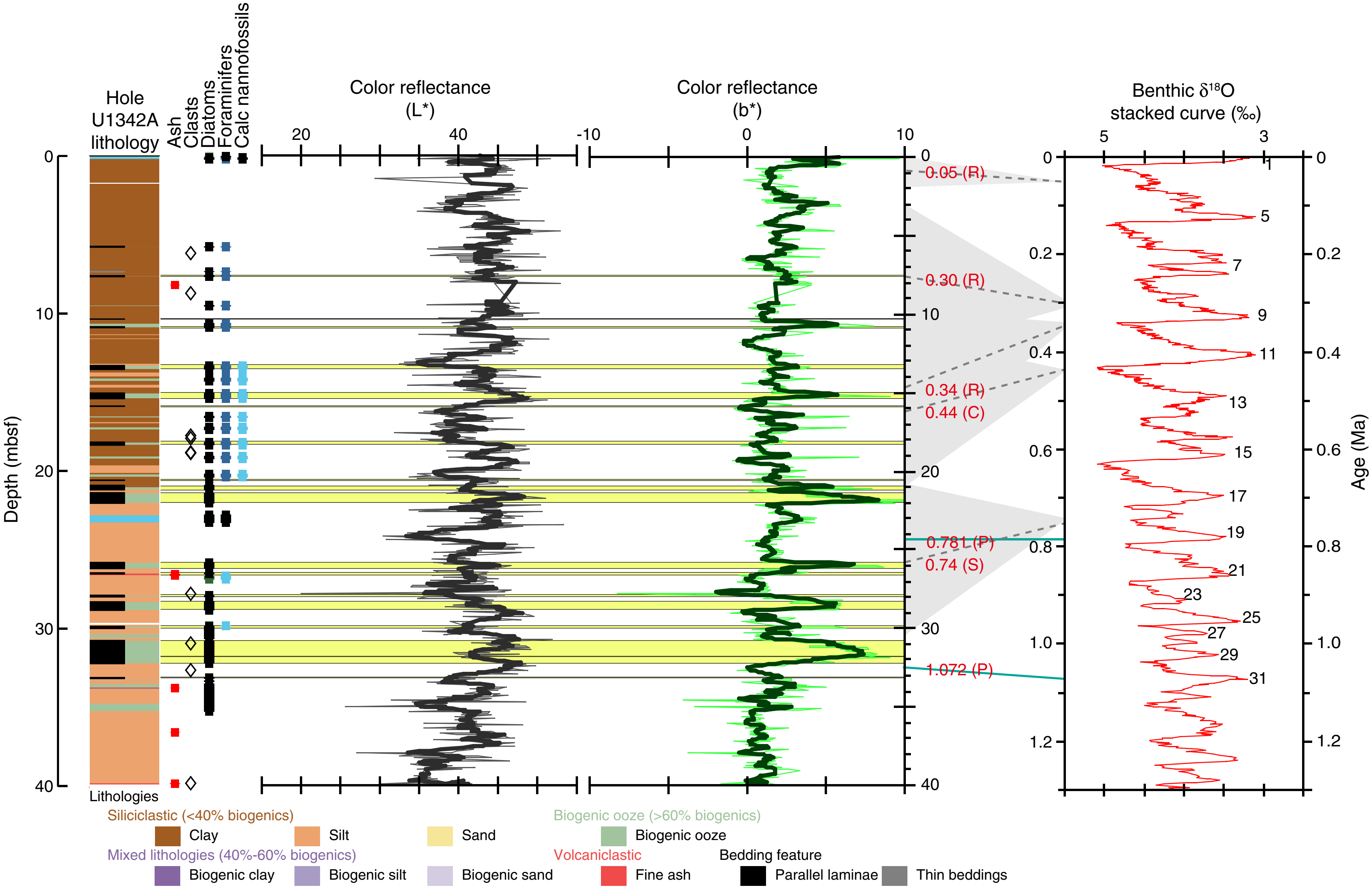

Figure F15. Age-depth plot for Site U1342 showing biostratigraphic datums based on radiolarians, diatoms, calcareous nannofossils, and silicoflagellates.

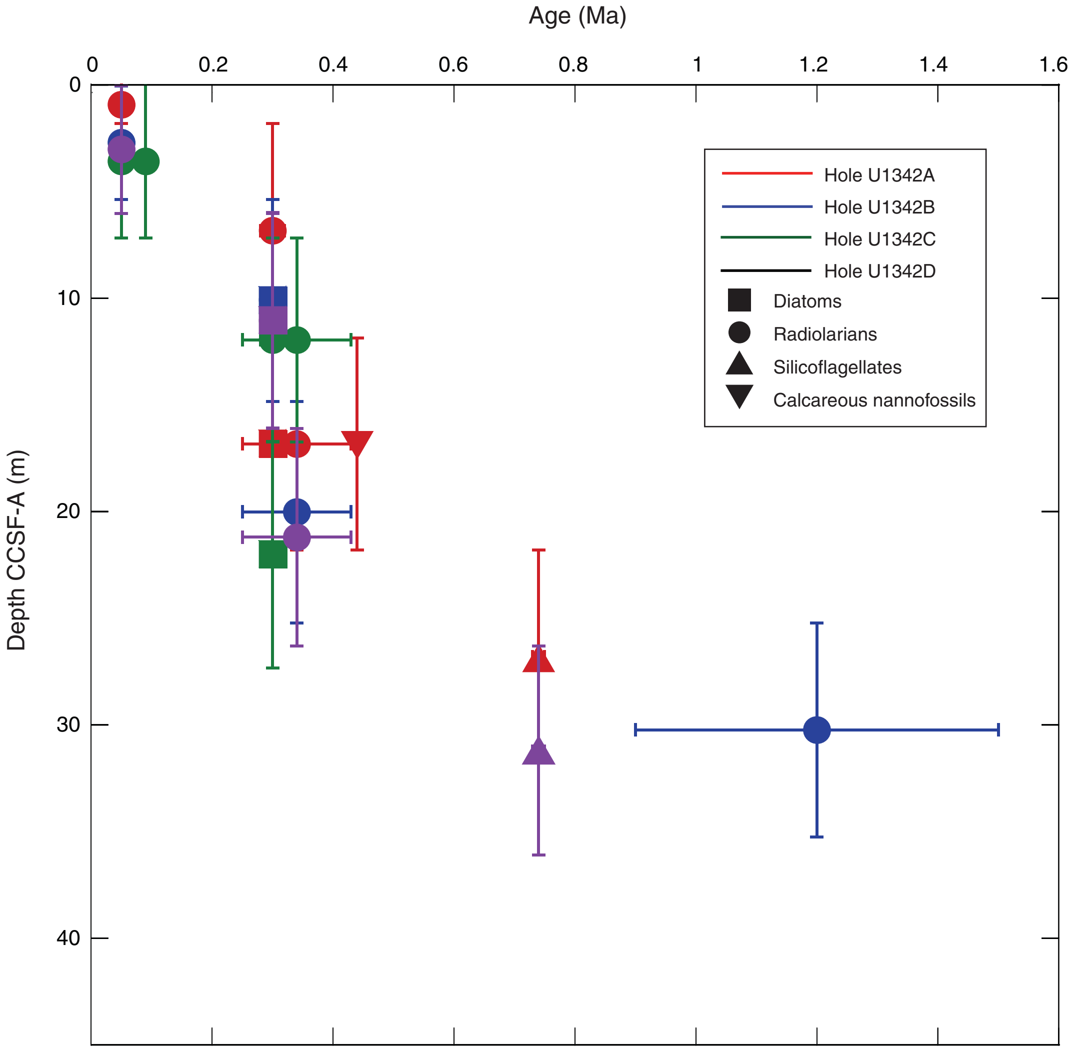

Figure F16. Planktonic foraminifer and calcareous nannofossil abundances, along with percentages of calcium carbonate and heavily silicified diatoms (*Coscinodiscus marginatus* and *Stephanopyxis horridus*). B = barren, P = present, R = rare, F = few, A = abundant, D = dominant.

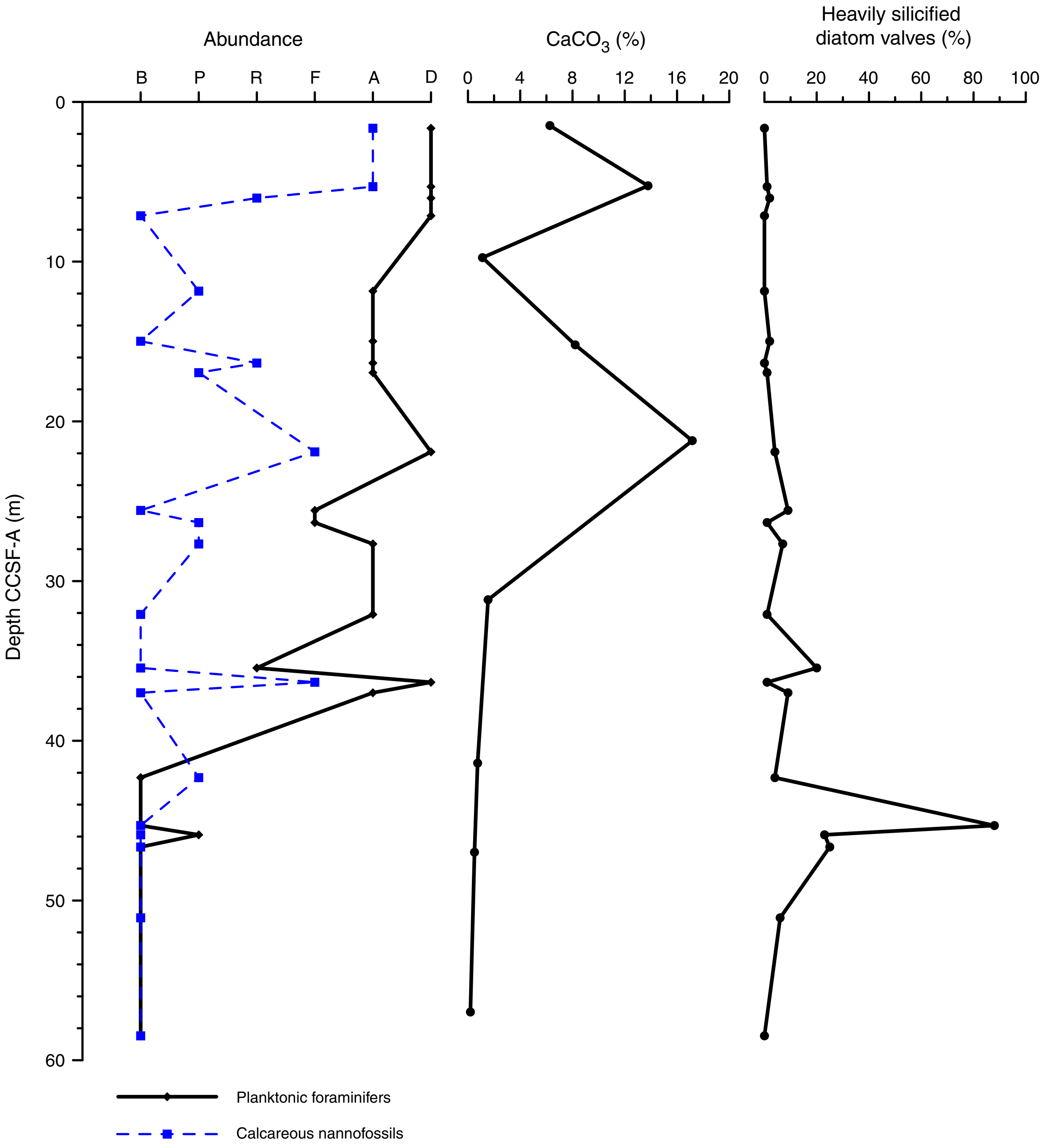

Figure F17. Abundances of sea ice diatoms, sea ice dinoflagellates, planktonic foraminifer species *Neogloboquadrina pachyderma* (sinistral), and subpolar species *Neogloboquadrina pachyderma* (dextral), *Globigerina bulloides*, and *Globigerina umbilicata*. B = barren, P = present, R = rare, F = few, A = abundant, D = dominant. Sea ice diatom species considered include *Thalassiosira antarctica* spores, *Dentonula confervacea, Fragilariopsis cylindrus*, and *Porosira glacialis*.

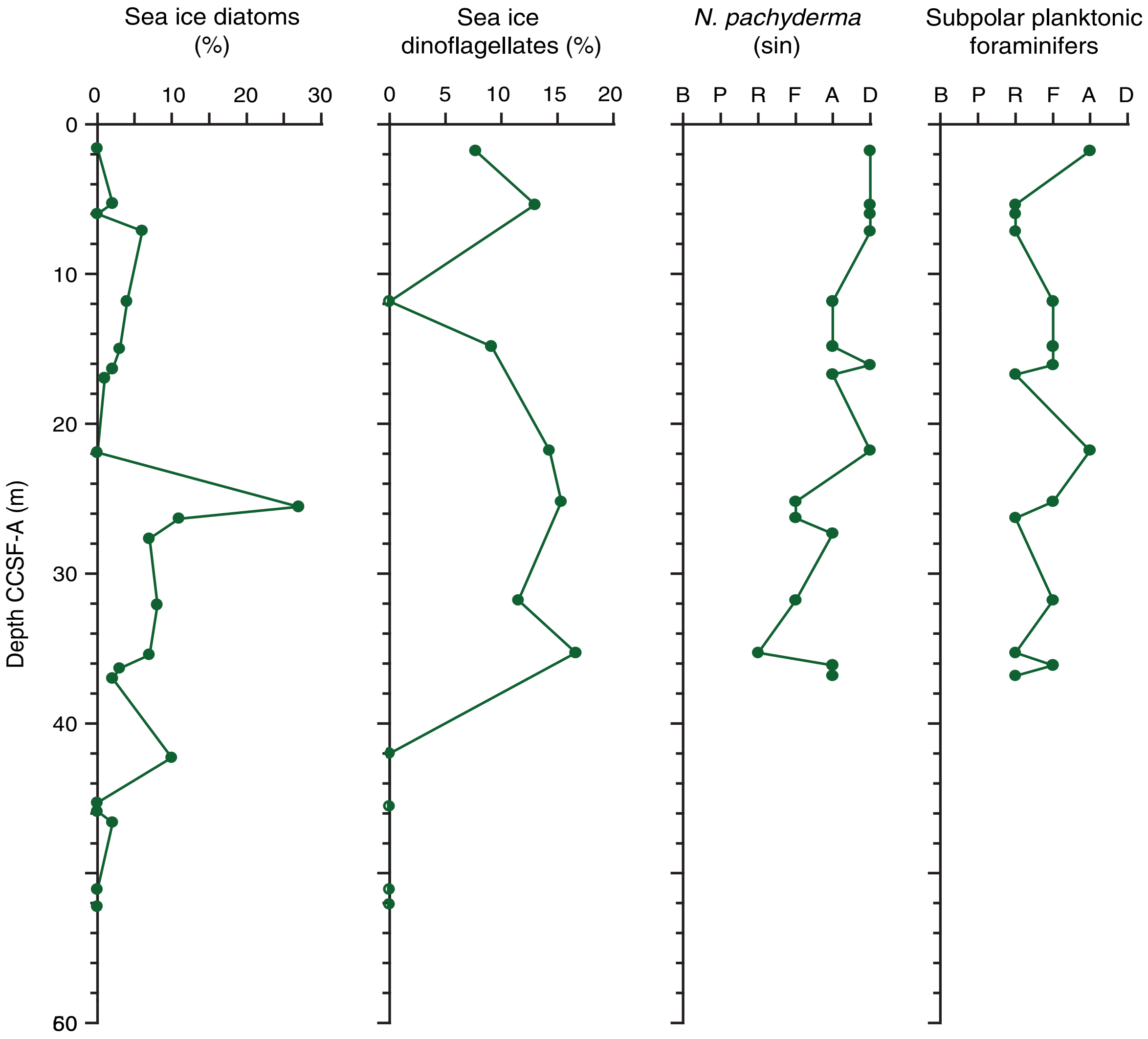

Figure F18. Composite record of gamma ray attenuation (GRA) bulk density and the semiquantitative ratio between *Bulimina* and *Uvigerina* species.

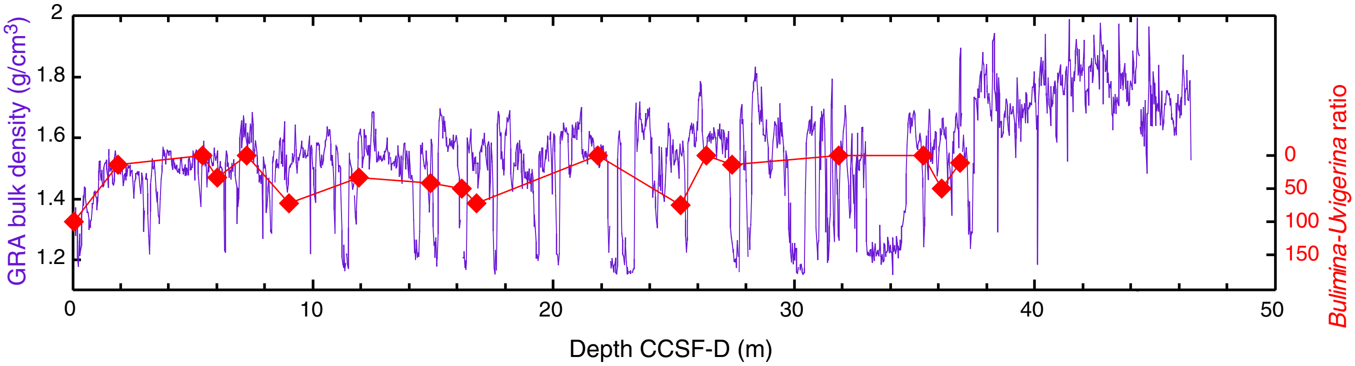

Figure F19. Inclination and intensity of remanent magnetization after 20 mT AF demagnetization ($Int_{20\ mT}$), Holes U1342A, U1342C, and U1342D. Intensity data are plotted with STMSL magnetic susceptibility data.

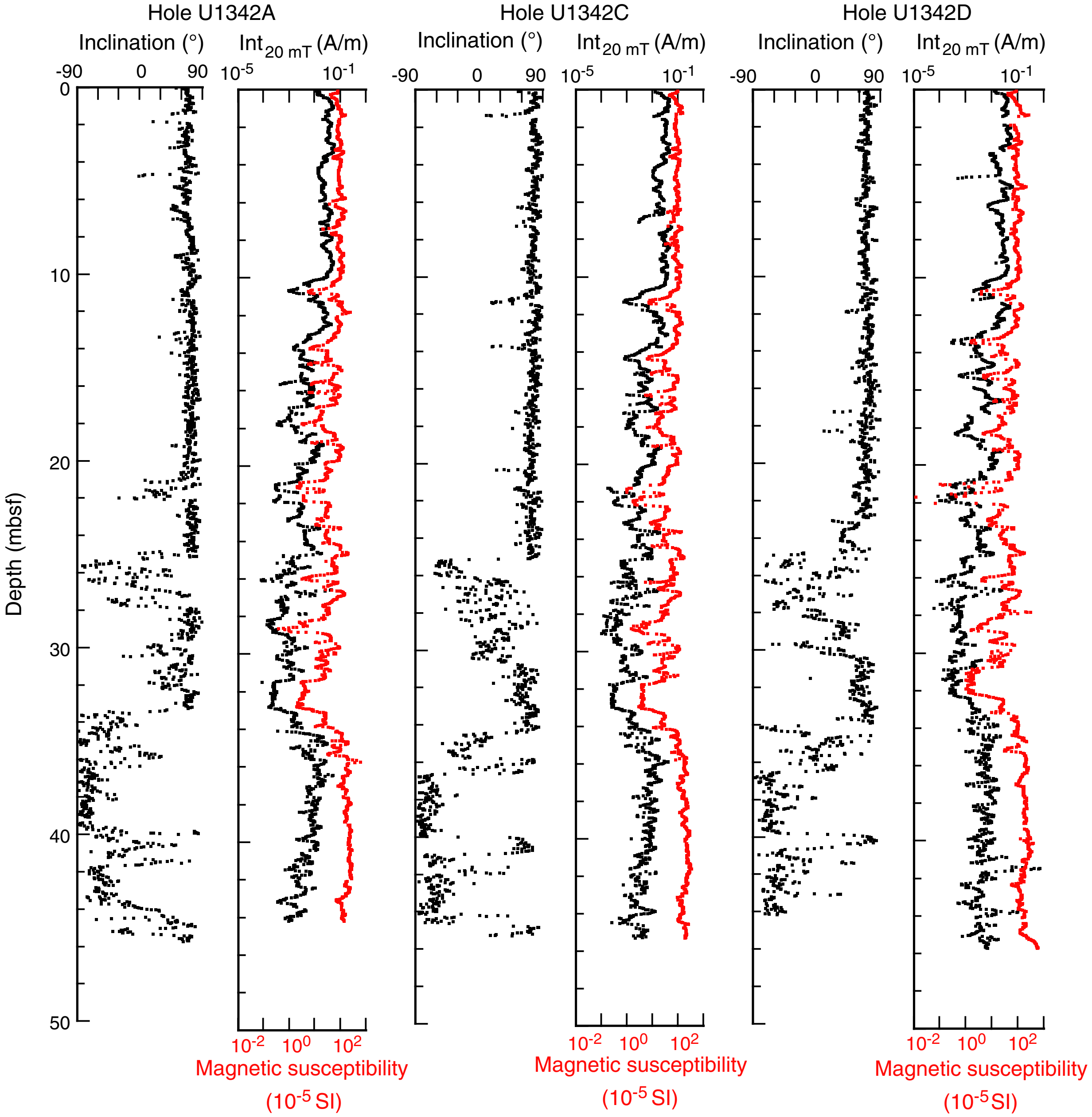

Figure F20. Inclination data (dots) and 60 point (corresponding to ~0.5 m) averaged inclination values (solid line), Holes U1342A, U1342C, and U1342D. Tentative polarity zonation (black = normal polarity, white = reversed polarity, and gray = uncertain polarity) and presumable correlation with reported geomagnetic excursions (names shown above the correlation lines) and polarity chrons are also shown.

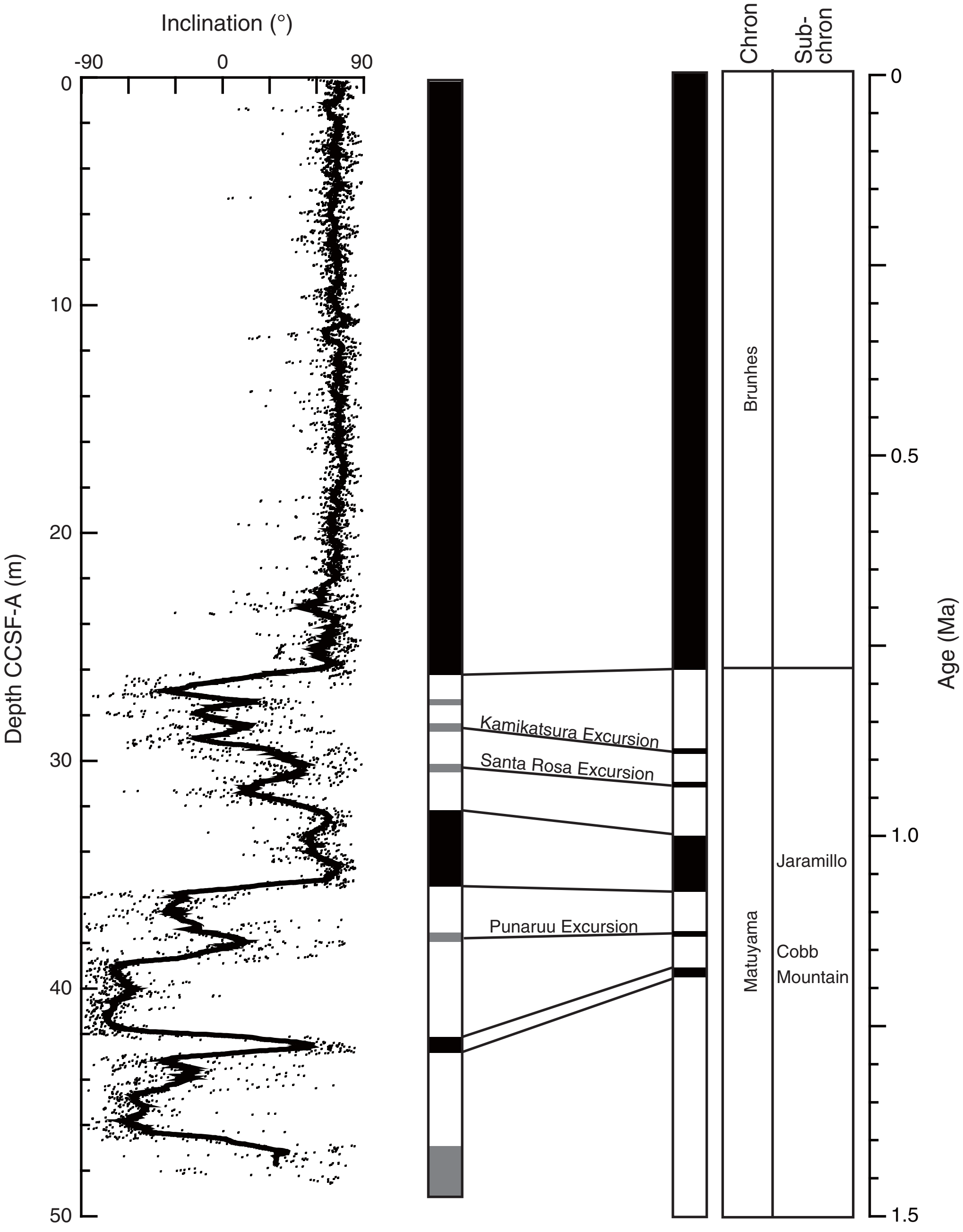

Figure F21. Magnetic susceptibility and relative paleointensity (Int$_{20\ \mathrm{mT}}$/Magnetic susceptibility), Site U1341. The Brunhes/Matuyama magnetic polarity boundary is at 90 m CCSF-A. Numbered features = best guesses for how each feature relates to a marine isotope stage.

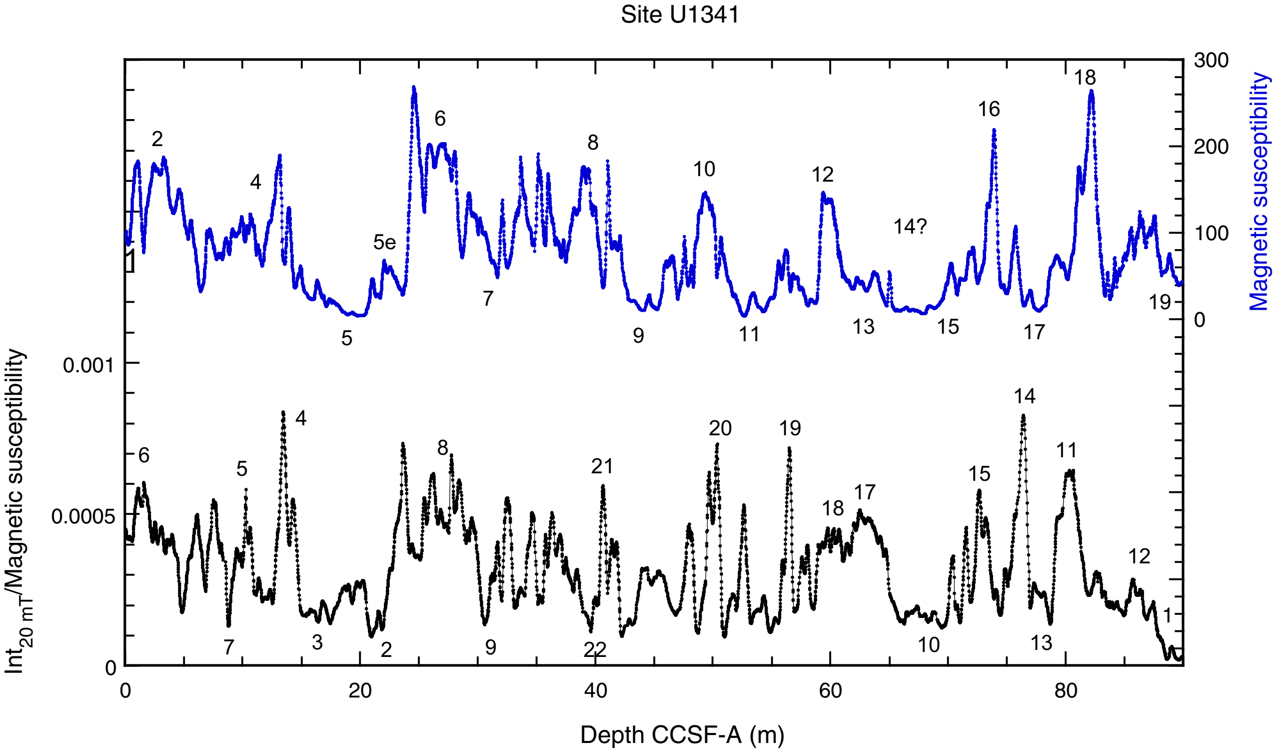

Figure F22. Magnetic susceptibility and relative paleointensity ($Int_{20\ mT}$/Magnetic susceptibility), Hole U1342A. The Brunhes/Matuyama (B/M) magnetic polarity boundary is at 25.25 mbsf. Numbered features = best guesses for how each feature relates to a marine isotope stage (MIS). These MIS estimates are the basis of the age assignments given in Figure F23.

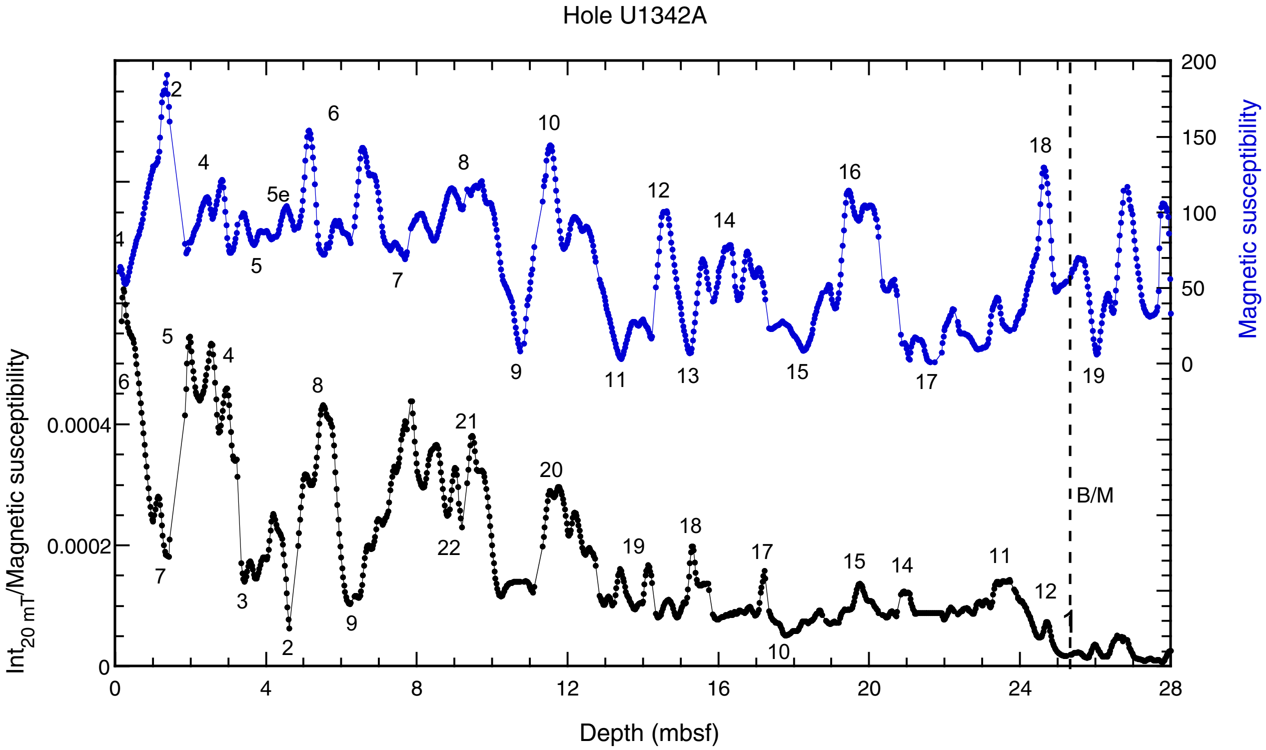

Figure F23. Age-depth plot for Hole U1342A based on paleomagnetic chronostratigraphic estimates. Solid squares = age correlations based on polarity transitions and geomagnetic excursions listed in Table T11, open squares = preliminary paleointensity estimate records shown in Figure F22.

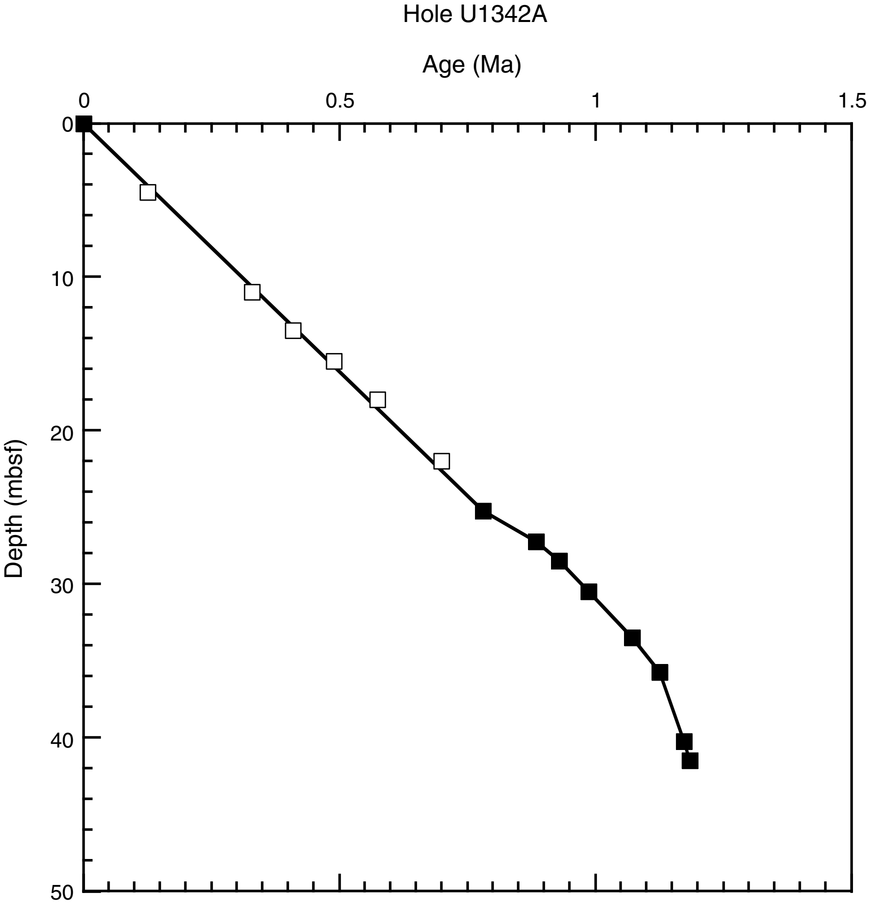

Figure F24. Rock magnetic summary for Hole U1342A showing magnetic susceptibility and remanent magnetization after 20 mT AF demagnetization ($Int_{20\ mT}$). Note the discrete intervals where both magnetic parameters undergo more than order-of-magnitude decreases.

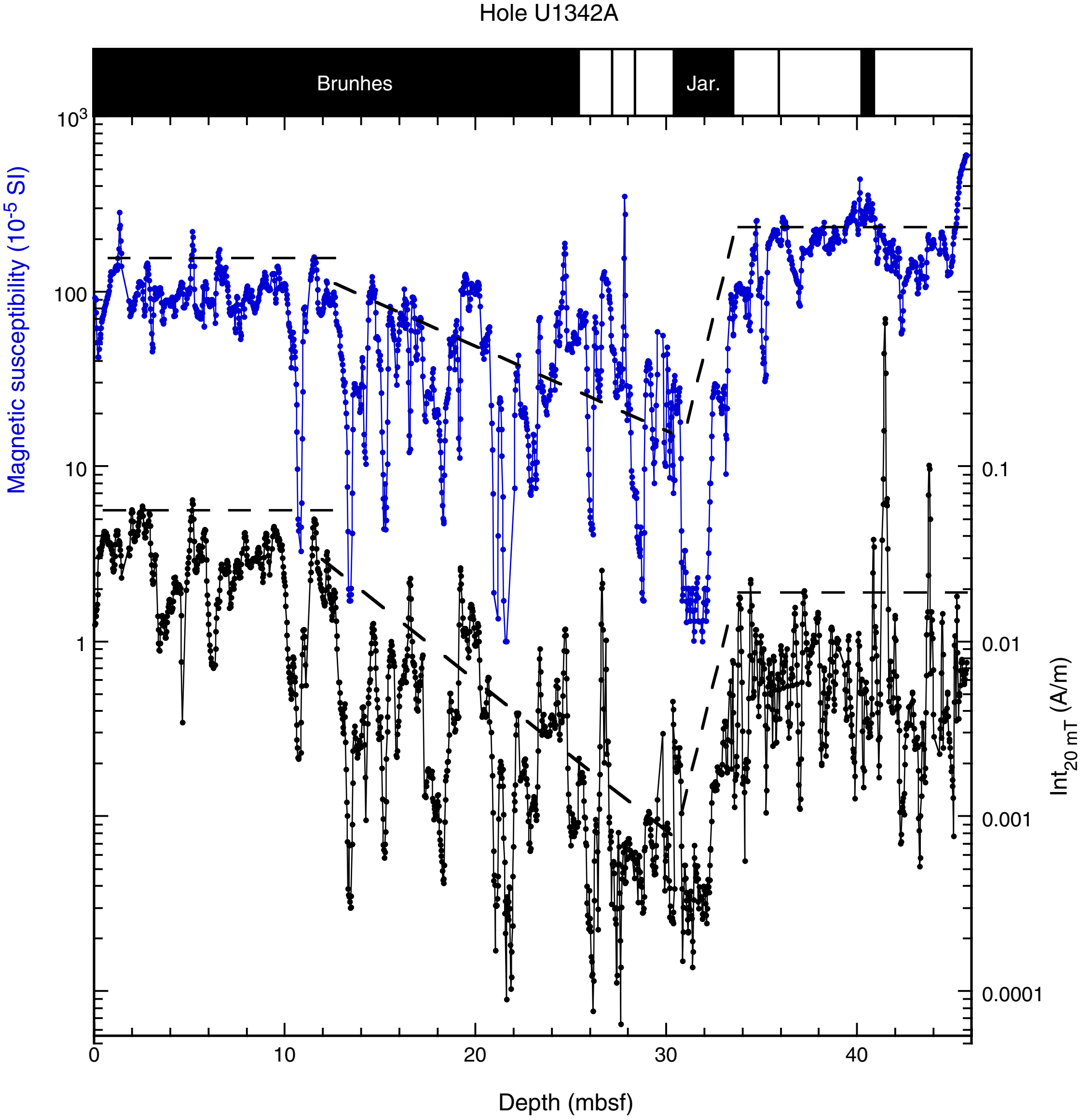

Figure F25. Dissolved chemical concentrations, Holes U1342A and U1342B. **A.** Dissolved inorganic carbon (DIC). **B.** pH. **C.** Alkalinity. **D.** Sulfate. **E.** Methane. **F.** Chloride. **G.** Phosphate. **H.** Ammonium.

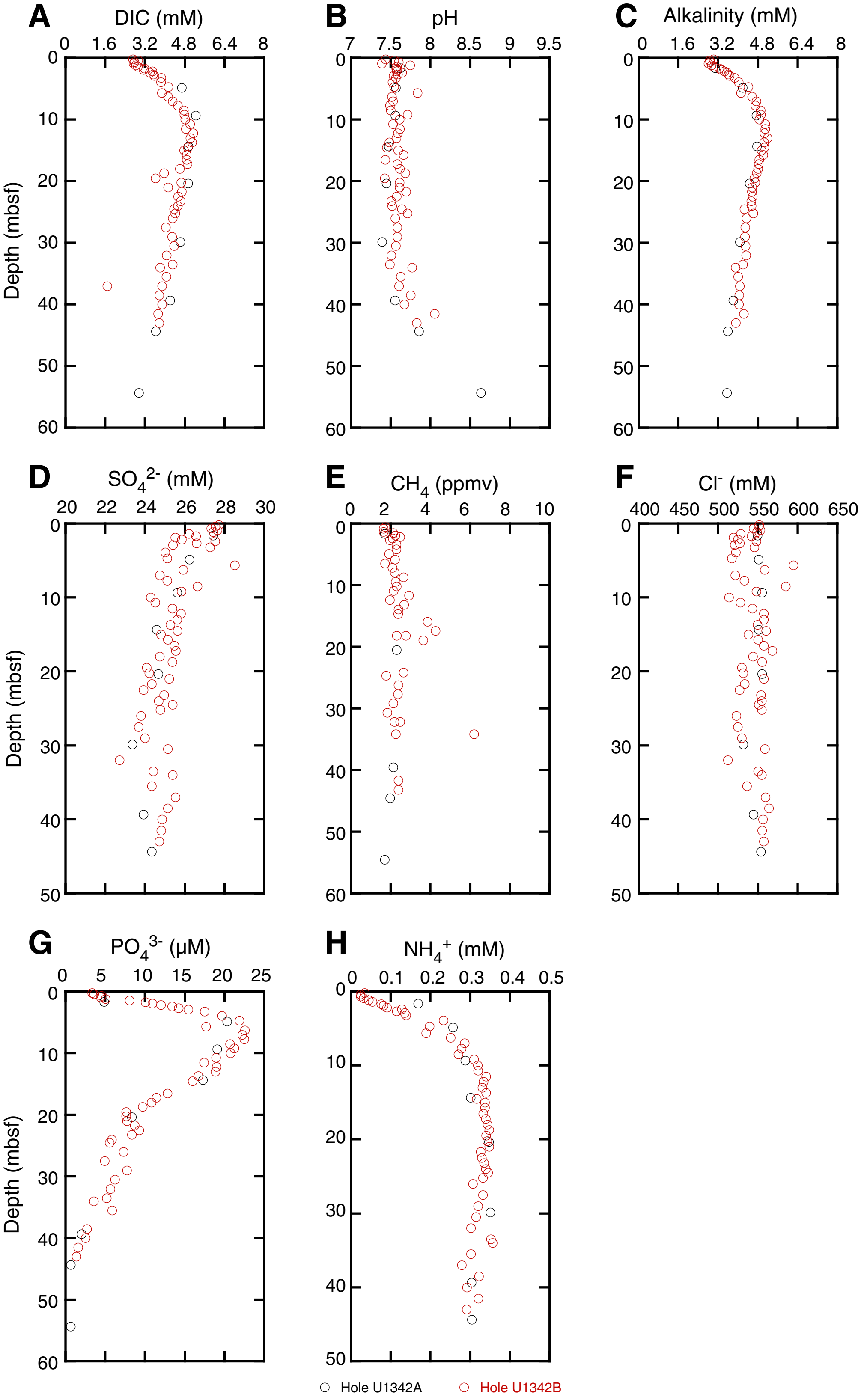

Figure F26. Dissolved chemical concentrations, Holes U1342A and U1342B. **A.** Calcium. **B.** Magnesium. **C.** Sodium. **D.** Potassium. **E.** Boron. **F.** Lithium. **G.** Strontium. **H.** Manganese. **I.** Iron. **J.** Silica.

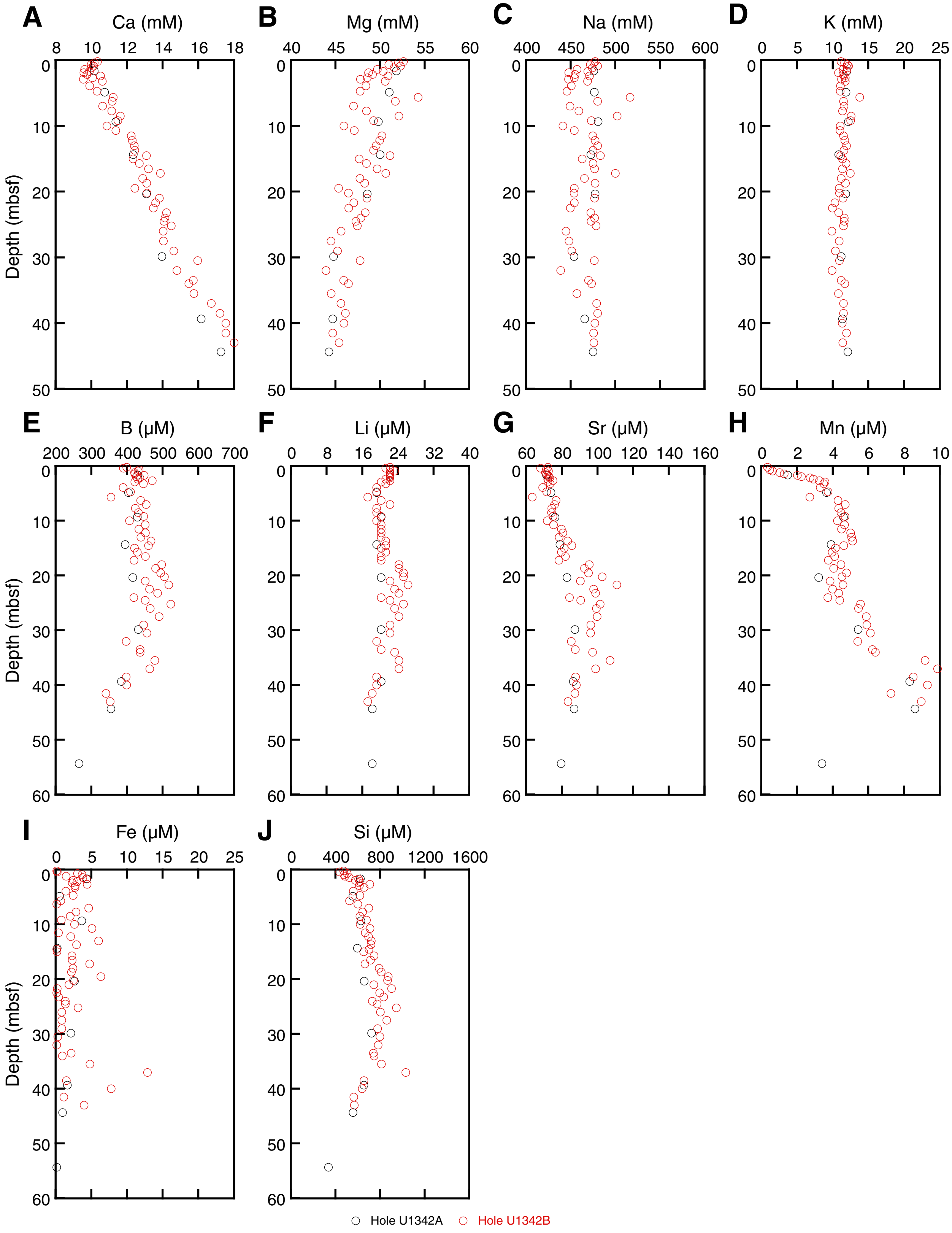

Figure F27. Solid-phase chemical concentrations, Holes U1342A and U1342B. **A.** Calcium carbonate ($CaCO_3$). **B.** Total organic carbon (TOC). **C.** Total sulfur (TS).

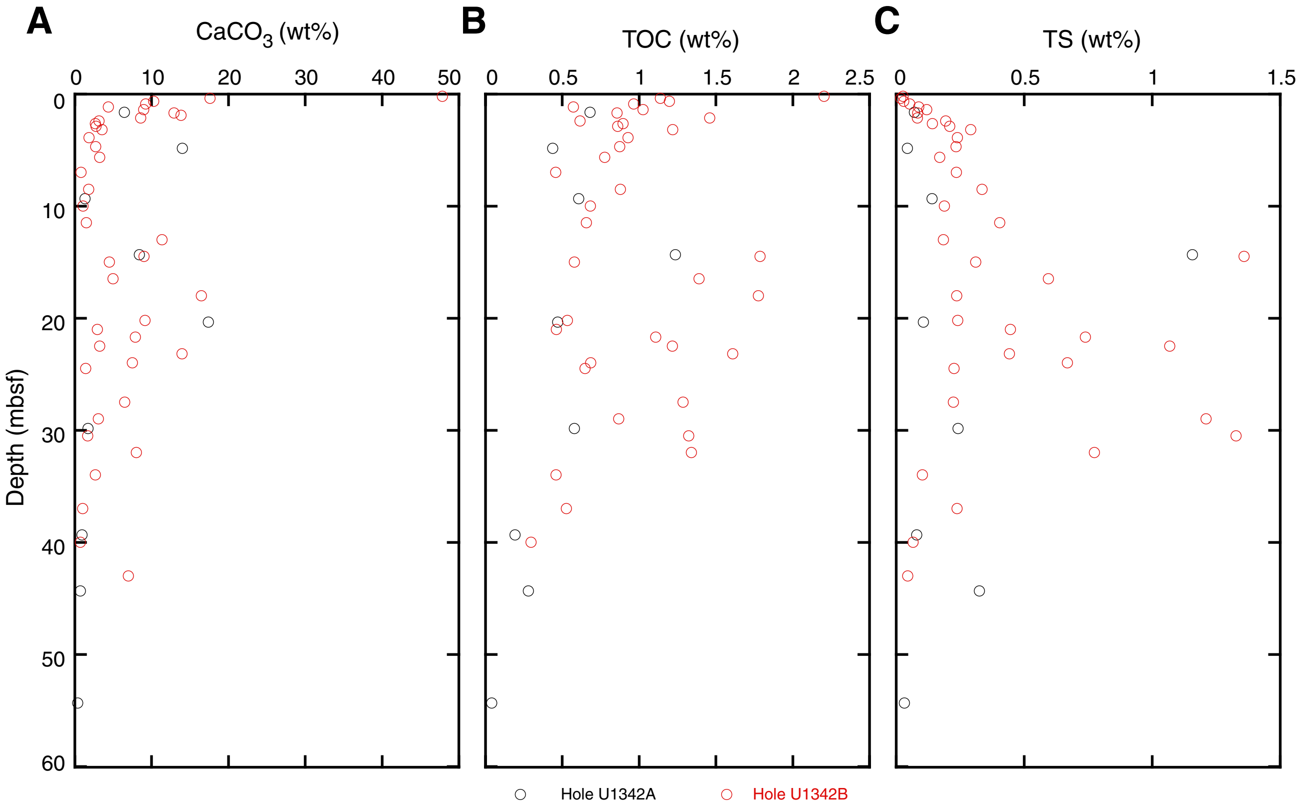

Figure F28. Comparison between solid-phase geochemical records and gamma ray attenuation (GRA) bulk density, Hole U1342B. **A.** Calcium carbonate ($CaCO_3$). **B.** Total organic carbon (TOC). **C.** Total sulfur (TS). Stars = data from solid-phase samples taken at a laminated layer. Green bars = estimated laminated layers recognized by gamma ray attenuation (GRA) bulk density.

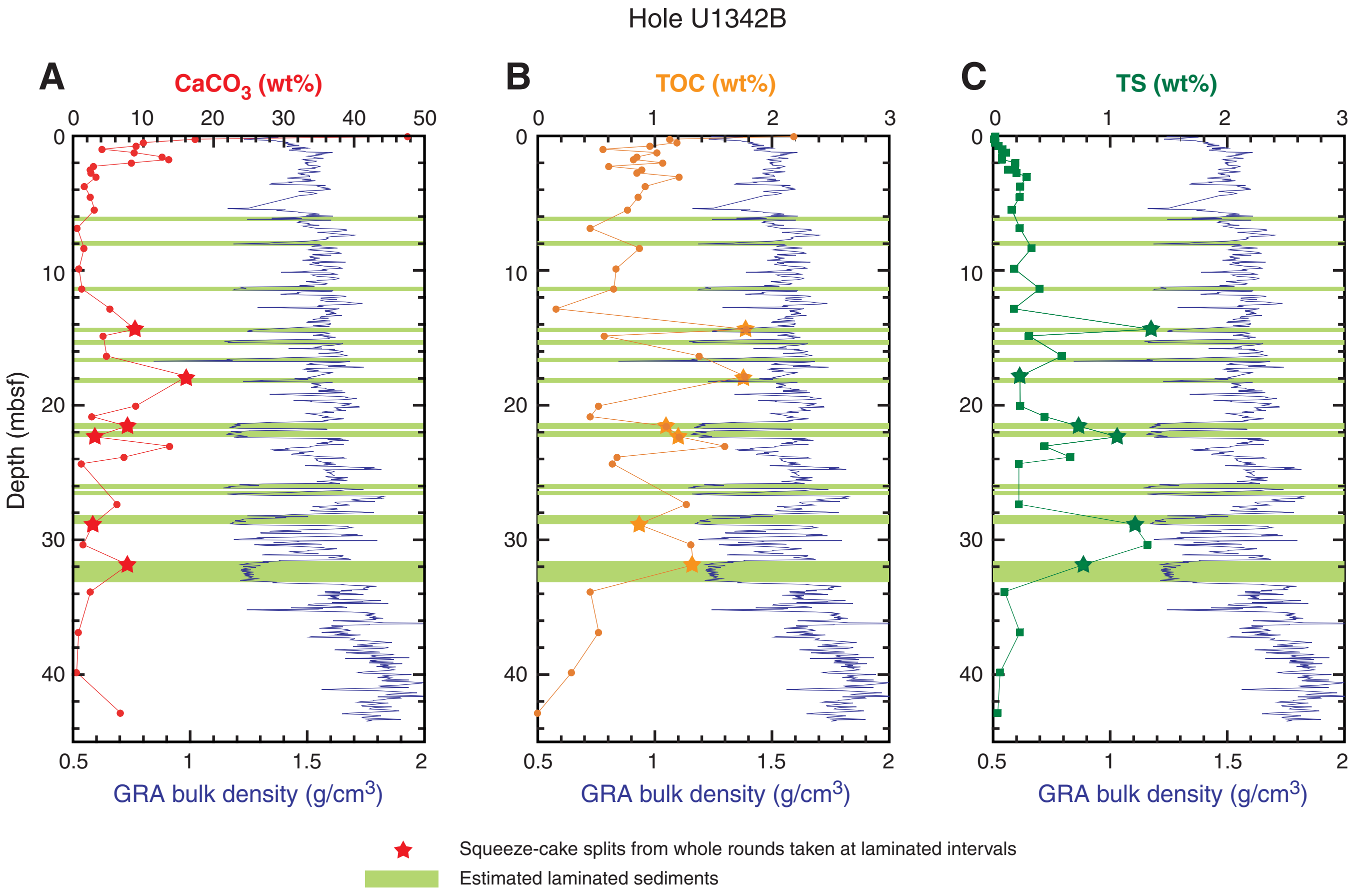

Figure F29. Downhole distribution of STMSL magnetic susceptibility, Hole U1342C.

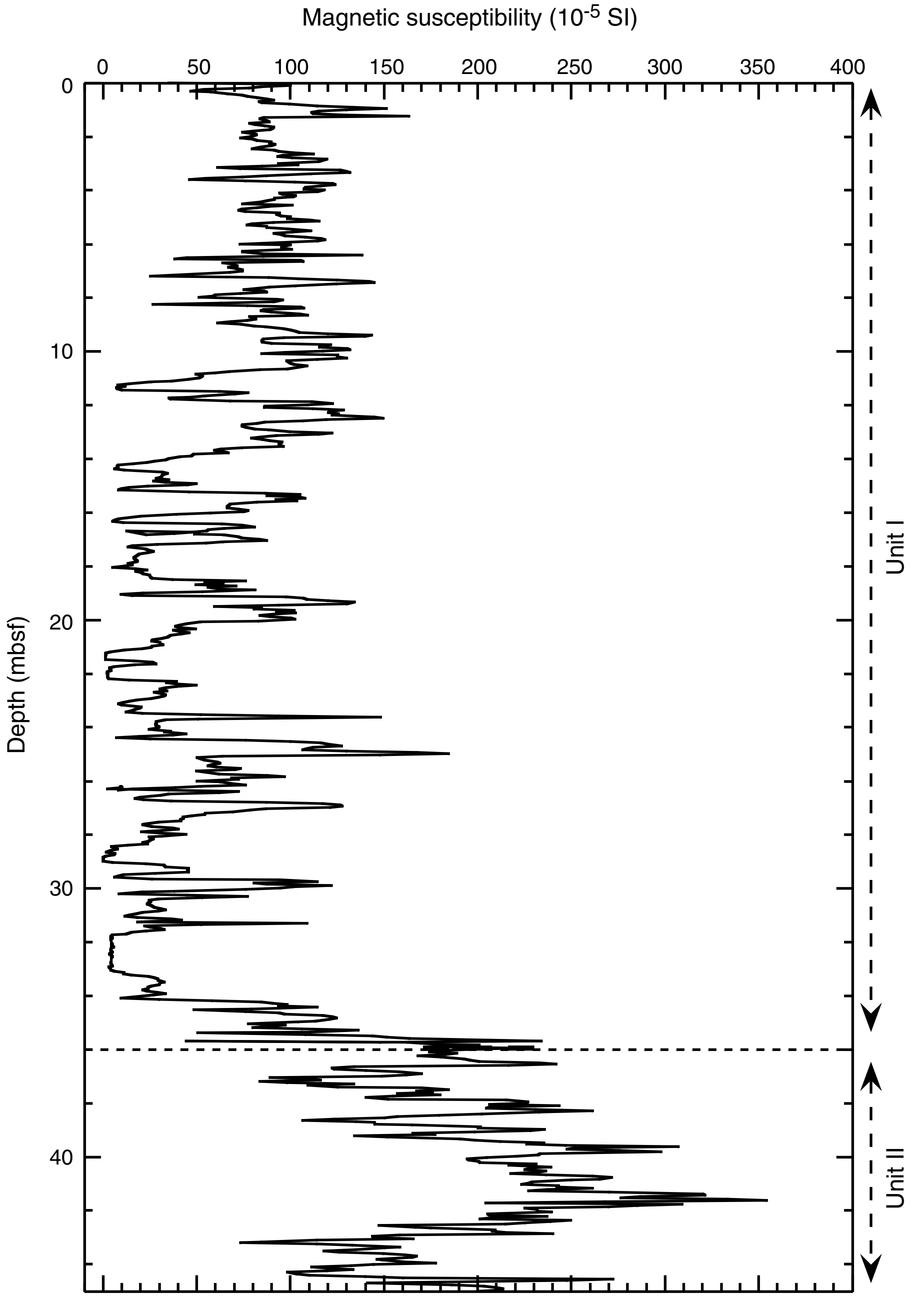

Figure F30. Downhole distribution of gamma ray attenuation (GRA) wet bulk density (solid line) and MAD measurements on sediment samples (open circles) collected from the working halves of split sections, Hole U1342C.

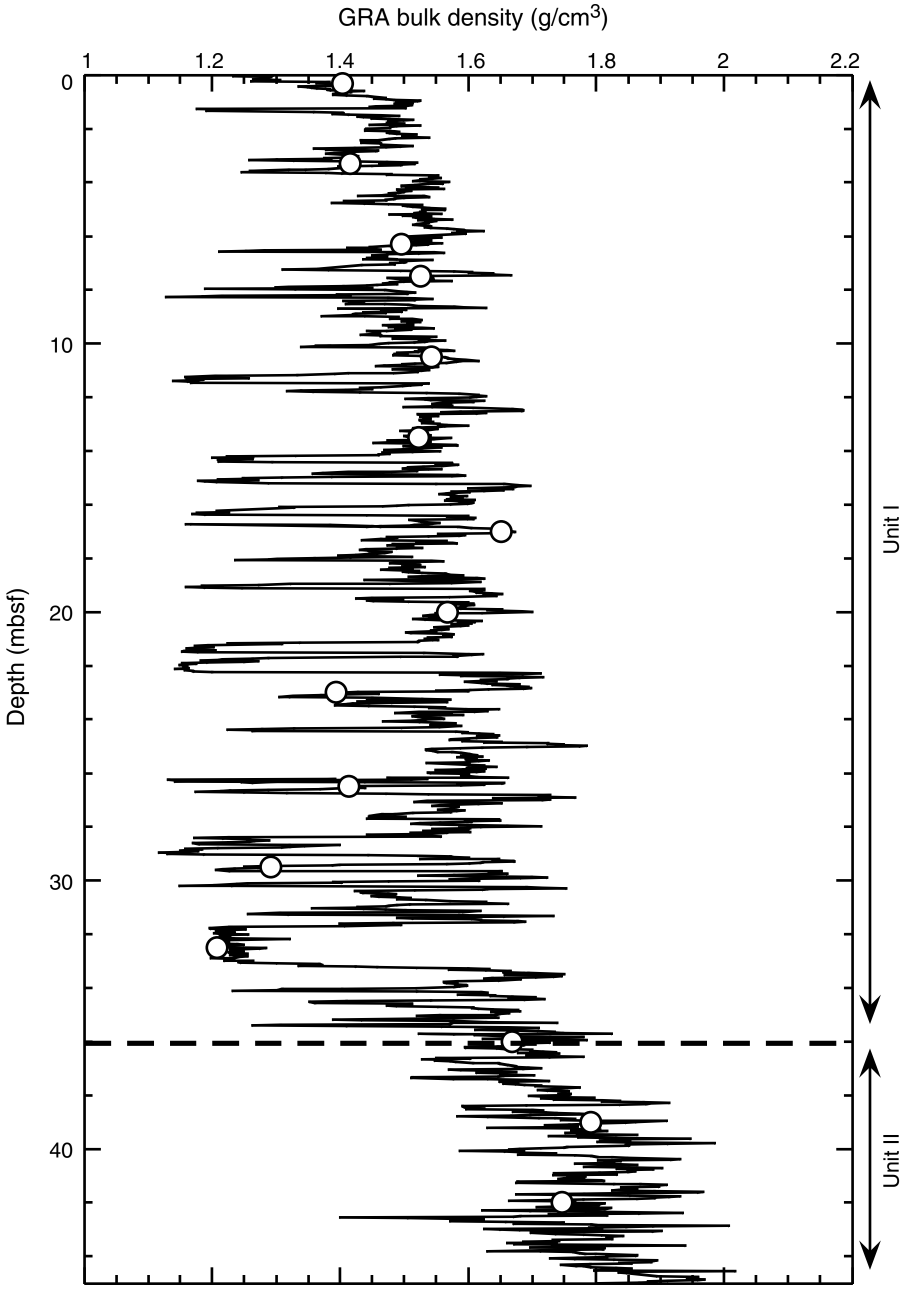

Figure F31. Downhole distribution of *P*-wave velocity recorded by the STMSL on whole-round sections, Hole U1342C.

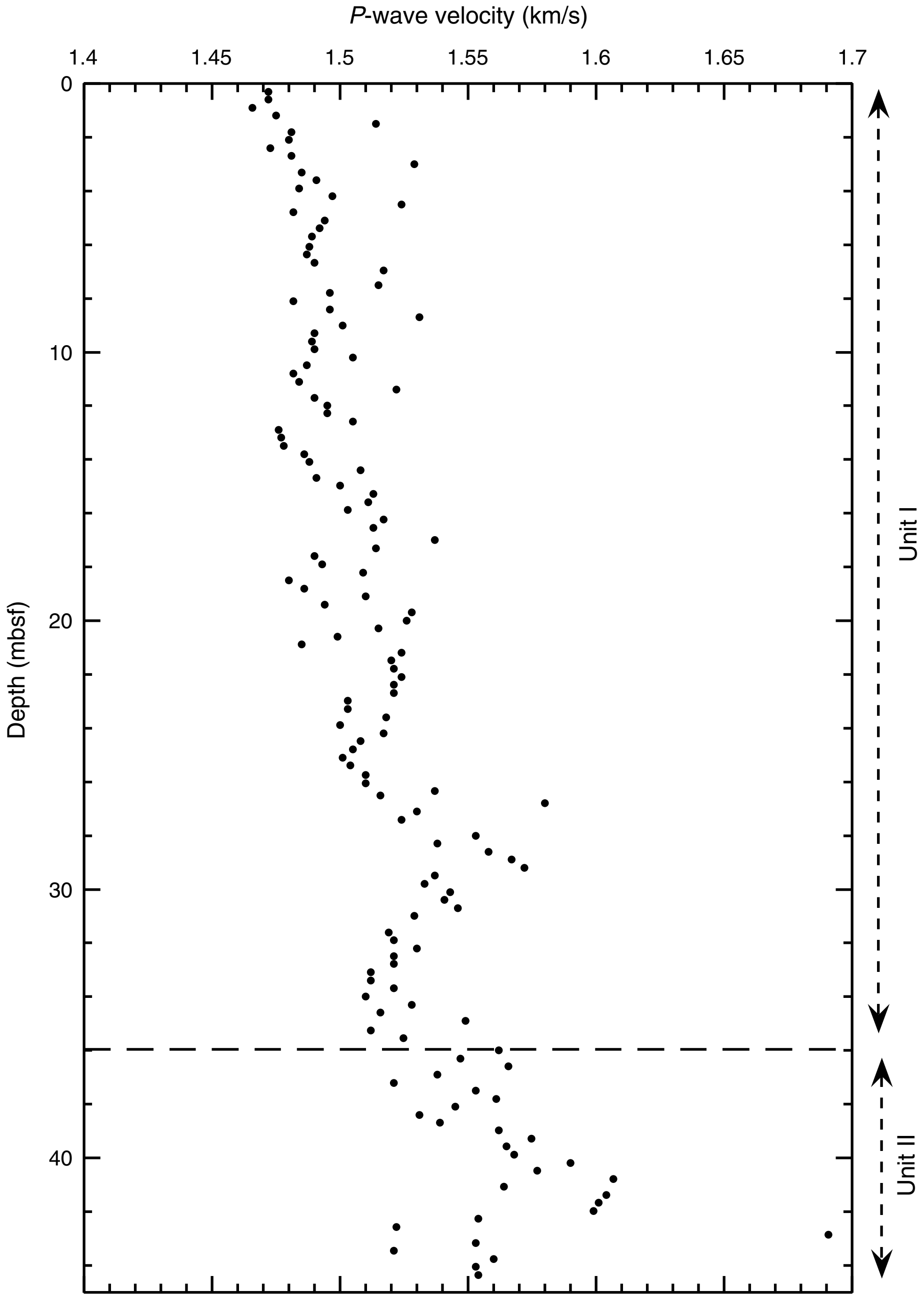

Figure F32. Downhole distribution of natural gamma radiation (NGR), Hole U1342C.

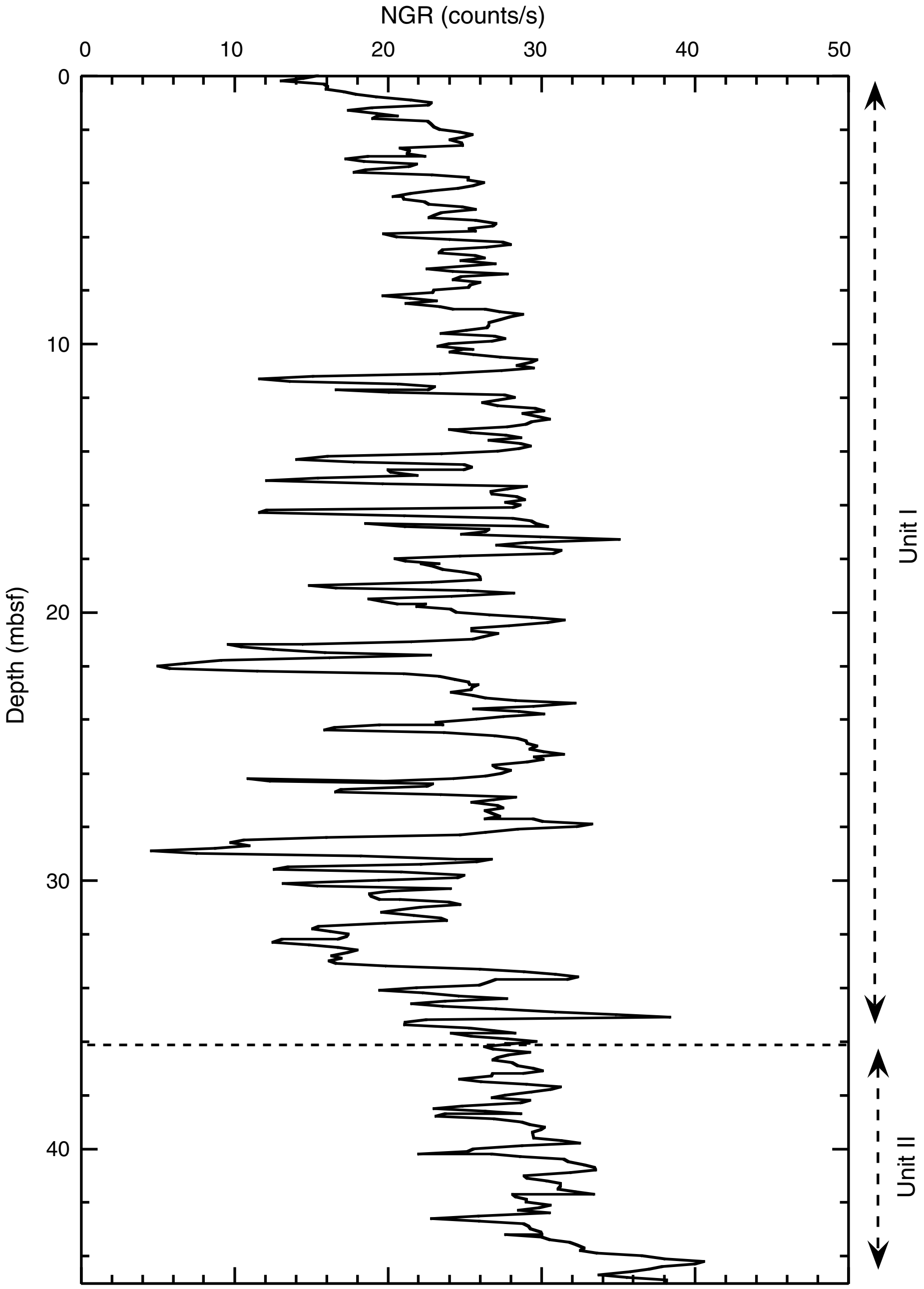

Figure F33. Downhole distribution of sediment water content (percent of total sediment weight) and porosity, Hole U1342C.

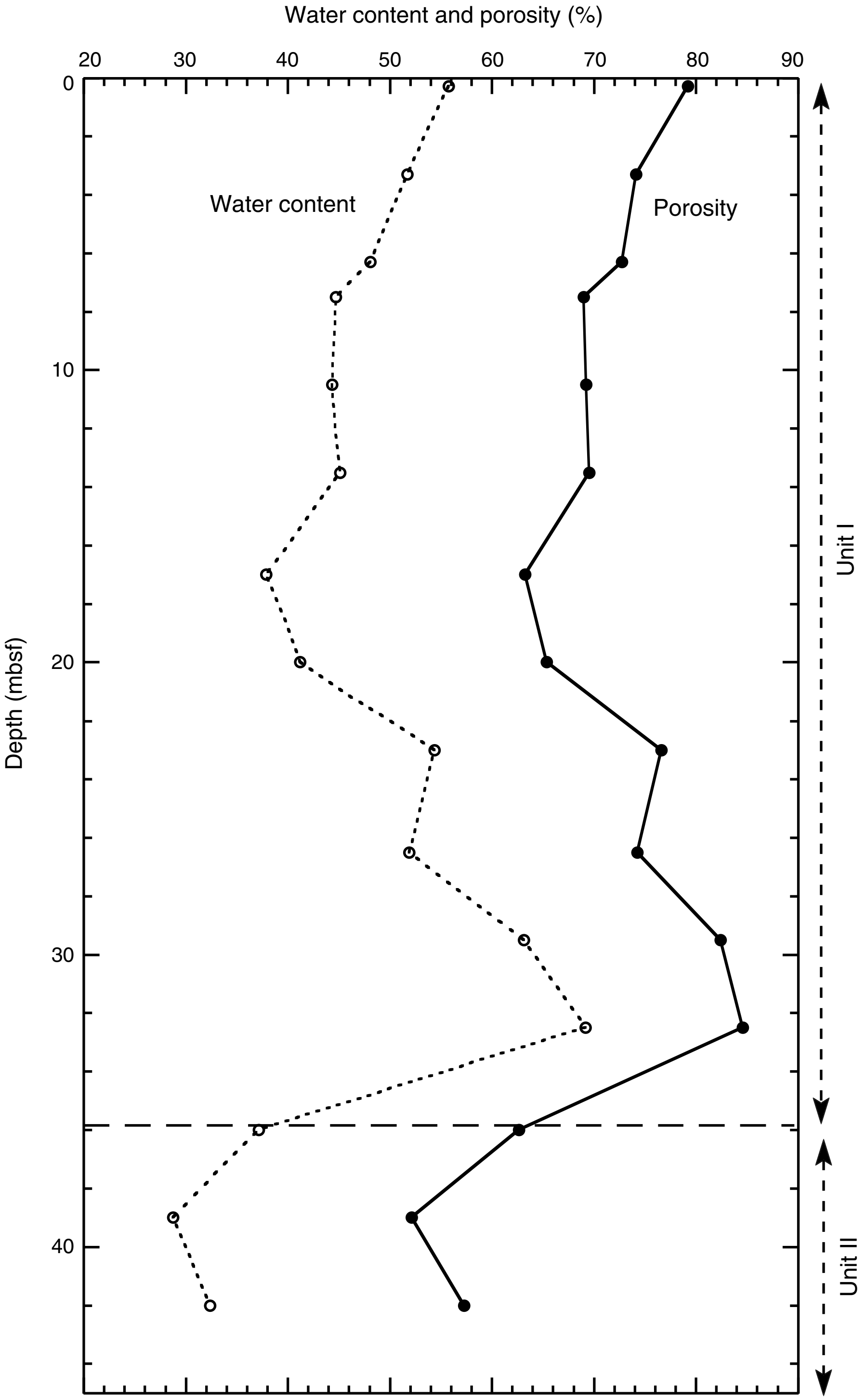

Figure F34. Downhole variations in dry grain density, Hole U1342C.

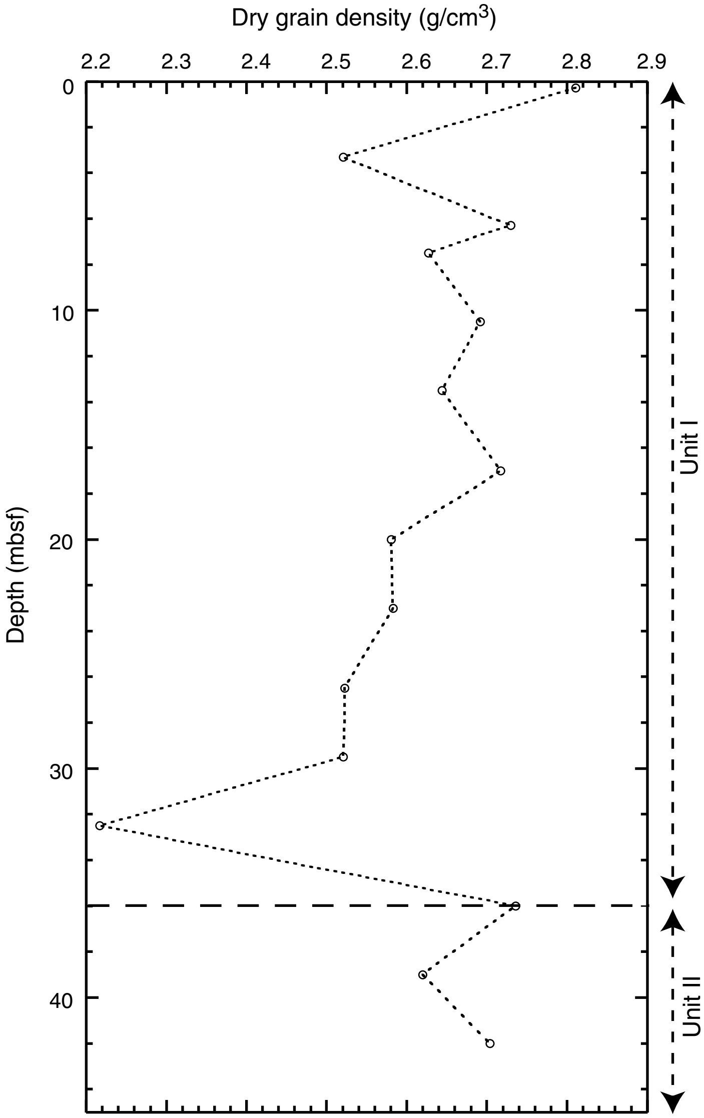

Figure F35. WRMSL magnetic susceptibility vs. composite depth, Site U1342. STMSL magnetic susceptibility data are shown for Hole U1342B because cores from this hole were not run through the WRMSL. For the splice record (top panel), depth on the CCSF-D scale is equivalent to depth on the CCSF-A scale.

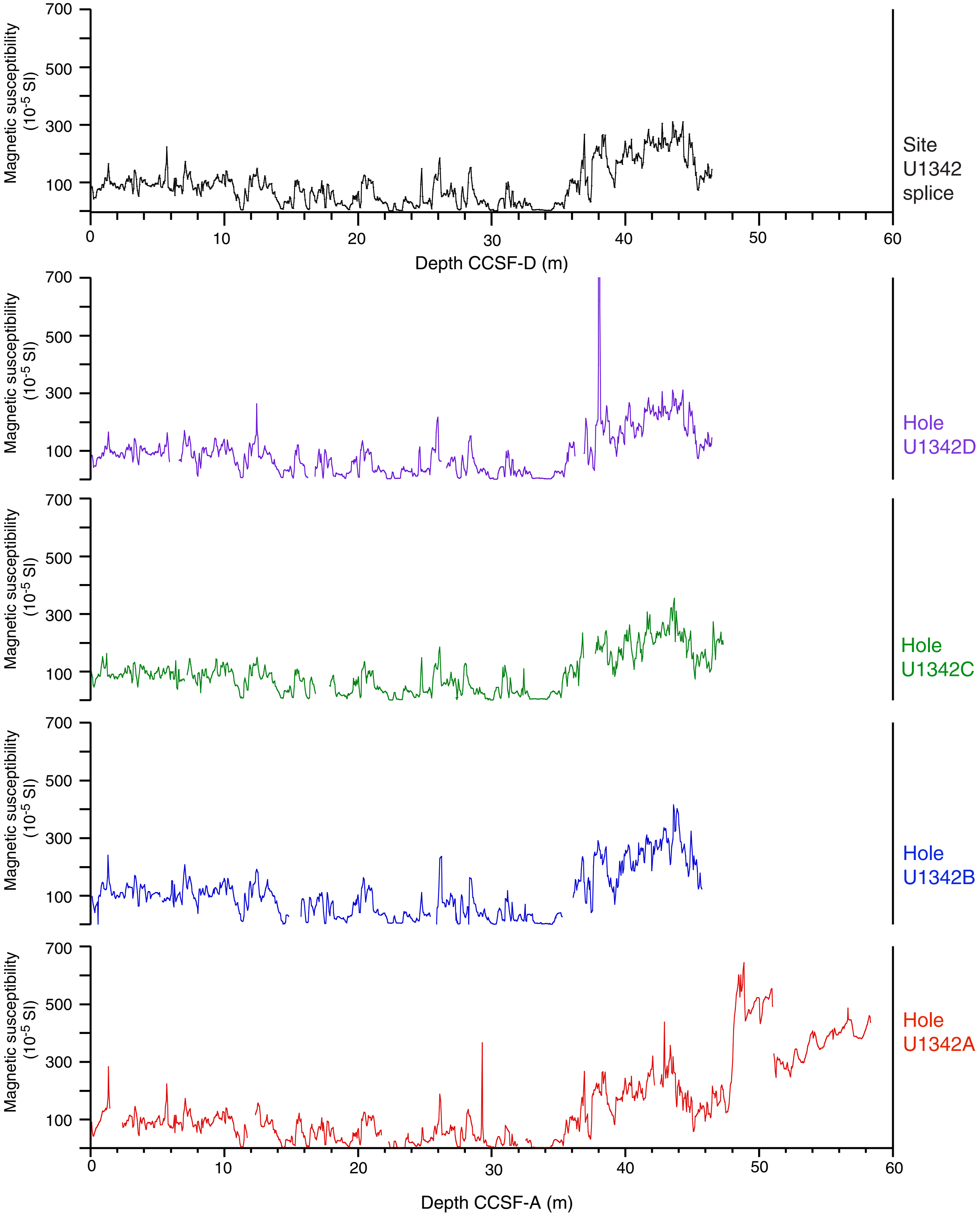

Figure F36. WRMSL gamma ray attenuation (GRA) bulk density vs. composite depth, Site U1342. STMSL GRA data are shown for Hole U1342B because cores from this hole were not run through the WRMSL. For the splice record (top panel), depth on the CCSF-D scale is equivalent to depth on the CCSF-A scale.

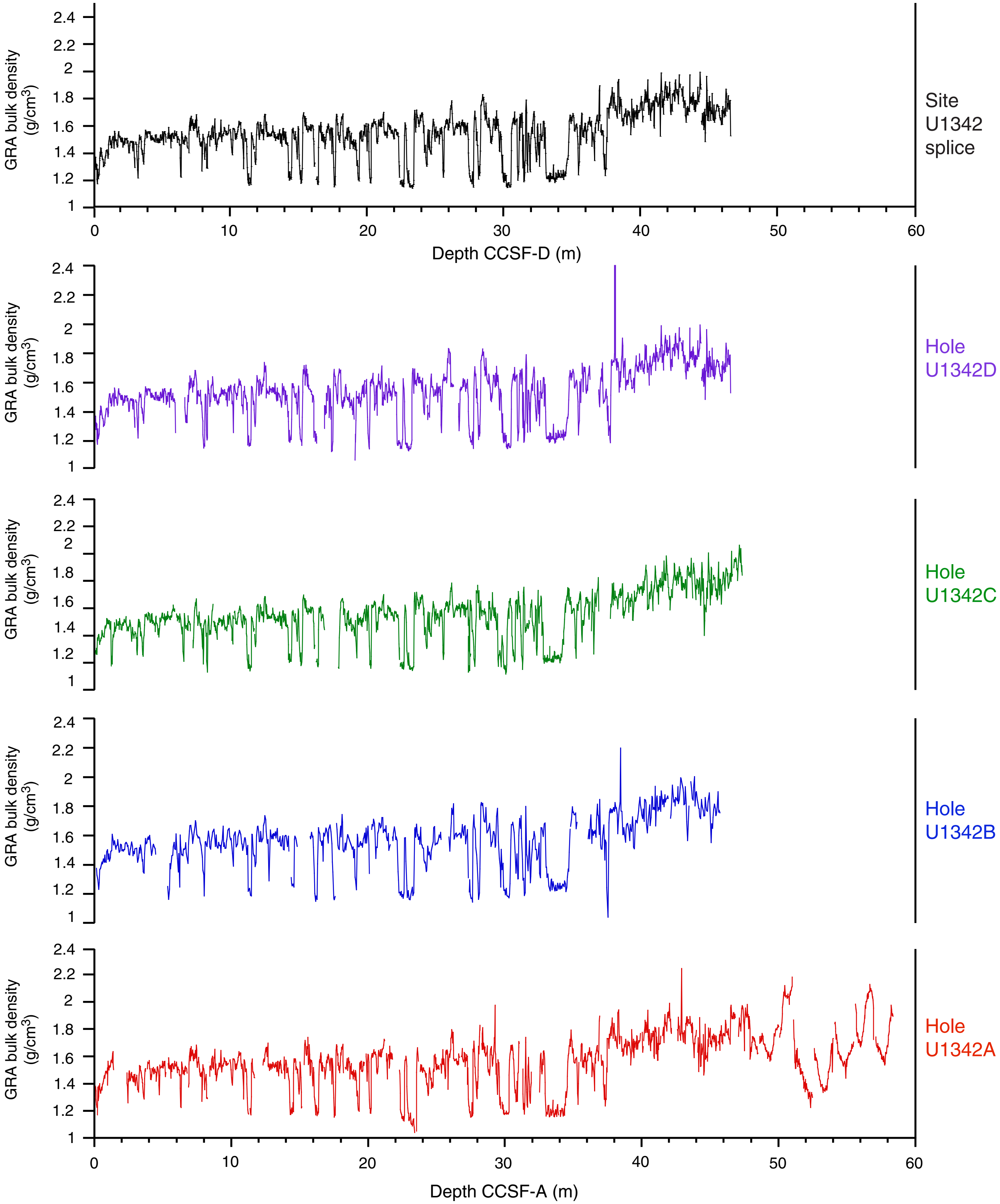

Figure F37. Natural gamma radiation (NGR) collected with the Natural Gamma Radiation Logger vs. composite depth, Site U1342. There are no NGR data for microbiology-dedicated Hole U1342B. For the splice record (top panel), depth on the CCSF-D scale is equivalent to depth on the CCSF-A scale.

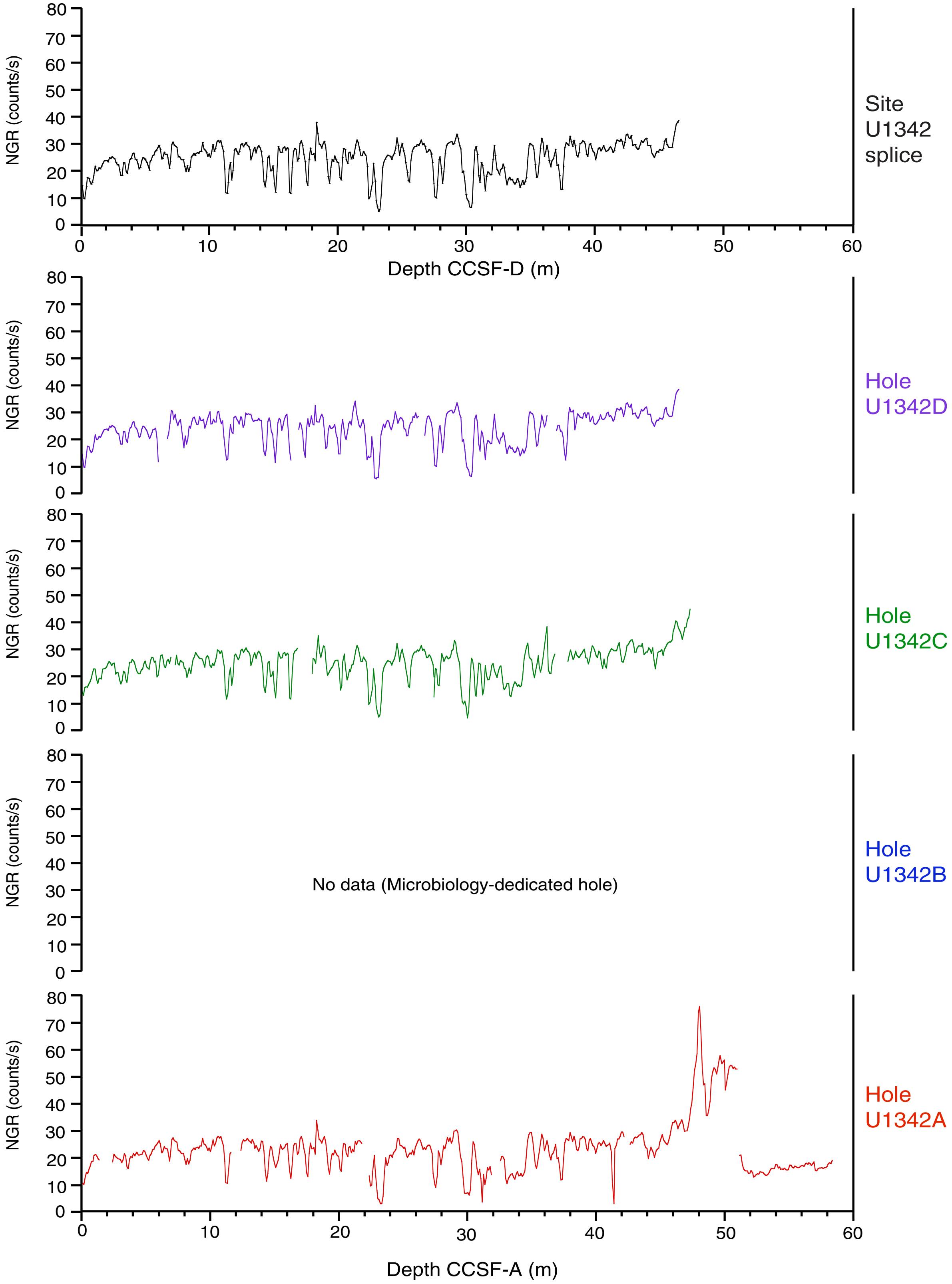

Figure F38. Color reflectance parameter b* collected with the SHMSL vs. composite depth, Site U1342. There are no color reflectance data for microbiology-dedicated Hole U1342B. For the splice record (top panel), depth on the CCSF-D scale is equivalent to depth on the CCSF-A scale.

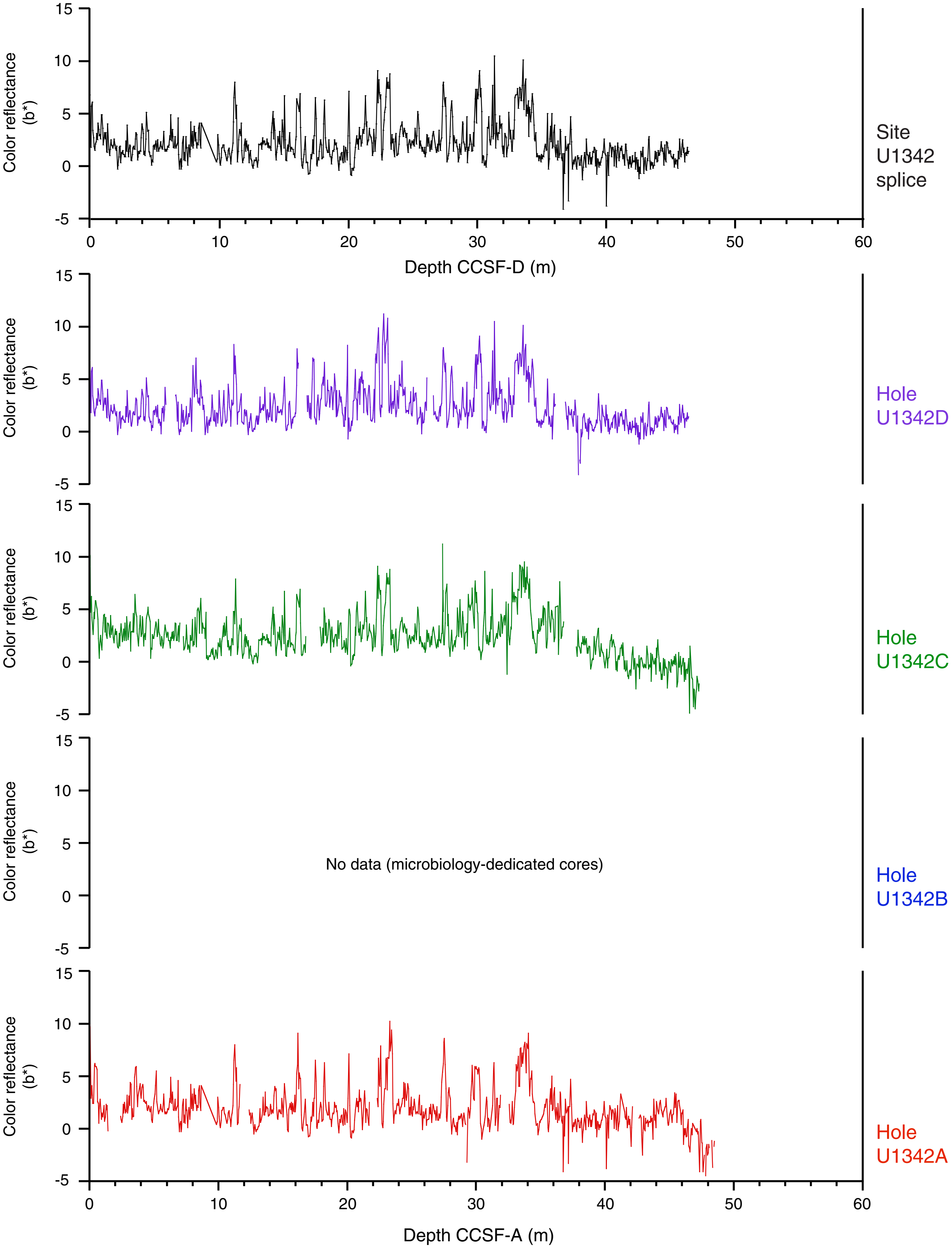

Figure F39. Spliced composite records of magnetic susceptibility, WRMSL gamma ray attenuation (GRA) bulk density, and natural gamma radiation (NGR) vs. composite depth, Site U1342.

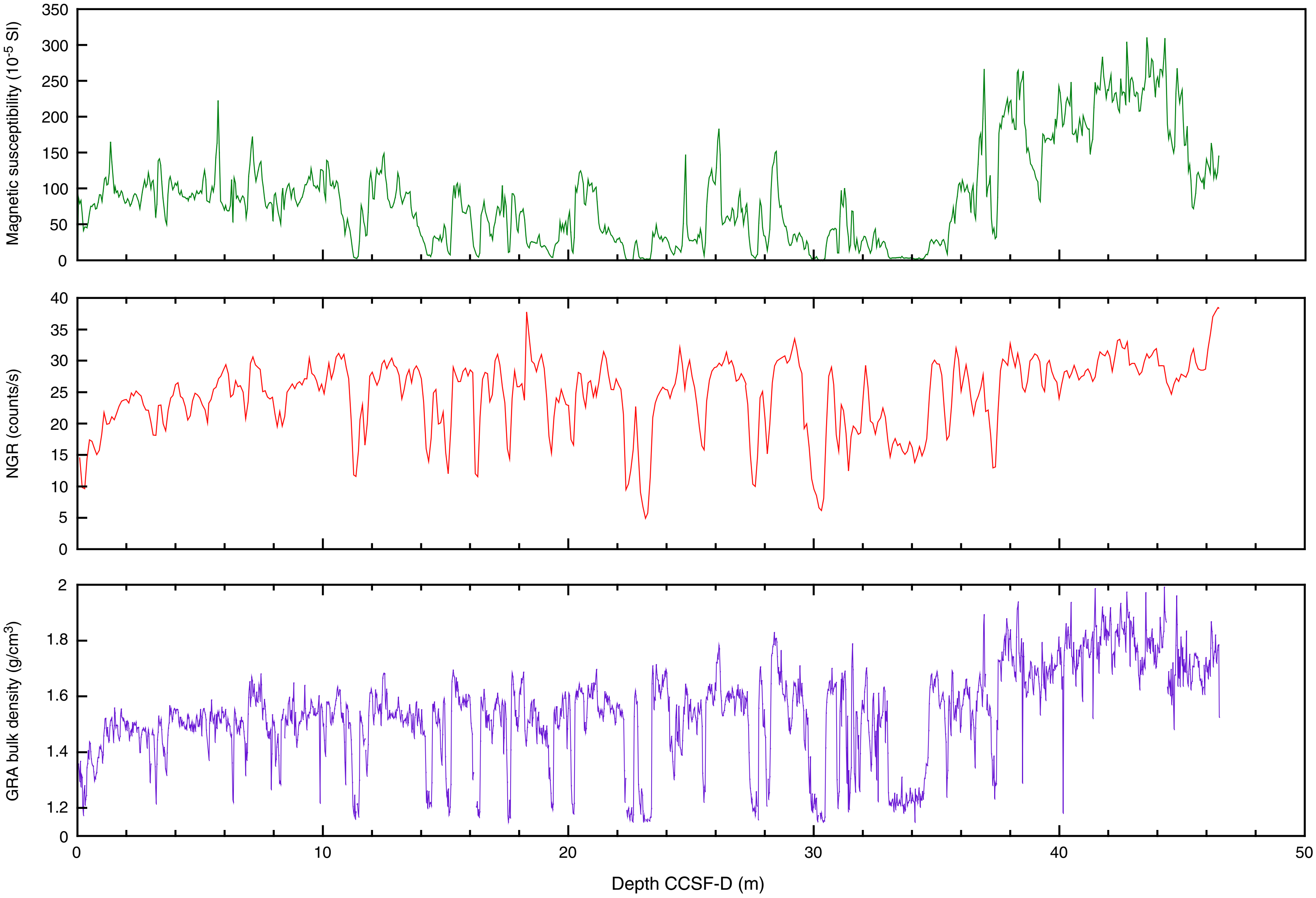

Figure F40. **A.** Mbsf vs. composite (CCSF-A) depth in the splice, Site U1342. A 1:1 line is also shown for comparison. **B.** Growth of cumulative depth offset (m) vs. mbsf in the splice. The affine growth factor is 1.06.

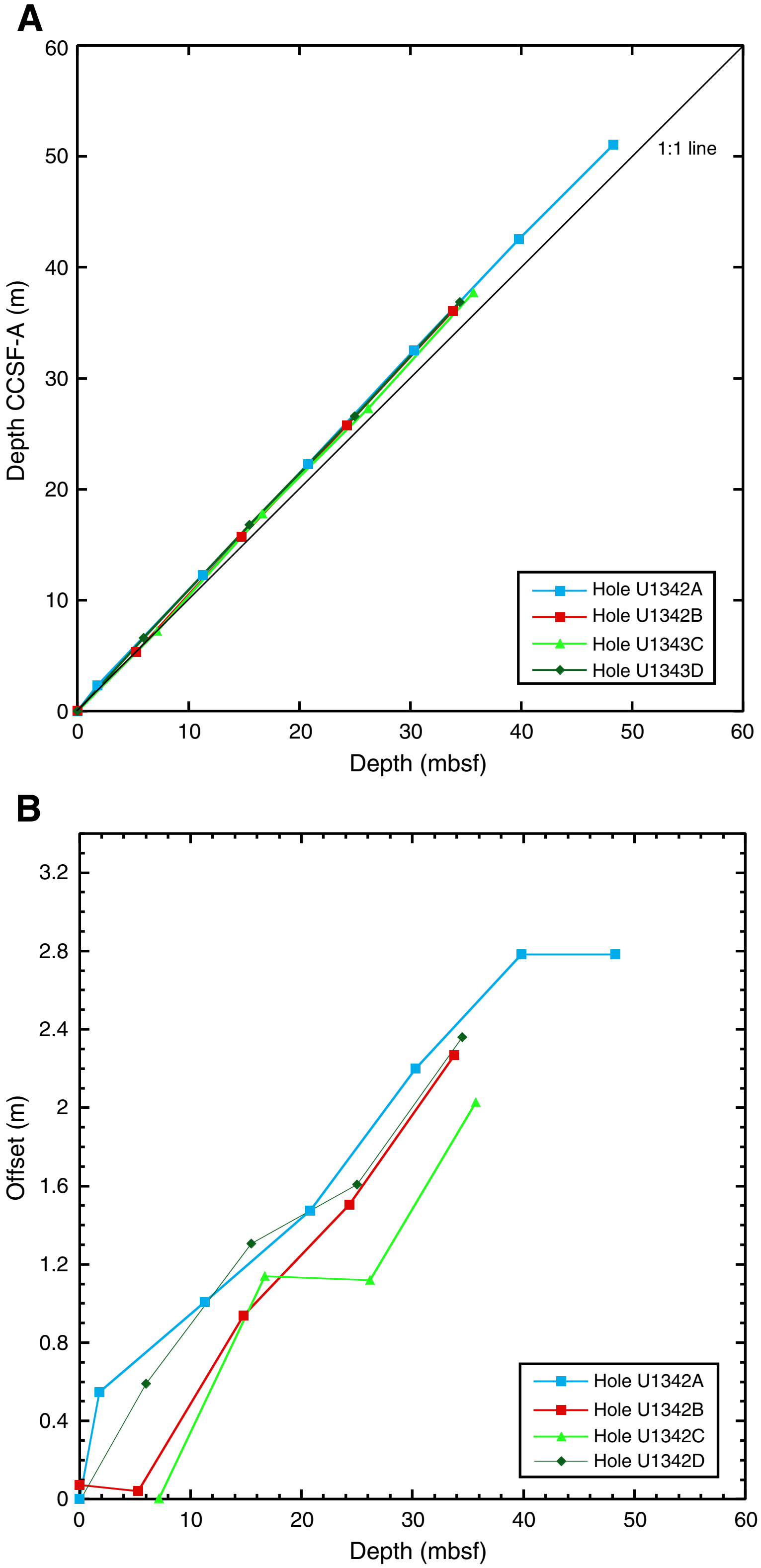

Figure F41. **A.** Records of APCT-3 penetrations and temperature decays, Hole U1342C. **B.** Summary of temperature measurements.

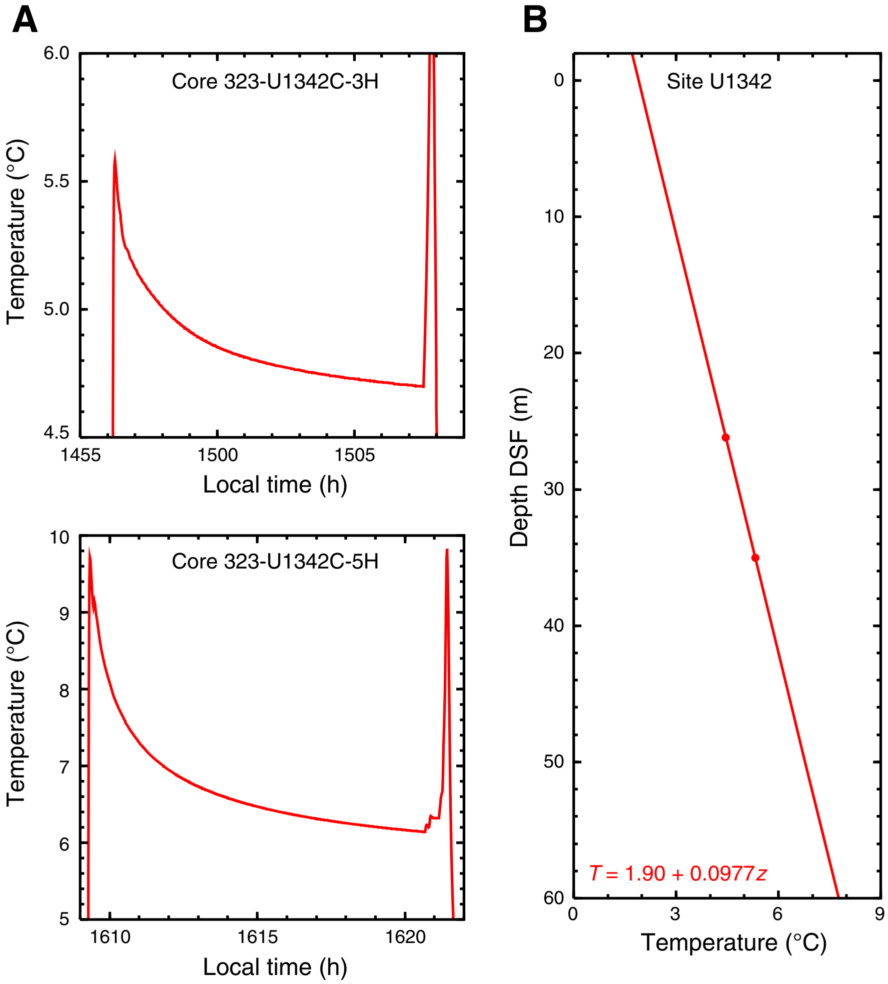

Figure F42. Summary of Bowers Ridge heat flow measurements recorded during Expedition 323 (black) compared with previously recorded values. All values are in mW/m²; the global heat flow database of the international heat flow commission can be found at **www.heatflow.und.edu/index.html.**

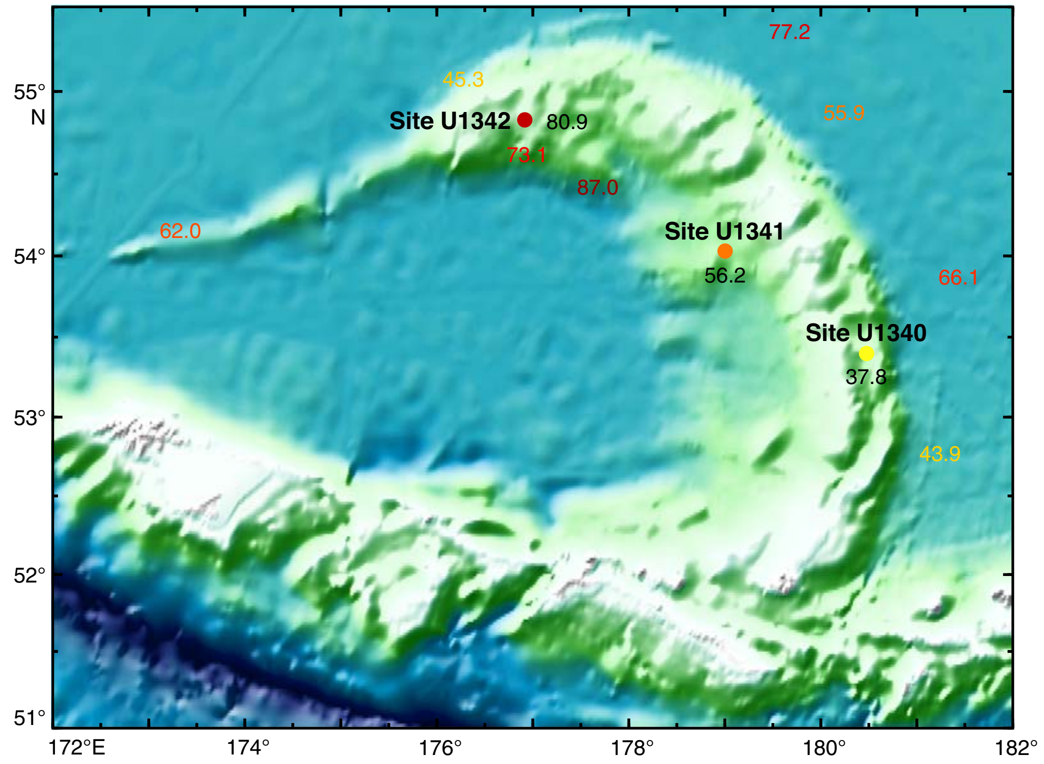

Table T1. Coring summary, Holes U1342A, U1342B, U1342C, and U1342D. (See table notes.) (Continued on next page.)

Hole U1342A
Latitude: 54°49.6987′N
Longitude: 176°55.0027′E
Time on hole (h): 13.83
Seafloor (drill pipe measurement from rig floor, m DRF): 829.7
Distance between rig floor and sea level (m): 11.4
Water depth (drill pipe measurement from sea level, m): 818.3
Total depth (drill pipe measurement from rig floor, m DRF): 883.00
Total penetration (mbsf): 53.3
Total length of cored section (m): 50.3
Total core recovered (m): 57.39
Core recovery (%): 114.1
Total number of cores: 9

Hole U1342B
Latitude: 54°49.7004′N
Longitude: 176°55.0232′E
Time on hole (h): 3.5
Seafloor (drill pipe measurement from rig floor, m DRF): 830.4
Distance between rig floor and sea level (m): 11.5
Water depth (drill pipe measurement from sea level, m): 818.9
Total depth (drill pipe measurement from rig floor, m DRF): 873.70
Total penetration (mbsf): 43.3
Total length of cored section (m): 43.3
Total core recovered (m): 44.83
Core recovery (%): 103.53
Total number of cores: 5

Hole U1342C
Latitude: 54°49.7017′N
Longitude: 176°55.0411′E
Time on hole (h): 6.166
Seafloor (drill pipe measurement from rig floor, m DRF): 830.3
Distance between rig floor and sea level (m): 11.5
Water depth (drill pipe measurement from sea level, m): 818.8
Total depth (drill pipe measurement from rig floor, m DRF): 875.70
Total penetration (mbsf): 45.4
Total length of cored section (m): 45.4
Total core recovered (m): 47.06
Core recovery (%): 103.66
Total number of cores: 6

Hole U1342D
Latitude: 54°49.7018′N
Longitude: 176°55.0581′E
Time on hole (h): 33.25
Seafloor (drill pipe measurement from rig floor, m DRF): 829.7
Distance between rig floor and sea level (m): 11.5
Water depth (drill pipe measurement from sea level, m): 818.2
Total depth (drill pipe measurement from rig floor, m DRF): 957.40
Total penetration (mbsf): 127.7
Total length of cored section (m): 109.1
Total core recovered (m): 86.37
Core recovery (%): 79.17
Total number of cores: 18

Core	Date (2009)	UTC (h)	Depth DSF (m)		Length (m)		Recovery (%)	Comments
			Top	Bottom	Cored	Recovered		
323-U1342A-								
1H	4 Aug	0030	0.0	1.8	1.8	1.75	97	Oriented nonmagnetic barrel
2H	4 Aug	0115	1.8	11.3	9.5	9.61	101	Oriented nonmagnetic barrel
3H	4 Aug	0150	11.3	20.8	9.5	9.71	102	Oriented nonmagnetic barrel
4H	4 Aug	0225	20.8	30.3	9.5	9.95	105	Oriented nonmagnetic barrel
5H	4 Aug	0300	30.3	39.8	9.5	9.92	104	Oriented nonmagnetic barrel
6H	4 Aug	0335	39.8	48.3	8.5	8.55	101	Oriented nonmagnetic barrel
7H	4 Aug	0425	48.3	49.3	1.0	7.44	744	Oriented nonmagnetic barrel
8D			*****Drilled from 49.30 to 52.30 m DSF*****					
9X	4 Aug	0830	52.3	53.3	1.0	0.46	46	Steel barrel
				Cored totals:	53.3	57.39	108	

Table T1 (continued).

Core	Date (2009)	UTC (h)	Depth DSF (m)		Length (m)		Recovery (%)	Comments
			Top	Bottom	Cored	Recovered		
323-U1342B-								
1H	4 Aug	1025	0.0	5.3	5.3	5.33	101	Oriented nonmagnetic barrel
2H	4 Aug	1100	5.3	14.8	9.5	9.78	103	Oriented nonmagnetic barrel
3H	4 Aug	1135	14.8	24.3	9.5	10.01	105	Oriented nonmagnetic barrel
4H	4 Aug	1150	24.3	33.8	9.5	9.77	103	Oriented nonmagnetic barrel
5H	4 Aug	1220	33.8	43.3	9.5	9.94	105	Oriented nonmagnetic barrel
				Cored totals:	43.3	44.83	104	
323-U1342C-								
1H	4 Aug	1345	0.0	7.2	7.2	7.22	100	Oriented nonmagnetic barrel
2H	4 Aug	1430	7.2	16.7	9.5	9.84	104	Oriented nonmagnetic barrel
3H	4 Aug	1515	16.7	26.2	9.5	10.00	105	Oriented nonmagnetic barrel
4H	4 Aug	1545	26.2	35.7	9.5	9.80	103	Oriented nonmagnetic barrel
5H	4 Aug	1629	35.7	45.2	9.5	9.98	105	Oriented nonmagnetic barrel
6H	4 Aug	1800	45.2	45.4	0.2	0.22	110	Oriented nonmagnetic barrel
				Cored totals:	45.4	47.06	104	
323-U1342D-								
1H	4 Aug	1940	0.0	6.0	6.0	6.11	102	Oriented nonmagnetic barrel
2H	4 Aug	2010	6.0	15.5	9.5	9.83	103	Oriented nonmagnetic barrel
3H	4 Aug	2040	15.5	25.0	9.5	9.62	101	Oriented nonmagnetic barrel
4H	4 Aug	2110	25.0	34.5	9.5	9.83	103	Oriented nonmagnetic barrel
5H	4 Aug	2140	34.5	44.0	9.5	9.90	104	Oriented nonmagnetic barrel
6D	*****Drilled from 44.00 to 62.60 m DSF*****							
7X	5 Aug	0255	62.6	66.6	4.0	0.55	14	Steel barrel
8X	5 Aug	0515	66.6	71.6	5.0	1.66	33	Steel barrel
9X	5 Aug	0625	71.6	75.6	4.0	3.84	96	Steel barrel
10X	5 Aug	0825	75.6	82.1	6.5	4.66	72	Steel barrel
11X	5 Aug	1030	82.1	87.9	5.8	3.34	58	Steel barrel
12X	5 Aug	1210	87.9	90.1	2.2	2.01	91	Steel barrel
13X	5 Aug	1340	90.1	94.9	4.8	4.64	97	Steel barrel
14X	5 Aug	1530	94.9	102.5	7.6	3.48	46	Steel barrel
15X	5 Aug	1710	102.5	106.1	3.6	1.48	41	Steel barrel
16X	5 Aug	1840	106.1	115.1	9.0	2.49	28	Steel barrel
17X	5 Aug	2030	115.1	117.7	2.6	5.70	219	Steel barrel
18X	5 Aug	2105	117.7	121.7	4.0	3.00	75	Steel barrel
19X	5 Aug	2340	121.7	127.7	6.0	4.23	70	Steel barrel
				Cored totals:	127.7	86.37	79	
				Site totals:	269.7	235.65	94.98	

Notes: DRF = drilling depth below rig floor, mbsf = meters below seafloor, DSF = drilling depth below seafloor. UTC = Universal Time Coordinated.

Table T2. Datum events of radiolarians, diatoms, calcareous nannofossils, and silicoflagellates, Holes U1342A, U1342B, U1342C, and U1342D. (See table notes.)

Datum event	Taxon	Age (Ma)	Depth (mbsf)				Depth CCSF-A (m)			
			Hole U1342A	Hole U1342B	Hole U1342C	Hole U1342D	Hole U1342A	Hole U1342B	Hole U1342C	Hole U1342D
LO *Lychnocanoma nipponica sakaii*	Radiolarian	0.05	0.9	2.7	3.6	3.1	0.9	2.7	3.6	3.0
LO *Amphimelissa setosa*	Radiolarian	0.08–1	—	—	3.6	—	—	—	3.6	—
LO *Spongodiscus* sp.	Radiolarian	0.28–0.32	6.6	10.2	12.1	11.0	6.8	10.1	11.9	11.0
LO *Axoprunum acquilonium*	Radiolarian	0.25–0.43	16.2	19.8	12.1	20.5	16.8	20.0	11.9	21.2
LO *Proboscia curvirostris*	Diatom	0.3	16.2	10.2	21.8	11.0	16.8	10.1	22.0	11.0
LO *Pseudoemiliania lacunosa*	Calcareous nannofossil	0.44	16.2	—	—	—	16.8	—	—	—
LO *Dictyocha subarctios*	Silicoflagellate	0.73–0.75	25.9	—	—	30.0	26.8	—	—	31.2
LO *Eucyrtidium matuyamai*	Radiolarian	0.9–1.5	—	29.3	—	—	—	30.3	—	—

Notes: For last occurrences (LO), the depth was estimated as the midpoint between the depth at which the species was last observed and the depth of the next sample above. — = not applicable.

Table T3. Calcareous nannofossil range chart, Holes U1342A, U1342B, U1342C, and U1342D. (See table notes.)

Core, section	Martini (1971) zone	Abundance	Preservation	*Coccolithus pelagicus*	*Cyclococcolithus leptoporus*	*Emiliania huxleyi*	*Gephyrocapsa* (small)	*Gephyrocapsa* (medium)	*Gephyrocapsa* (large)	*Pseudoemiliania lacunosa*	*Reticulofenestra minuta*	*Reticulofenestra minutula*	Other taxa	Comments
323-U1342A-														
1H-CC	NN21	A	G	A		F								
2H-CC		R	M-G	R			R	R						
3H-CC	NN19	C	M-G	F			F	F		R				
4H-CC		B												
5H-CC		R	G	R										
6H-CC		B												
7H-CC		B												
8H-CC		—												Drilled interval
9X-CC		—												Hard rock
323-U1342B-														
1H-CC		A	M-G	A			F	R			R			
2H-CC		B												
3H-CC		B												
4H-CC		B												
5H-CC		B												
323-U1342C-														
1H-CC		B												
2H-CC		R	G	R										
3H-CC		R	M				R							
4H-CC		B												
5H-CC		B												
6H-CC		B												
323-U1342D-														
1H-CC		F	M-G	F		R	R	R						Reworked specimens (*Dictyococcites* spp. and *Discoaster* spp.)
2H-CC	NN21	F	M-G	F	R	R	R							Reworked specimens (*Reticulofenestra asanoi* and *Coccolithus pelagicus*)
3H-CC		R	M-G	R			R							
4H-CC		C	M-G	C										Reworked specimens (*Coccolithus pelagicus* and *Coccolithus miopelagicus*)
5H-CC		B												
6H-CC		—												Drilled interval
7H-CC		—												Drilled interval
8H-CC		—												Drilled interval
9X-CC		B												

Notes: Abundance: A = abundant, C = common, F = few, R = rare, B = barren, — = no sample. Preservation: G = good, M = moderate.

Table T4. Planktonic foraminifer range chart, Holes U1342A, U1342B, U1342C, and U1342D. (See table notes.)

Core, section, interval (cm)	Abundance	Preservation	*Globigerina bulloides*	*Globigerina umbilicata*	*Neogloboquadrina pachyderma* (dex)	*Neogloboquadrina pachyderma* (sin)	*Turborotalia quinqueloba*	Other observations
323-U1342A-								
Mudline	D	G	F			D		Dominant foraminifers, abundant diatoms, few sponge spicules, rare rock fragments
1H-CC	D	G	A			D		Dominant foraminifers, abundant rock fragments, rare sponge spicules
2H-CC	A	G	F			A		Dominant sand, abundant sponge spicules
3H-CC	D	G			A	D		Dominant foraminifers, abundant rock fragments, rare sponge spicules
4H-CC	A	G	F	P	F	F		Dominant sand, abundant sponge spicules, few bubble-walled glass shards
5H-CC	B							Dominant sand, glauconite, rare sponge spicules
6H-CC	B							Dominant sand, glauconite, rare sponge spicules
7H-CC	B							Dominant sand, glauconite, rare sponge spicules
323-U1342B-								
Mudline	D	G	R			D		Dominant foraminifers, few diatoms
1H-CC	D	G	R	R		D		Dominant foraminifers
2H-CC	A	G	F	P	R	A		Dominant sand, abundant sponge spicules
3H-CC	F	G	R	P	F	F		Dominant sand, abundant sponge spicules
4H-CC	R	M			R	R		Dominant sand, abundant sponge spicules, few bubble-walled glass shards
5H-CC	B							Dominant sand, abundant sponge spicules, few bubble-walled glass shards
323-U1342C-								
Mudline	D	VG	F			D		Dominant foraminifers, few diatoms
1H-CC	D	VG	R			D		Dominant foraminifers
2H-2W, 24–26	D	G	R	R		D		Dominant foraminifers, abundant large bivalve fragments, abundant diatoms
2H-CC	A	G	R	P		A		Dominant sand, abundant sponge spicules, few bubble-walled glass shards
3H-CC	A	G				A		Dominant sand, abundant sponge spicules, few bubble-walled glass shards
4H-CC	A	G	R		R	A		Dominant sand, abundant sponge spicules
5H-CC	B							Dominant rock fragments with “breadcrust”-like surface, abundant sponge spicules and frames
6H-CC	B							Dominant sand, glauconite, rare sponge spicules
323-U1342D-								
Mudline	D	VG	R	R		D	P	Dominant foraminifers, abundant diatoms, few sponge spicules, rare sand
1H-CC	D	VG	R	R		D		Dominant foraminifers
2H-CC	A	VG	F	F	P	D		Dominant sand, abundant sponge spicules
3H-CC	F	G	R			F		Dominant sand, abundant sponge spicules
4H-CC	D	G	A		F	A		Dominant foraminifers
5H-CC	P	G	P					Dominant sand, glauconite, rare sponge spicules
9X-CC	B							Rock fragments

Notes: Abundance: D = dominant, A = abundant, F = few, R = rare, P = present, B = barren. Preservation: VG = very good, G = good, M = moderate. Dex = dextral, sin = sinistral.

Table T5. Benthic foraminifer and ostracode range chart, Holes U1342A, U1342B, U1342C, and U1342D. (See table notes.)

Core, section, interval (cm)	Abundance	Preservation	*Alabaminella weddellensis*	*Bolivina* sp.	*Brizalina* cf. *spathula*	*Brizalina earlandi*	*Brizalina pygmaea*	*Bulimina* aff. *exilis*	*Cancris* cf. *philippinensis*	*Cassidulina laevigata* var. *carinata*	*Cassidulina* sp.	*Cassidulinoides tenuis*	*Cibicidoides* sp.	*Cibicidoides* cf. *subhaidingeri*	*Cyclammina cancellata*	*Eggerella bradyi*	*Epistominella pulchella*	*Globobulimina pacifica*	*Gyroidinoides soldanii*	*Islandiella norcrossi*	*Lagena* spp.	*Lenticulina* sp.	*Melonis barleeanum*	*Nodosaria advena*	*Nodosaria* spp.	*Nonionella labradorica*	*Nonionella turgida digitata*	*Oridorsalis umbonatus*	*Procerolagena* cf. *gracillima*	*Pullenia* sp.	*Pyrgo* sp.	*Stainforthia* aff. *fusiformis*	*Triloculina* cf. *trihedra*	*Uvigerina auberiana*	*Uvigerina* cf. *peregrina*	*Valvulineria* sp.	*Krithe* sp.	Other observations
323-U1342A-																																						
Mudline	A	VG			A	F	A	F			A							R														R				R		Dominant planktonic foraminifers, abundant diatoms and sponge spicules
1H-CC	A	G		P				R	R	F	A							R						P					P		P		R		A	R	P	Planktonic ooze, some sponge spicules
2H-CC	D	G	F			R	F	A	F		R						F	A																	D	F		Rare sponge spicules
3H-CC	A	G	R				P				R								F	F		R													A	F		Planktonic ooze, some sponge spicules
4H-CC	A	G																																	A			Monospecific fauna—winnowed?, sponge spicules
5H-CC	B																																					Sand, glauconite concretions
6H-CC	B																																					Sand, glauconite concretions
7H-CC	B														P																							Sand, glauconite concretions
323-U1342B-																																						
Mudline	D	VC			F	A	R	F			D							R			R								P	P		R	P			R		Dominant foraminifers
1H-CC	D	G			R		P			R	D		P												P					R	P	P		P	A			Sand
2H-CC	F	G			F	R	R	F			F							R	R	F						P								R	F	R		Sand, sponge spicules
3H-CC	R	G						R		P	R					P														P					P			Sand, sponge spicules
4H-CC	R	M			P						R														P										R			Sand, sponge spicules
5H-CC	B																																					Sand, sponge spicules
323-U1342C-																																						
Mudline	D	VG			F	A	A	A	F											F																		Planktonic ooze
1H-CC	D	VG	F								F						A	P								F		R							D	F		Abundant shells (bivalve?)
2H-CC	A	G					P	A			R	P						R	R																F	R		Sand, sponge spicules
2H-2, 24–26	A	G				A	R	A			F							P																	F	R		
3H-CC	R	G			P			R		P	P							P																	A			Sand, sponge spicules
4H-CC	F	G					P	P		R	R			P					P								R								F			Sand, sponge spicules
5H-CC	B																																					Rock fragments, abundant sponge spicules
6H-CC	B																																					Sand, glauconite concretions
323-U1342D-																																						
Mudline	D	VG			A	F	A	F			D							P														R				R		Dominant planktonic foraminifers, abundant sponge spicules
1H-CC	D	VG			P	P		A	A	R	D								F				P												D	R		Planktonic ooze
2H-CC	A	VG				P		F	R		P							F		F										P					F	F		
3H-CC	A	G					F											R		F															A	A		
4H-CC	D	G			A	R		A	R	R										A					R	R				R					A			Planktonic ooze
5H-CC	P	G																																	P			Sand, glauconite concretions
9X-CC	B																																					Rock fragments

Notes: Abundance: D = dominant, A = abundant, F = few, R = rare, P = present, B = barren. Preservation: VG = very good, G = good, M = moderate.

Table T6. Diatom range chart, Holes U1342A, U1342B, U1342C, and U1342D. (See table notes.)

Core, section	Depth (mbsf)		Abundance	Preservation	*Actinocyclus curvatulus*	*Actinocyclus ingens*	*Actinocyclus ingens nodus*	*Actinocyclus ochotensis*	*Actinocyclus oculatus*	*Actinoptychus senarius*	*Arachnoidiscus* spp.	*Asteromphalus brookei*	*Asteromphalus robustus*	*Bacteriosira fragilis*	*Chaetoceros* resting spore	*Chaetoceros* vegetative spore	*Cocconeis costata*	*Coscinodiscus marginatus*	*Coscinodiscus oculus-iridis*	*Cyclotella* spp.	*Delphineis surirella*	*Denticulopsis* spp.	*Detonula confervacea*	*Eunotia* spp.	*Fragilariopsis cylindrus*	*Mediaria splendida*	*Navicula* spp.	*Neodenticula kamtschatica*	*Neodenticula koizumii*	*Neodenticula seminae*	*Nitzschia* spp.	*Odontella aurita*	*Opephora marina*	*Paralia sol*	*Paralia sulcata*	*Porosira glacialis*	*Proboscia barboi*	*Proboscia curvirostris*	*Rhabdonema* spp.	*Rhizosolenia hebetata* f. *hebetata*	*Rhizosolenia hebetata* f. *hiemalis*	*Rhizosolenia hebetata* f. *semispina*	*Rhizosolenia* spp.	*Stellarima microtrias*	*Stephanopyxis horridus*	*Stephanopyxis turris*	*Stephanopyxis zabelinae*	*Tabellaria* spp.	*Thalassionema bacillaris*	*Thalassionema nitzschioides*	*Thalassiosira antarctica* spore	*Thalassiosira antiqua*	*Thalassiosira* cf. *leptopus*	*Thalassiosira jouseae*	*Thalassiosira latimarginata* s.l.	*Thalassiosira oestrupii*	*Thalassiothrix longissima*	Diatom zone (NPD) in Yanagisawa and Akiba (1998)
	Top	Bottom																																																								
323-U1342A-																																																										
1H-CC	1.55	1.75	F	P													C				C								C	A					C							C															C		*Neodenticula seminae* (NPD12)
2H-CC	11.19	11.41	A	M-G	C																									D												F									F				C	F		
3H-CC	20.80	21.01	F	P-M	A			R	C									F	F		R							R	R	C							C	F		R		F				R				R					C	C	F	*Proboscia curvirostris* (NPD11)
4H-CC	30.48	30.75	A	G	C				C								R	R											C	A						F	F	R				R		R							F				C	R	F	
5H-CC	40.00	40.22	C	M-G	C			R	A				R	R				R	R						R				C	C				R		R	F			R					F						C		R	C	R	C	C	*Neodenticula koizumii* (NPD9) ?
6H-CC	48.25	48.35	R	P-M	A				C		F							C												F							C	F							F	C								F	C		F	Undefined
7H-CC	55.64	55.74	F	P-M	F	C	F			C	R						R					D				R			R																													
323-U1342B-																																																										
1H-CC	5.14	5.33	R-F	P	F													R												R					C					F	D										F			R	F		C	*Neodenticula seminae* (NPD12)
2H-CC	14.81	15.08	F	P	C										F	F		F												A								F	R	R	R		F								F			R	C	R	R	*Proboscia curvirostris* (NPD11)
3H-CC	24.46	24.81	F	M	C					R		R				R		C						R						C	R				R	R		F		F	R					C					A	R		R	C		F	
4H-CC	33.80	34.07	C	M	F				R									C			R									A						R	C	C		R	C		F								F		R		C		R	
5H-CC	43.50	43.74	C	M	A				F									R											F	C							C	R							C	F	F					R			C			*Neodenticula koizumii* (NPD9) ?
7H-CC	55.64	55.64	R	P	C				C																					A					C			C			C												C		C			Undefined
323-U1342C-																																																										
1H-CC	7.09	7.22	A	M-G	C							R																	R	C										C		F									C	R			A	F	R	*Neodenticula seminae* (NPD12)
2H-CC	16.85	17.04	R	P	C																									A					A			F		C						F				C	F				F	C		
3H-CC	26.37	26.70	20.80	21.01	C								R	R	C	C		R	R	R			R				F			C			R					F		F	C	R				F		R			F				C		C	*Proboscia curvirostris* (NPD11)
4H-CC	35.75	36.00	30.48	30.48	C													C											R	D								R		R	R					R					F				F		R	
5H-CC	45.20	45.42	B																																																							Undefined
6H-CC	45.32	45.68	F	P		C				R								D	F																																							
323-U1342D-																																																										
1H-CC	5.95	6.11	C	P-M	C													R	F		R								R	A										A		R													C	R	R	*Neodenticula seminae* (NPD12)
2H-CC	15.69	15.83	F	P-M	A				F										R											C		R			C		F	F		C											F				F	R	C	*Proboscia curvirostris* (NPD11)
3H-CC	24.94	25.12	C	P	A													R	R										R	C					F		C	F		C		R								R	C				F	F	F	
4H-CC	34.62	34.83	A	M-G	C														F										C	A						R	R	R		R		F				R					R				C	F	F	
5H-CC	44.18	44.40	F	P-M	A				R										F										R	F					C		C					R				C	R	C				R				F	C	F	*Neodenticula koizumii* (NPD9) ?

Notes: Abundance: A = abundant, F = few, R = rare, B = barren. Preservation: G = good, M = moderate, P = poor.

Table T7. Silicoflagellate and ebridian range chart, Holes U1342A and U1342D. (**See table notes.**)

	Depth (mbsf)				Silicoflagellates									Ebridians	
Core, section	Top	Bottom	Abundance	Preservation	Aberrant silicoflagellates	*Dictyocha subarctios*	*Distephanus speculum*	*Distephanus speculum**	*Distephanus medianoctisol*	*Distephanus medianoctisol**	*Distephanus octangulatus*	*Distephanus octonarius*	*Distephanus quinquangellus*	*Ebriopsis antiqua antiqua*	Zone in Ling (1992)
323-U1342A-															
1H-CC	1.65	1.75	B												Undefined
2H-CC	11.31	11.41	C	M-G		T	T				F	F			
3H-CC	20.91	21.01	R	P-M							R				
4H-CC	30.65	30.75	C	M		C	R	R	R						
5H-CC	40.12	40.22	F	M	T		R	R							
6H-CC	48.25	48.35	B												
7H-CC	55.64	55.74	F	M			R	R					R	R	
323-U1342D-															
1H-CC	6.01	6.11	R	P-M							R				Undefined
2H-CC	15.73	15.83	F	M			F			T					
3H-CC	25.02	25.12	B												
4H-CC	34.73	34.83	C	M-G	T	R	R		T	R		C			
5H-CC	44.30	44.40	R	M-G			R							R	

Notes: * = with short radial spines. Abundance: C = common, F = few, R = rare, T = trace, B = barren. Preservation: G = good, M = moderate, P = poor.

Table T8. Radiolarian datum events, Holes U1342A, U1342B, U1342C, and U1342D. (See table note.)

			Hole U1342A				Hole U1342B			
			Core, section		Depth (mbsf)		Core, section		Depth (mbsf)	
Zone	Marker species	Age (Ma)	Top	Bottom	Top	Bottom	Top	Bottom	Top	Bottom
Botryostrobus aquilonaris	T *Lychnocanoma nipponica sakaii*	0.05		1H-CC	0	1.75		1H-CC	0	5.33
	T *Amphimelissa setosa*	0.08–0.10	Not found				Not found			
	T *Spongodiscus* sp.	0.28–0.32	1H-CC	2H-CC	1.75	11.41	1H-CC	2H-CC	5.33	15.08
	T *Axoprunum acquilonium*	0.25–0.43	2H-CC	3H-CC	11.41	21.01	2H-CC	3H-CC	15.08	24.56
Stylatractus universus	T *Stylatractus universus*	0.41–0.51	6H-CC	7H-CC	48.35	55.74	Not found			
Eucyrtidium matuyamai	T *Eucyrtidium matuyamai*	0.9–1.5	Not found				3H-CC	4H-CC	24.56	34.07
	B *Eucyrtidium matuyamai*	1.7–1.9								

Note: T = top, B = bottom.

Table T8 (continued).

			Hole U1342C				Hole U1342D			
			Core, section		Depth (mbsf)		Core, section		Depth (mbsf)	
Zone	Marker species	Age (Ma)	Top	Bottom	Top	Bottom	Top	Bottom	Top	Bottom
Botryostrobus aquilonaris	T *Lychnocanoma nipponica sakaii*	0.05		1H-CC	0	7.19		1H-CC	0	6.11
	T *Amphimelissa setosa*	0.08–0.10		1H-CC	0	7.19	Not found			
	T *Spongodiscus* sp.	0.28–0.32	1H-CC	2H-CC	7.19	17.04	1H-CC	2H-CC	6.11	15.83
	T *Axoprunum acquilonium*	0.25–0.43	1H-CC	2H-CC	7.19	17.04	2H-CC	3H-CC	15.83	25.12
Stylatractus universus	T *Stylatractus universus*	0.41–0.51	Not found				Not found			
Eucyrtidium matuyamai	T *Eucyrtidium matuyamai*	0.9–1.5	Not found				Not found			
	B *Eucyrtidium matuyamai*	1.7–1.9								

Table T9. Radiolarian range chart, Holes U1342A, U1342B, U1342C, and U1342D. (**See table notes.**)

Core, section	Depth (mbsf)		Abundance	Preservation	*Actinomma boreale*	*Actinomma medianum*	*Amphimelissa setosa*	*Axoprunum acquilonium*	*Botryostrobus aquilonaris*	*Ceratospyris borealis*	*Collosphaera pyloma*	*Cycladophora cornutoides*	*Cycladophora cosma*	*Cycladophora davisiana*	*Cycladophora sakaii*	*Cyrtocapsella japonica*	*Dendrospyris sakaii*	*Dictyophimus bullatus*	*Dictyophimus hirundo*	*Eucyrtidium asanoi*	*Eucyrtidium inflatum*	*Eucyrtidium matuyamai*	*Lamprocyrtis heteroporos*	*Larcopyle butschlii*	*Lipmanella redondoensis*	*Lithelius barbatus*	*Lychnocanoma magnacornuta*	*Lychnocanoma nipponica sakaii*	*Lychnocanoma parallelipes*	*Phormostichoartus fistula*	*Porodiscus circularis*	*Sphaeropyle langii-robusta* group	*Spongodiscus* sp.	*Spongopyle osculosa*	*Spongotrochus glacialis*	*Spongurus pylomaticus*	*Stichocorys delmontensis*	*Stichocorys peregrina*	*Stylatractus universus*	*Stylochlamydium venustum*	*Stylodictya validispina*	*Thecosphaera akitaensis*
	Top	Bottom																																								
323-U1342A-																																										
1H-CC	1.65	1.75	F	M	F					F		F		F					F									F							F					F	F	
2H-CC	11.31	11.41	C	M	F				F	F				C					F					F				F					F		F					F	F	
3H-CC	20.91	21.01	C	P				F	F	C				A					F														F		F					F	F	
4H-CC	30.65	30.75	F	M				F		C				C					F														F		F						F	
5H-CC	40.12	40.22	C	P				F		F				F					F					F											F						F	
6H-CC	48.25	48.35	F	M				F		F				F																					F						F	
7H-CC	55.64	55.74	F	M																													F	F		F			F			
323-U1342B-																																										
1H-CC	5.23	5.33	F	M	F	F				F																		F													F	
2H-CC	14.98	15.08	C	M	F				F	C				C										F				F					A		F					F	F	
3H-CC	24.46	24.56	F	M				F		C				F																			C		F							
4H-CC	33.97	34.07	C	M				F		C				F								F											F	F	F						F	
5H-CC	43.64	43.74	F	G				F		C				F	F																		F		F						F	
323-U1342C-																																										
1H-CC	7.09	7.19	C	G			F			C				A										F				F							F					F	F	
2H-CC	16.94	17.04	F	P	F			F		C				C					F									F					F		F						F	
3H-CC	26.60	26.70	C	M	C	F		F		C				C					F														F		F						F	
4H-CC	35.90	36.00	F	M					F	F				C														F					F		F							
5H-CC	45.37	45.42	N	P																																						
6H-CC	45.58	45.68	F	M																				F									F		F					F	F	
323-U1342D-																																										
1H-CC	6.01	6.11	C	P					F	C				F										F				C							F						C	
2H-CC	15.73	15.83	F	M	F				F	F				F										F									F								F	
3H-CC	25.02	25.12	F	P				F	F	F				F																			F		F						F	
4H-CC	34.73	34.83	F	M	F			F		F				F										F								F	F		F							
5H-CC	44.30	44.40	F	M				F		C				F	F																			F	F						F	

Notes: Abundance: A = abundant, F = few, C = common, N = none. Preservation: G = good, M = moderate, P = poor.

Table T10. Dinoflagellate cyst, pollen, and palynomorph range chart, Holes U1342A and U1342B. (**See table notes.**)

	Depth (mbsf)			Marine		Pollen and spores					Dinoflagellate cyst assemblages															
Core, section	Top	Bottom	Preservation	Dinoflagellate cysts	Organic lining of foraminifers	Pollen (herbs)	Pollen (trees)	Pollen (shrubs)	Spores (moss and fern)	Reworked palynomorphs	*Bitectatodinium tepikiense*	*Brigantedinium cariacoense*	*Brigantedinium simplex*	*Brigantedinium* spp.	*Gymnodinium catenatum*	*Impagidinium pallidum*	*Impagidinium* spp.	*Islandinium imnutum*	*Islandinium* morphotype *cesare*	*Nematosphaeropsis lemniscata*	*Operculodinium centrocarpum*	*Operculodinium centrocarpum* var. short processes	*Pentapharsodinium dalei*	*Polykrikos* - Arctic morphotype	*Polykrikos schwartzii*	*Protoperidinium americanum*
323-U1342A-																										
1H-CC	1.65	1.75	G	C	C	R	R	F	F	R	A	R	A	D				F								
2H-CC	11.31	11.41	M	C	C		C	R	F	F			A	D												
3H-CC	20.91	21.01	G	A	C	R	C	C	C	F	F	R	F	A			R	R		F	A	A	R	A		
4H-CC	30.65	30.75	M	C	C		C	R	R	F	R	A	A	D				A		R						
5H-CC	40.12	40.22	M	C	C		F	R	R	R	D			D												F
6H-CC	48.25	48.35	P	R			R	F			P															
7H-CC	55.64	55.74	P	F	C	R	F	R	R	R			P	P												
323-U1342B-																										
1H-CC	5.23	5.33	G	C	C	R	R	R	R	R		F	A	D	F			F						R	F	
2H-CC	14.98	15.08	M	C	C	R	C	C	R	R	F	F		D		F					F		F			
3H-CC	24.71	24.81	M	C	C		C		F	C		F	D	D				A								
4H-CC	33.97	34.07	M	C	C		C	R	C			R	A	D			R	A								
5H-CC	43.64	43.74	P	C	C		F	C	F	C				P												

Notes: Preservation: G = good, M = moderate, P = poor. Absolute abundance: A = abundant (>2000/cm^3), C = common (>200/cm^3), F = few (>100/cm^3), R = rare (<100/cm^3). Relative abundance of dinoflagellate cysts: D = dominant (>30%), A = abundant (>10%), F = few (>5%), R = rare (<5%), P = occurrence (when counts are <20).

Table T11. Chron ages and preliminary depths, Holes U1342A, U1342C, and U1342D. (**See table notes.**)

		Hole U1342A			Hole U1342C			Hole U1342D		
Event	Age (ka)	Core, section, interval (cm)	Depth (mbsf)	Sed. rate (cm/k.y.)	Core, section, interval (cm)	Depth (mbsf)	Sed. rate (cm/k.y.)	Core, section, interval (cm)	Depth (mbsf)	Sed. rate (cm/k.y.)
		323-U1342A-			323-U1342C-			323-U1342D-		
	0		0	3.2		0	3.2		0	3.2
B Brunhes	781	4H-3, 110	24.9	2.3	3H-6, 90	25.1	1.8	3H-7, 30	24.8	2.1
Kamikatsura Excursion	885	4H-5, 45	27.25	3.3	4H-1, 80	27	4.4	4H-2, 50	27	3.3
Santa Rosa Excursion	930				4H-2, 130	29	2.5	4H-3, 50	28.5	2.6
T Jaramillo	998				4H-4 (T)	30.7	5.1	4H-4, 80	30.3	5.0
B Jaramillo	1072	5H-3, 15	33.45	4.3	4H-6, 75	34.45	3.4	4H-7 (T)	34	4.2
Punaruu Excursion	1125	5H-4, 95	35.75	9.4	5H-1, 52.5	36.25	7.9	5H-2, 25	36.25	7.6
T Cobb Mountain	1173	6H-1, 45	40.25	10.4	5H3, 135	40.05	7.1	5H-4, 90	39.9	5.8
B Cobb Mountain	1185	6H-2, 20	41.5		5H-4, 70	40.9		5H-5, 10	40.6	

Notes: B = bottom, T = top. Sed. rate = sedimentation rate.

Table T12. Depths of possible dissolved magnetic grains, U1342A. (See table note.)

Depth (mbsf)	Corresponding MIS	Comments
10.6–11.0	9	Large decrease in intensity
13.2–13.6	11	Large decrease in intensity
15.1–15.4	13	Large decrease in intensity
18.1–18.4	15	Moderate decrease in intensity
20.8–21.2	17	Large decrease in intensity
21.4–22.0	17	Large decrease in intensity
25.8–26.2	19	Large decrease in intensity
28.2–28.9	25	Large decrease in intensity
30.8–32.3	29	Largest decrease in intensity

Note: MIS = marine isotope stage.

Table T13. Depths of possible authigenic magnetic minerals or ash, Hole U1342A. (See table notes.)

Depth (mbsf)	Corresponding MIS	Comments
1.35	2	Increase in MS only
5.20	6	
24.70	18	
27.85	22	Increase in MS only
41.50		Increase in remanence, not in MS
43.80		Increase in remanence, not in MS

Notes: MIS = marine isotope stage. MS = magnetic susceptibility.

Table T14. Moisture and density, Hole U1342C.

Core, section, interval (cm)	Depth (mbsf)	Density (g/cm^3)			Void ratio	Water content (%)	Porosity (%)
		Dry grain	Wet bulk	Dry bulk			
323-U1342C-							
1H-1, 29–31	0.3	2.81	1.40	0.62	3.80	55.76	79.19
1H-3, 29–31	3.3	2.52	1.42	0.68	2.86	51.74	74.10
1H-5, 29–31	6.3	2.73	1.50	0.78	2.67	48.08	72.74
2H-1, 29–31	7.5	2.63	1.53	0.84	2.23	44.71	69.02
2H-3, 29–31	10.5	2.69	1.54	0.86	2.25	44.36	69.23
2H-5, 29–31	13.5	2.64	1.52	0.84	2.28	45.14	69.54
3H-1, 29–31	17.0	2.72	1.65	1.03	1.72	37.86	63.26
3H-3, 29–31	20.0	2.58	1.57	0.92	1.89	41.19	65.34
3H-5, 29–31	23.0	2.58	1.39	0.64	3.28	54.37	76.63
4H-1, 29–31	26.5	2.52	1.41	0.68	2.88	51.88	74.23
4H-3, 29–31	29.5	2.52	1.29	0.48	4.69	63.10	82.44
4H-5, 29–31	32.5	2.22	1.21	0.37	5.49	69.20	84.59
5H-1, 29–31	36.0	2.74	1.67	1.05	1.68	37.13	62.68
5H-3, 29–31	39.0	2.62	1.79	1.28	1.09	28.76	52.14
5H-5, 29–31	42.0	2.70	1.75	1.18	1.34	32.40	57.27

Table T15. Affine table indicating the amount that each core in each hole needs to be offset in order to construct a continuous record, Site U1342. (See table note.)

	Depth (mbsf)		Offset	Depth CCSF-A (m)		Recovered	Recovery
Core	Top	Bottom	(m)	Top	Bottom	(m)	(%)
323-U1342A-							
1H	0.00	1.80	0.00	0.00	1.80	1.75	97
2H	1.80	11.30	0.55	2.35	11.85	9.61	101
3H	11.30	20.80	1.01	12.31	21.81	9.71	102
4H	20.80	30.30	1.47	22.27	31.77	9.95	105
5H	30.30	39.80	2.20	32.50	42.00	9.92	104
6H	39.80	48.30	2.78	42.58	51.08	8.55	101
7H	48.30	49.30	2.78	51.08	52.08	7.44	744
8D	49.30	52.30	—	—	—	0.00	0
9X	52.30	53.30	—	—	—	0.46	46
323-U1342B-							
1H	0.00	5.30	0.07	0.07	5.37	5.33	101
2H	5.30	14.80	0.04	5.34	14.84	9.78	103
3H	14.80	24.30	0.94	15.74	25.24	10.01	105
4H	24.30	33.80	1.50	25.80	35.30	9.77	103
5H	33.80	43.30	2.27	36.07	45.57	9.94	105
323-U1342C-							
1H	0.00	7.20	–0.03	–0.03	7.17	7.22	100
2H	7.20	16.70	0.01	7.21	16.71	9.84	104
3H	16.70	26.20	1.14	17.84	27.34	9.67	102
4H	26.20	35.70	1.12	27.32	36.82	9.80	103
5H	35.70	45.20	2.03	37.73	47.23	9.98	105
6H	45.20	45.40	—	—	—	0.22	110
323-U1342D-							
1H	0.00	6.00	–0.01	–0.01	5.99	6.11	102
2H	6.00	15.50	0.59	6.59	16.09	9.83	103
3H	15.50	25.00	1.31	16.81	26.31	9.62	101
4H	25.00	34.50	1.61	26.61	36.11	9.83	103
5H	34.50	44.00	2.36	36.86	46.36	9.90	104
6D	44.00	62.60	—	—	—	0.00	0
7X	62.60	66.60	—	—	—	0.55	14
8X	66.60	71.60	—	—	—	1.66	33
9X	71.60	75.60	—	—	—	3.84	96
10X	75.60	82.10	—	—	—	4.66	72
11X	82.10	87.90	—	—	—	3.34	58
12X	87.90	90.10	—	—	—	2.01	91
13X	90.10	94.90	—	—	—	4.64	97
14X	94.90	102.50	—	—	—	3.48	46
15X	102.50	106.10	—	—	—	1.48	41
16X	106.10	115.10	—	—	—	2.49	28
17X	115.10	117.70	—	—	—	5.70	219
18X	117.70	121.70	—	—	—	3.00	75
19X	121.70	127.70	—	—	—	4.23	70

Note: — = not applicable.

Table T16. Splice table indicating tie points between holes, Site U1342. Sampling along the splice should be used to construct a continuous record.

	Depth				Depth	
Hole, core, section, interval (cm)	mbsf	CCSF-D (m)		Hole, core, section, interval (cm)	mbsf	CCSF-D (m)
323-				323-		
U1342D-1H-4, 75.1	5.25	5.24	Tie to	U1342A-2H-2, 139.8	4.70	5.24
U1342A-2H-7, 16.1	10.96	11.51	Tie to	U1342C-2H-3, 130.2	11.50	11.51
U1342C-2H-7, 28.2	16.48	16.49	Tie to	U1342A-3H-3, 118.1	15.48	16.49
U1342A-3H-6, 125.8	20.06	21.06	Tie to	U1342C-3H-3, 22.5	19.93	21.06
U1342C-3H-7, 34.6	26.05	27.19	Tie to	U1342D-4H-1, 57.7	25.58	27.19
U1342D-4H-7, 5.6	34.06	35.66	Tie to	U1342A-5H-3, 16.5	33.46	35.66
U1342A-5H-6, 103.9	38.84	41.04	Tie to	U1342D-5H-3, 117.7	38.68	41.04

Table T17. Temperature data, Hole U1342C. (**See table note.**)

Core	Depth (mbsf)	Thermal resistance (m^2K/W)	T (°C)
323-U1342C-			
3H	26.2	27.0	4.46
5H	35.0	37.7	5.32

Note: T = formation temperature.